Title: Mixed plastics waste valorization via tandem chemical oxidation and biological funneling

Authors: Kevin P. Sullivan,[1,2,†] Allison Z. Werner,[1,2,†] Kelsey J. Ramirez,[1,2,†] Lucas D. Ellis,[1,2,†] Jeremy Bussard,[1,2] Brenna A. Black,[1,2] David G. Brandner,[1,2] Felicia Bratti,[1,2] Bonnie L. Buss,[1,2] Xueming Dong,[1] Stefan J. Haugen,[1] Morgan A. Ingraham,[1] Mikhail O. Konev,[1,2] William E. Michener,[1] Joel Miscall,[1,2] Isabel Pardo,[1] Sean P. Woodworth,[1] Adam M. Guss,[2,3] Yuriy Román-Leshkov,[4] Shannon S. Stahl,[5,*] Gregg T. Beckham[1,2,*]

Affiliations:

[1]Renewable Resources and Enabling Sciences Center, National Renewable Energy Laboratory; Golden CO USA

[2]BOTTLE Consortium, Golden CO USA

[3]Biosciences Division, Oak Ridge National Laboratory, Oak Ridge, TN, USA

[4]Department of Chemical Engineering, Massachusetts Institute of Technology, Cambridge, MA, USA

[5]Department of Chemistry, University of Wisconsin Madison, Madison, WI USA

[†]These authors contributed equally to this work

*Corresponding author. Email: gregg.beckham@nrel.gov; stahl@chem.wisc.edu

Abstract: Mixed plastics waste, which is rapidly accumulating in landfills and the environment, represents an abundant and largely untapped feedstock for production of valuable products. The chemical diversity and complexity of these materials, however, present major barriers to realizing this opportunity. Here, we show that metal-catalyzed autoxidation depolymerizes co-mingled polymers into a mixture of oxygenated small molecules that are advantaged substrates for biological conversion. A robust soil bacterium, *Pseudomonas putida*, is engineered to funnel these oxygenated compounds into a single exemplary chemical product, either β-ketoadipate or polyhydroxyalkanoates. This hybrid process establishes a strategy for selective conversion of mixed plastics waste into useful chemical products.

One-Sentence Summary: Autoxidation is applied to mixed plastics to generate oxygenates, which are converted to a single product by an engineered bacterium.

Main Text:

Plastics have revolutionized modern life due to their low cost and utility in a vast range of applications. However, the accumulation of synthetic polymers in landfills and the environment has created a global pollution crisis that the existing reclamation and recycling infrastructure is not equipped to resolve (*1-3*). This challenge has accelerated investigation into new chemical recycling technologies that could enable the conversion of plastic waste streams into valuable chemicals and support creation of a circular plastics economy (*3-11*). Many chemical recycling approaches focus on selective depolymerization of single plastic streams. However, plastics chemistry is diverse in both monomer and bond type, and plastics in post-consumer waste are physically mixed and include complex materials such as multilayer packaging. These features complicate and increase the cost of separation methods required to isolate individual polymers for recycling (*3*). Chemical recycling processes that enable deconstruction of mixed plastics into valuable products without requiring sorting could bypass this limitation and significantly enhance plastics reclamation and recycling infrastructure.

Here, we present a strategy whereby mixed plastics are converted into single products through a tandem catalytic and biological process (**Fig. 1**). The initial catalytic step uses metal-promoted autoxidation to depolymerize mixed plastics into oxygenated intermediates that represent advantaged substrates for subsequent bioconversion (*12*). The biological step employs a robust engineered bacterial strain to funnel the mixed oxygenates into the target product, in this case illustrated by either β-ketoadipate or polyhydroxyalkanoates. This approach is demonstrated with mixtures of high-density polyethylene (HDPE), polystyrene (PS), and poly(ethylene terephthalate) (PET), which are among the most abundant components of post-consumer plastics waste.

Autoxidation is a complex chemical process in which initiation reactions generate organic radicals that react with O_2 and undergo chain propagation to generate oxygenated products. A notable example of industrial autoxidation is the conversion of *p*-xylene to terephthalic acid in the Amoco process, which operates at ~80M tons/year, where acetate salts of cobalt and manganese are used as catalysts with bromine radicals initiating the reaction, using O_2 as the oxidant (*13*). Partenheimer showed that similar conditions support depolymerization of several pristine polymers (*14*). Autoxidation of polymers is initiated by H-atom transfer from C–H bonds in the polymer backbone to generate alkyl radicals, which react at diffusion-controlled rates with O_2 to form peroxide intermediates (**Fig. 2A**). Homolytic cleavage of the O–O bond, aided by the Co and Mn catalysts, forms alkoxyl radicals that can undergo C–C cleavage via β-scission steps. This collection of H-atom transfer, radical trapping by O_2, and C–C cleavage steps ultimately affords a mixture of low-molecular-weight oxygenated products with identities reflecting the polymer precursor, for example, benzoic acid from PS, terephthalic acid from PET, and α,ω-dicarboxylic acids from HDPE (*14*). This precedent, among other studies (*15-17*), prompted us to explore a similar approach as the initial stage of our mixed plastics valorization process.

Autoxidation studies began with single-component commercial polymer resins comprising HDPE beads, PS beads, or PET powder. Use of bromide as a co-catalyst was avoided in our studies, as it is corrosive and requires specialized reactor materials. *N*-hydroxyphthalimide (NHPI) has precedent as an initiator and co-catalyst in autoxidation (*18*) and proved to be an effective alternative to bromide.

Under autoxidation conditions, depolymerization of PS yields benzoic acid (63.7 ± 1.0 mol%), HDPE yields a distribution of C_4-C_{22} dicarboxylic acids (34.2 ± 0.7 mol%), and PET generates

terephthalic acid (68.3 ± 0.7 mol%) (**Fig. 2B**, **figs. S1-12, tables S1-3**). To compare results more easily between different polymers, molar yields were determined in terms of moles of carbon in the isolated product relative to the starting polymer, such that the maximum theoretical yield is 87.5% for PS, 100% for PE and 80% for PET, respectively. This difference accounts for the loss of the methylene carbon in PS and the ethylene glycol carbons in PET. The molecular weight of the starting polymer had little influence on the product yields (**figs. S3a, S8a**), suggesting that depolymerization occurs through random chain scission. The yields obtained for the single-component substrates in this study are comparable to those observed previously by Partenheimer when using bromide-containing systems (*14*), and generated the expected products from the polymer precursor. Depolymerization of PS and PET affords a single major product, benzoic acid and terephthalic acid, respectively, while HDPE depolymerization led to a more complex product mixture, including dicarboxylic acids and five-membered lactone-containing products (**figs. S13-16**, **tables S3-4**). Experiments with PS and PET demonstrate that product yields are similar over a range of 1–10 wt% loadings, while higher HDPE loadings afford lower yields that are attributed to in situ degradation of the dicarboxylic acid products (**fig. S17**).

Efforts then shifted to reactions of mixed plastics, including mixtures of PS and HDPE, and ternary mixtures of PS, HDPE, and PET, for both commercial resins and post-consumer plastics. The latter were derived from expanded PS (EPS, i.e., Styrofoam^{TM}) cups, HDPE bottles (milk containers), or PET (single-use beverage bottles). Depolymerization of PS and PET is favored at higher temperatures (180 and 210 °C, respectively) and longer reaction times (5.5 h) relative to HDPE (160 °C, 2.5 h) (**Fig. 2B, figs. S1, S6, S9**), as HDPE generates products that degrade at higher temperatures (*14, 19*). Despite these differences, we identified conditions that support effective autoxidative depolymerization of mixed PS and HDPE, and mixed PS, HDPE, and PET. Treatment of the mixed PS and HDPE commercial resins at 180 °C for 5.5 h led to benzoic acid (68.9 ± 0.6 mol%) and dicarboxylic acids (22.5 ± 0.5 mol%) (**Fig. 2C, figs. S18-22**). Very similar results were obtained from reactions of mixed PS and HDPE post-consumer plastics, showing a slight increase in benzoic acid (71.0 ± 0.1 mol%) and similar dicarboxylic acid (22.1 ± 0.3 mol%) yields. Analogous results were obtained from the ternary PS, HDPE, and PET mixture of commercial resins and post-consumer plastics (**Fig. 2C**). These reactions were conducted at elevated temperature (210 °C) to facilitate PET depolymerization, but despite this adjustment, autoxidation of these mixtures afforded the same products, in similar (benzoic acid, 58.0 ± 1.2 mol%) or moderately reduced (dicarboxylic acids, 20.2 ± 1.1 mol%; terephthalic acid, 52.1 ± 5.5 mol%) yields, relative to those observed from depolymerization of the individual polymers (**Figs. 2B** and **2C**).

The mixture of oxygenates obtained from autoxidation of mixed plastics is sufficiently complex that it would require advanced separation methods to isolate and purify individual products suitable for downstream application. This challenge is akin to that encountered in thermal treatments of mixed plastics waste, such as pyrolysis. The autoxidation products are appealing, however, because they have enhanced water solubility that make them advantaged feedstocks for biological funneling, wherein an engineered microbe converts diverse chemicals to a single product (*20*). To pursue this opportunity, we engineered two strains of *Pseudomonas putida* (*21, 22*): first, to convert acetate, C_4-C_{17} dicarboxylates, benzoate, and terephthalate to polyhydroxyalkanoates, a natural polyester with growing industrial applications (*23*); and second, to utilize acetate and dicarboxylates for growth while converting benzoate and terephthalate to β-ketoadipate, a monomer for performance-advantaged polymers (*24*) (**Fig. 3**).

P. putida natively utilizes acetate, benzoate, and C_4-C_5 dicarboxylates as carbon sources (**figs. S23-24**), and we previously engineered a strain of *P. putida* to utilize terephthalate and ethylene glycol (*25*), which was used a base strain for further engineering in the present study. Ackermann *et al.* enabled adipate (C_6) utilization in *P. putida* by combining the native phenylacetate pathway with select transport and β-oxidation reactions from *Acinetobacter baylyi* ADP1 (**fig. S25**) *(26).* We took a similar approach by heterologously expressing the *A. baylyi dcaAKIJP* operon (*27*) and deleting genes encoding two native repressors of phenylacetate catabolism and β-oxidation, PaaX and PsrA (*28, 29*). The resulting strain, AW162, grew on C_4-C_{10} dicarboxylates as sole carbon sources, simultaneously utilized mixed C_4-C_{14} dicarboxylates, and was not inhibited by trace catalyst, initiator, or lactone acid species (**figs. S24-37, tables S5-8**).

Metal catalysts were recovered from crude, deconstructed polymers by suspension in water, NaOH addition, and filtration to remove the precipitated metal hydroxides (**fig. S38**). The resulting solutions contained substrates congruent with the feedstocks, trace (< 5 μM) Co/Mn metals, and acetate (**tables S9-12**). These "effluent" streams were used directly in microbial cultivations.

We next engineered and demonstrated biological funneling of intermediates from both commercial polymer resins and post-consumer plastics to polyhydroxyalkanoates, and separately to β-ketoadipate. AW162 grew on effluent from mixed PS and HDPE commercial polymer resin, as well as effluent from mixed EPS and HDPE post-consumer products, with simultaneous utilization of benzoate and C_4-C_{17} dicarboxylates (**Fig. 4A-C**, **fig. S39**). In effluent from mixed PS, HDPE, and PET commercial polymer resin, AW162 cultivations simultaneously utilized the aromatic and aliphatic substrates during growth (**Fig. 4D-E, fig. S40**). AW162 was also used for polyhydroxyalkanoates production by cultivation in nitrogen-limited medium: polyhydroxyalkanoates were produced from both effluent from mixed PS beads and HDPE beads, as well as effluent from mixed postconsumer EPS cups and HDPE bottles (**fig. S41**) and primarily comprised 3-hydroxydodecanoic acid and 3-hydroxydecanoic acid (**Fig. 4F, fig. S42**). In previous work, deletion of *pcaIJ* in *P. putida* enabled conversion of benzoate to β-ketoadipate at 41 g/L, 0.8 g/L/h, and quantitative yield in bioreactors (*24*). Here, *pcalJ* was deleted in strain AW162, resulting in strain AW307, to enable conversion of benzoate and terephthalate to β-ketoadipate (**Fig. 4G**). β-Ketoadipate production by AW307 was evaluated, with aliphatic substrates supporting growth and conversion of aromatic substrates to β-ketoadipate. Yields are reported as mol β-ketoadipate per mol aromatic monomer where the theoretical yield is 1 mol/mol; see **Table S13** for consideration of aliphatic carbon that is used as the substrate for cellular growth. In effluent from mixed PS and HDPE commercial polymer resins, all dicarboxylates except C_6-C_7 were completely utilized, and benzoate was converted to β-ketoadipate at an 81.0 ± 7.2% molar yield (**Fig. 4H-I, fig. S43b**). AW307 cultivations in effluent from mixed postconsumer EPS cups and HDPE bottles displayed similar growth and substrate utilization, generating β-ketoadipate at 84.8 ± 4.7% molar yield (**Fig. 4I, fig. S43c**). Incomplete utilization of C_6-C_7 dicarboxylates was observed and β-ketoadipate decreased at extended timepoints (**fig. S43**), which may indicate promiscuous activity of PcaIJ on C_6-C_7 dicarboxylates and/or DcaIJ on β-ketoadipate. In effluent from mixed PS, HDPE, and PET commercial polymer resins, β-ketoadipate was produced at a 75.5 ± 8.5% molar yield (**Fig. 4J-K**, **fig. S44-45**). Assuming no losses occurred during the processing of samples between the chemical and biological processes, overall molar β-ketoadipate yields from the aromatic constituents of the original plastics were 69% for mixed PS and HDPE commercial polymer resins, 72% for mixed PS and HDPE post-consumer plastics, and 57% for mixed PS, HDPE, and PET commercial polymer resins (**tables S13-S14**).

This work demonstrates a process concept for pairing chemical catalysis and bioconversion to convert mixed plastics into valuable products. Metal-catalyzed autoxidation offers a feedstock-agnostic approach for mixed-polymer deconstruction into oxygenated small molecules with advantages for biological funneling, owing to their bioavailability. Extensions from the individual and mixed PS, HDPE, and PET materials demonstrated here to other polymers susceptible to autoxidation, including polypropylene and polyvinyl chloride (*14*), are readily envisioned. These efforts will be supported by technical advances that improve the process performance and economic viability. For example, continuous reactor systems, such as those used in the Amoco process, should support higher polymer loadings by improving oxygen delivery and continuous removal of products to limit in situ degradation. Improvements in process integration will increase recovery of acetic acid and catalysts between the chemical and biological steps (*30*). Separations could also enable isolation of valuable autoxidation products prior to bioconversion. Further metabolic engineering of microbes will enable bioprocess improvements to access higher titers and rates, in addition to production of other products (*31*), beyond the two examples demonstrated here. Ideal targets include the synthesis of monomers for intrinsically circular polymers (*10, 32*). Techno-economic and life cycle assessment will guide future progress toward economical and sustainable processes (*11*).

References and Notes

1. S. B. Borrelle *et al.*, Predicted growth in plastic waste exceeds efforts to mitigate plastic pollution. *Science* **369**, 1515-1518 (2020).
2. A. Milbrandt, K. Coney, A. Badgett, G. T. Beckham, Quantification and evaluation of plastic waste in the United States. *Resour. Conserv. Recycl.* **183**, 106363 (2022).
3. K. Ragaert, L. Delva, K. Van Geem, Mechanical and chemical recycling of solid plastic waste. *Waste Manage.* **69**, 24-58 (2017).
4. A. Rahimi, J. M. García, Chemical recycling of waste plastics for new materials production. *Nat. Rev. Chem.* **1**, 1-11 (2017).
5. G. W. Coates, Y. D. Getzler, Chemical recycling to monomer for an ideal, circular polymer economy. *Nat. Rev. Mater.*, 1-16 (2020).
6. I. Vollmer *et al.*, Beyond mechanical recycling: Giving new life to plastic waste. *Angew. Chemie* **59**, 15402-15423 (2020).
7. L. D. Ellis *et al.*, Chemical and biological catalysis for plastics recycling and upcycling. *Nat. Catal.* **4**, 539-556 (2021).
8. S. C. Kosloski-Oh, Z. A. Wood, Y. Manjarrez, J. P. de los Rios, M. E. Fieser, Catalytic methods for chemical recycling or upcycling of commercial polymers. *Mater. Horiz.* **8**, 1084-1129 (2021).
9. A. J. Martín, C. Mondelli, S. D. Jaydev, J. Pérez-Ramírez, Catalytic processing of plastic waste on the rise. *Chem*, (2021).
10. C. Jehanno *et al.*, Critical advances and future opportunities in upcycling commodity polymers. *Nature* **603**, 803-814 (2022).
11. S. R. Nicholson *et al.*, The critical role of process analysis in chemical recycling and upcycling of waste plastics. *Ann. Rev. Chem. Biomolec. Eng.* **13**, (2021).
12. R. Wei *et al.*, Possibilities and limitations of biotechnological plastic degradation and recycling. *Nat. Catal.* **3**, 867-871 (2020).
13. R. A. F. Tomás, J. C. M. Bordado, J. F. P. Gomes, *p*-Xylene oxidation to terephthalic acid: A literature review oriented toward process optimization and development. *Chem. Rev.* **113**, 7421-7469 (2013).

14. W. Partenheimer, Valuable oxygenates by aerobic oxidation of polymers using metal/bromide homogeneous catalysts. *Catal. Today* **81**, 117-135 (2003).
15. A. Pifer, A. Sen, Chemical recycling of plastics to useful organic compounds by oxidative degradation. *Angew. Chemie* **37**, 3306-3308 (1998).
16. E. Bäckström, K. Odelius, M. Hakkarainen, Trash to treasure: Microwave-assisted conversion of polyethylene to functional chemicals. *Ind. Eng. Chem. Res* **56**, 14814-14821 (2017).
17. M. W. Guzik *et al.*, Robust process for high yield conversion of non-degradable polyethylene to a biodegradable plastic using a chemo-biotechnological approach. *Waste Manage.* **135**, 60-69 (2021).
18. Y. Ishii, S. Sakaguchi, Recent progress in aerobic oxidation of hydrocarbons by N-hydroxyimides. *Catal. Today* **117**, 105-113 (2006).
19. F. Gugumus, Re-examination of the thermal oxidation reactions of polymers 2. Thermal oxidation of polyethylene. *Polym. Degrad. Stab.* **76**, 329-340 (2002).
20. J. G. Linger *et al.*, Lignin valorization through integrated biological funneling and chemical catalysis. *Proc. Natl. Acad. Sci.* **111**, 12013-12018 (2014).
21. I. Poblete-Castro, J. Becker, K. Dohnt, V. M. Dos Santos, C. Wittmann, Industrial biotechnology of *Pseudomonas putida* and related species. *Appl. Microbiol. Biotechnol.* **93**, 2279-2290 (2012).
22. P. I. Nikel, V. de Lorenzo, *Pseudomonas putida* as a functional chassis for industrial biocatalysis: From native biochemistry to trans-metabolism. *Metab. Eng.* **50**, 142-155 (2018).
23. M. P. Mezzina, M. T. Manoli, M. A. Prieto, P. I. Nikel, Engineering native and synthetic pathways in *Pseudomonas putida* for the production of tailored polyhydroxyalkanoates. *Biotechnol. J.* **16**, e2000165 (2021).
24. C. W. Johnson *et al.*, Innovative chemicals and materials from bacterial aromatic catabolic pathways. *Joule* **3**, 1523-1537 (2019).
25. A. Z. Werner *et al.*, Tandem chemical deconstruction and biological upcycling of poly(ethylene terephthalate) to β-ketoadipic acid by *Pseudomonas putida* KT2440. *Metab. Eng.* **67**, 250-261 (2021).
26. Y. S. Ackermann *et al.*, Engineering adipic acid metabolism in *Pseudomonas putida*. *Metab. Eng.* **67**, 29-40 (2021).
27. D. Parke, M. A. Garcia, L. N. Ornston, Cloning and genetic characterization of *dca* genes required for beta-oxidation of straight-chain dicarboxylic acids in *Acinetobacter* sp. strain ADP1. *Appl. Environ. Microbiol.* **67**, 4817-4827 (2001).
28. G. Thompson Mitchell *et al.*, Fatty acid and alcohol metabolism in *Pseudomonas putida*: Functional analysis using random barcode transposon sequencing. *Appl. Environ. Microbiol.* **86**, e01665-01620 (2020).
29. C. Fernández, E. Díaz, J. L. García, Insights on the regulation of the phenylacetate degradation pathway from *Escherichia coli*. *Environ. Microbiol. Rep.* **6**, 239-250 (2014).
30. N. A. Rorrer *et al.*, Production of β-ketoadipic acid from glucose in *Pseudomonas putida* KT2440 for use in performance-advantaged nylons. *Cell Rep. Phy. Sci.*, **3**, 100840 (2022).
31. S. Y. Lee *et al.*, A comprehensive metabolic map for production of bio-based chemicals. *Nat. Catal.* **2**, 18-33 (2019).

32. C. Shi *et al.*, Design principles for intrinsically circular polymers with tunable properties. *Chem* **7**, 2896-2912 (2021).

Acknowledgments: We thank Robert Allen, Amy Cuthbertson, Sarah Hesse, Katrina Knauer, Jacob Kruger, Ciaran Lahive, David Moore, Nicholas Rorrer, Christopher Tassone, Nick Wierckx, Yannic Ackermann, Wilson McNeary, Hannah Alt, and members of the BOTTLE Consortium for helpful discussions.

Funding: Funding was provided by the U.S. Department of Energy, Office of Energy Efficiency and Renewable Energy, Advanced Manufacturing Office (AMO) and Bioenergy Technologies Office (BETO). This work was performed as part of the BOTTLE™ Consortium and was supported by AMO and BETO under contract no. DE-AC36-08GO28308 with the National Renewable Energy Laboratory, operated by Alliance for Sustainable Energy, LLC. The BOTTLE Consortium includes members from MIT, funded under contract no. DE-AC36-08GO28308 with NREL. Contributions by SSS were supported by U.S. Department of Energy, Office of Basic Energy Sciences under Sciences, under award no. DEFG02-05ER15690.

Author contributions:

Conceptualization: GTB, KPS, AZW, KJR, LDE, SSS

Investigation: KPS, AZW, KJR, LDE, JB, BAB, XD, IP

Visualization: AZW, KPS

Funding acquisition: GTB, AMG, YR

Resources: DGB, FB, BLB, SJH, MAI, MOK, WEM, JM, SPW

Supervision: GTB, SSS, YR

Writing – original draft: KPS, AZW, GTB

Writing – review & editing: All authors have reviewed and approved of the manuscript

Competing interests: GTB, LDE, KPS, and AZW have filed a patent application on this concept: PCT/US2021/063725 Upcycling Mixed Waste Plastic Through Chemical Depolymerization and Biological Funneling. The patent filer is the Alliance for Sustainable Energy, LLC.

Data and materials availability: All data are available in the manuscript or the Supplementary Materials. Strains and plasmids are available upon request via a Materials Transfer Agreement with the National Renewable Energy Laboratory.

Figures and Legends

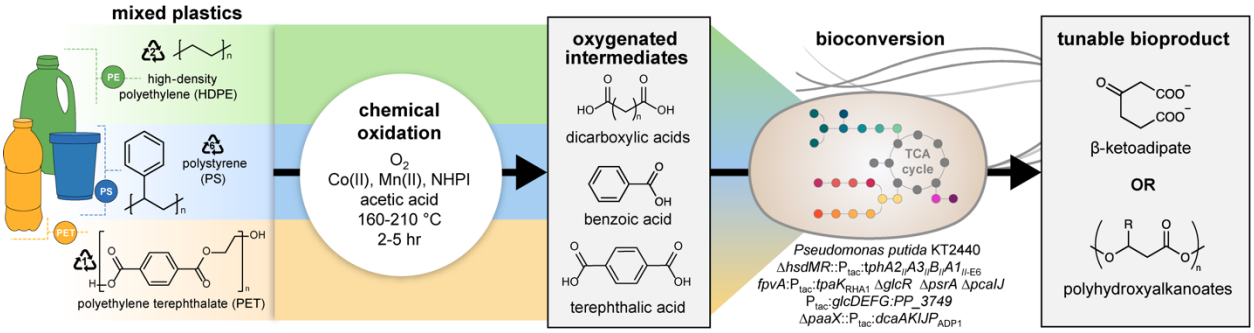

Fig. 1. Concept for upcycling of mixed plastic waste via tandem chemical oxidation and bioconversion. Metal-promoted autoxidation simultaneously deconstructs multiple polymers, generating a mixture of oxygenated intermediates that are advantaged substrates for bioconversion. An engineered *Pseudomonas putida* strain funnels the heterogeneous mixture of oxygenates into a single target product.

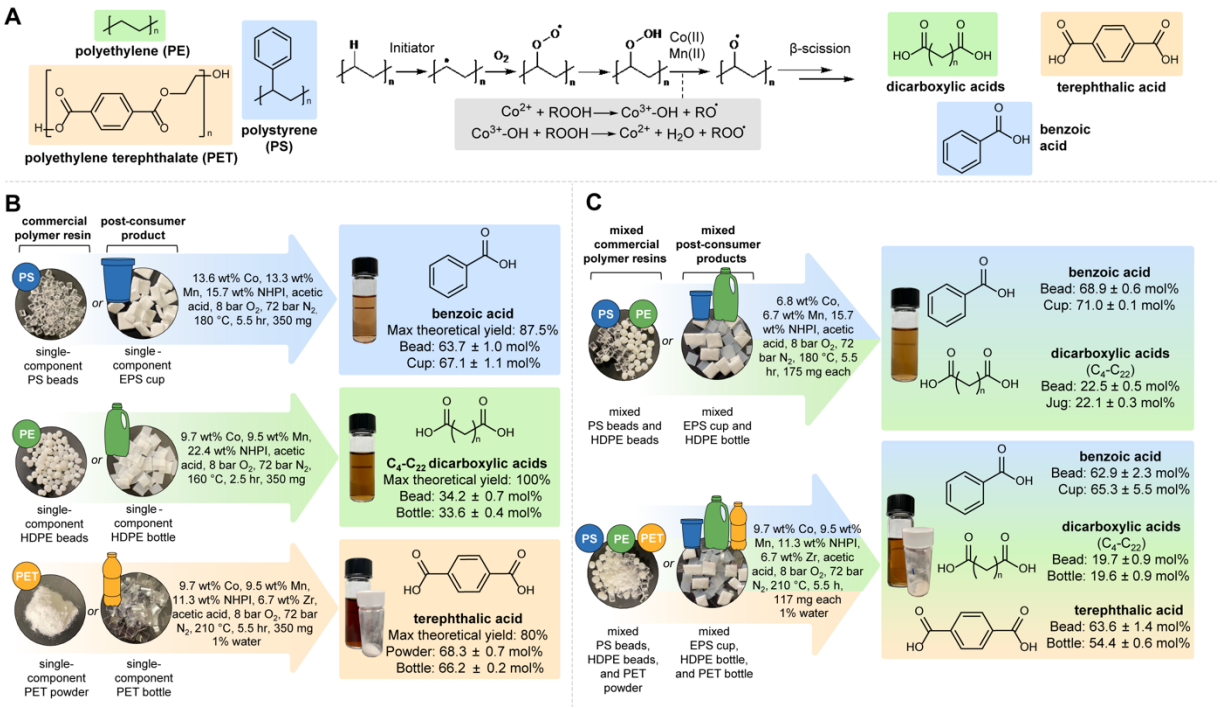

Fig. 2. Oxidative depolymerization of mixed plastics. (**A**) Autoxidation scheme, illustrated for HDPE, with products for all polymers shown. (**B**) Oxidation of single-component commercial polymer resins and post-consumer plastics. (**C**) Oxidation of mixed plastic substrates. Experimental details are in the **Supplementary Materials**. Mean ± SD; $N = 3$. Mol% indicates mol % carbon in isolated products relative the total carbon in the starting polymer, wt% is relative to the total plastics loading.

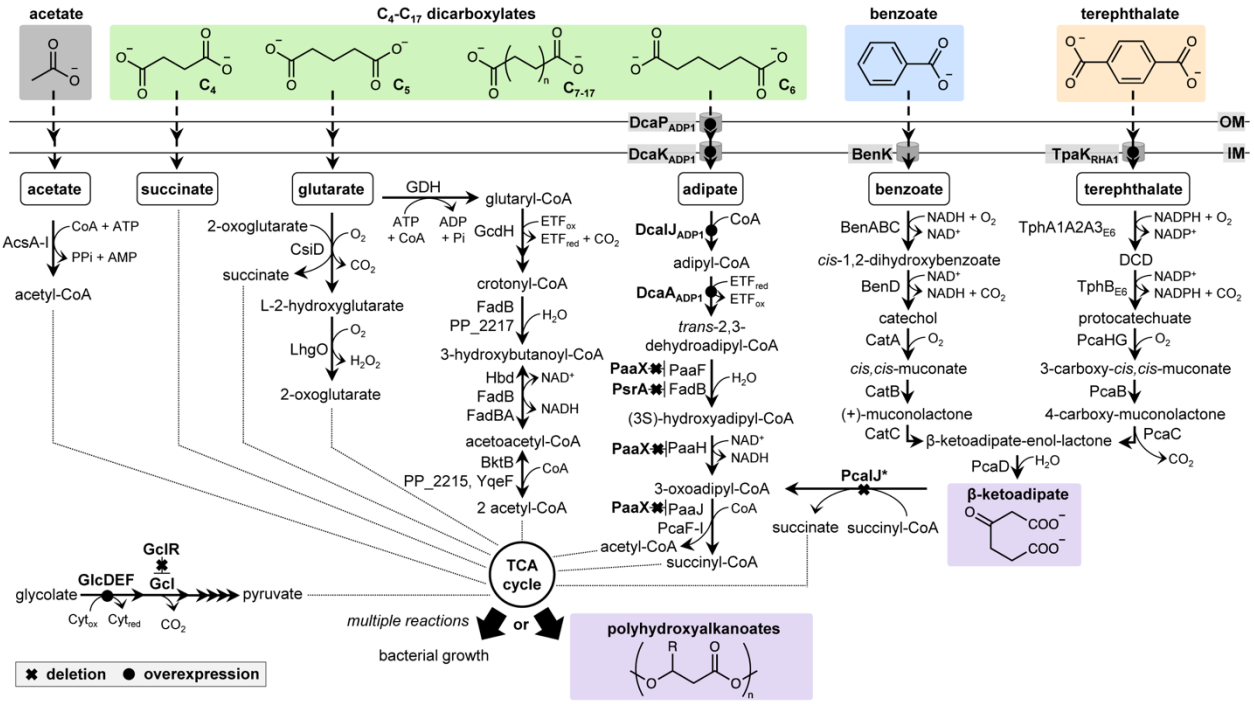

Fig. 3. Engineered metabolic pathways for biological funneling of PS, HDPE, and PET-derived oxygenated intermediates to β-ketoadipate or polyhydroxyalkanoates. Engineered expression changes to genes encoding the corresponding proteins are depicted in bold font where gene deletion is indicated by an "X", and gene overexpression is indicated by a circle. Subscript indicates a protein of heterologous origin, where ADP1 indicates *A. baylyi* ADP1, RHA1 indicates *R. jostii* RHA1, and E6 indicates *Comamonas* sp. E6. AW162: *P. putida* Δ*hsdMR*::P$_{tac}$:*tphA2*$_{II}$*A3*$_{II}$*B*$_{II}$*A1*$_{II\text{-}E6}$ *fpvA*:P$_{tac}$:*tpaK*$_{RHA1}$ Δ*glcR* P$_{tac}$:*glcDEFG:PP_3749* Δ*paaX*::P$_{tac}$:*dcaAKIJP*$_{ADP1}$ Δ*psrA*. AW307: AW162 Δ*pcaIJ*. Genotypes and strain construction details are provided in **tables S5-8**.

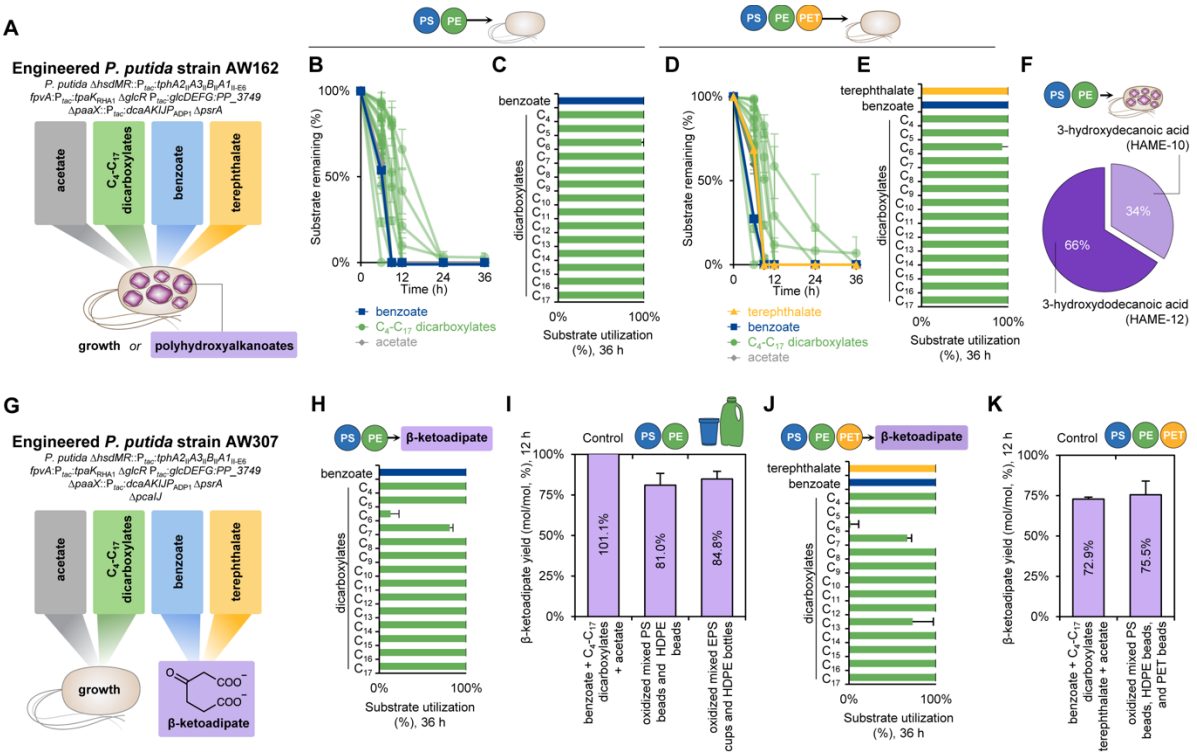

Fig. 4. Bioconversion of effluent from mixed plastics to target products. (**A**) AW162 was engineered to utilize all intermediates as substrates for growth or polyhydroxyalkanoates production. Utilization of intermediates in (**B-C**) effluent from mixed PS beads and PE beads, or (**D-E**) effluent from mixed PS beads, HDPE beads, and PET powder by AW162. (**F**) Composition of polyhydroxyalkanoates produced from effluent from mixed PS beads and HDPE beads by AW162. (**G**) AW307 was engineered to utilize acetate and dicarboxylates for growth and convert benzoate and terephthalate to β-ketoadipate. (**H**) Utilization of intermediates in effluent from mixed PS beads and HDPE beads by AW307. (**I**) β-ketoadipate yields (% of theoretical maximum) from control mixtures, effluent from mixed PS beads and HDPE beads, or effluent from mixed postconsumer EPS cups and HDPE bottles by AW307. (**J**) Utilization of intermediates in effluent from mixed PS beads, HDPE beads, and PET powder by AW307, and (**K**) β-ketoadipate yields from the same or control mixtures. Mean ± SD; $N = 3$. Genotypes and strain construction details are in **tables S5-8**.

List of Supplementary Content:

Materials and Methods
Supplementary Text
Figs. S1 to S45
Tables S1 to S14
References (*33*)-(*56*)

Science
AAAS

Supplementary Materials for

Mixed plastics waste valorization via tandem chemical oxidation and biological funneling

Authors: Kevin P. Sullivan,[1,2,†] Allison Z. Werner,[1,2,†] Kelsey J. Ramirez,[1,2,†] Lucas D. Ellis,[1,2,†] Jeremy Bussard,[1,2] Brenna A. Black,[1,2] David G. Brandner,[1,2] Felicia Bratti,[1,2] Bonnie L. Buss,[1,2] Xueming Dong,[1] Stefan J. Haugen,[1] Morgan A. Ingraham,[1] Mikhail O. Konev,[1,2] William E. Michener,[1] Joel Miscall,[1,2] Isabel Pardo,[1] Sean P. Woodworth,[1] Adam M. Guss,[2,3] Yuriy Román-Leshkov,[4] Shannon S. Stahl,[5,*] Gregg T. Beckham[1,2,*]

Affiliations:

[1]Renewable Resources and Enabling Sciences Center, National Renewable Energy Laboratory; Golden CO USA

[2]BOTTLE Consortium, Golden CO USA

[3]Biosciences Division, Oak Ridge National Laboratory, Oak Ridge, TN, USA

[4]Department of Chemical Engineering, Massachusetts Institute of Technology, Cambridge, MA, USA

[5]Department of Chemistry, University of Wisconsin Madison, Madison, WI USA

[†]These authors contributed equally to this work

*Corresponding author. Email: gregg.beckham@nrel.gov; stahl@chem.wisc.edu

This PDF file includes:

Other Supplementary Materials for this manuscript include the following:

Supplementary Excel 1

List of Figures

List of Tables

Materials and Methods

Chemicals

The following chemicals were used:

Polymer substrates:

- 280 kDa polystyrene beads (Sigma-Aldrich, CAS:9003-53-6, Lot#: MKCL4619)
- 185 kDa polystyrene beads, atactic (Alfa Aesar, CAS: 9003-53-6, Lot#: W02G019)
- 35 kDa polystyrene pellets (Sigma-Aldrich, CAS: 9003-53-6, Lot#: MKCG5477)
- 125 kDa high-density polyethylene granules (Alfa Aesar, CAS:9002-88-4, Lot#: S02D047)
- 54 kDa linear polyethylene (NIS0T NBS Standard Reference Material 1475, Lot# JRMPMMA-1B152)
- 38 kDa polyethylene terephthalate powder (Goodfellows, Lot# ES306031/1)
- post-consumer 290 kDa EPS cup (Reynolds Hefty® 16 oz Foam Cups)
- post-consumer 99 kDa HDPE bottle (Meadow Gold Fat Free Milk, half gallon jug)
- post-consumer 42 kDa PET soda bottle (Diet Dr. Pepper, 16 oz.)

Catalysts, initiators, and gases:

- *N*-hydroxyphthalimide (NHPI) (Sigma-Aldrich, Cat. #H53704)
- cobalt(II) acetate (Sigma-Aldrich, Cat. #399973)
- manganese(II) acetate (Sigma-Aldrich, Cat. #330825)
- zirconium (IV) acetylacetonate (Sigma-Aldrich, Cat. #338001)
- glacial acetic acid (JT Bakter Inc., Cat. #9507)
- ultra-high purity (UHP) helium (CAS: 7440-59-7, Air Gas)
- ultra-zero compressed air (Matheson, UN1002)

Other chemicals:

- benzoic acid (Sigma-Aldrich, Cat. # 242381), used for biological cultivations
- benzoic acid (Acros Organics, Cat. # 14913), used for analytical standards
- terephthalic acid (Sigma-Aldrich, CAS: 100-21-0), used for analytical standards
- 2-hydroxyethyl terephthalic acid (Chiroblock, batch REL 5782 a18 VI), used for analytical standards
- malonic acid (Sigma-Aldrich, Cat. # M1296)
- succinic acid (Sigma-Aldrich, Cat. # S3674)
- glutaric acid (Sigma-Aldrich, Cat. # G3407)
- adipic acid (Sigma-Aldrich, Cat. # A26357)
- pimelic acid (Sigma-Aldrich, Cat. # P45001)
- suberic acid (Sigma-Aldrich, Cat. # S5200)
- azelaic acid (Sigma-Aldrich, Cat. # 246379)
- sebacic acid (Sigma-Aldrich, Cat. # 283258)
- undecanedioic acid (Sigma-Aldrich, Cat. # 177962)
- dodecanedioic acid (Sigma-Aldrich, Cat. # D1009)
- tridecanedioic acid (Sigma-Aldrich, Cat. # U601)
- tetradecanedioic acid (Sigma-Aldrich, Cat. # D221201)
- 1,15-pentadecanedioic acid (Synthonix, Cat. # P58506)
- hexadecanedioic acid (Sigma-Aldrich, Cat. # 177504)

- heptadecanedioic acid (Toronto Research Chemicals, Cat. # H998558)
- octadecanedioic acid (Toronto Research Chemicals, Cat. # O235303)
- nonadecanedioic acid (Toronto Research Chemicals, Cat. # N649003)
- eicosanedioic acid (Toronto Research Chemicals, Cat. # E476860)
- docosanedioic acid (Sigma-Aldrich, Cat. # 306673)
- succinic-2,2,3,3-d4 acid (CDN Isotopes, Cat. # D-0197)
- pentanedioic-2,2,4,4-d4 acid (CDN Isotopes, Cat. # D-1197)
- hexanedioic-2,2,5,5-d4 acid (CDN Isotopes, Cat. # D-0907)
- 1,12-dodecanedioic-2,2,11,11-d4 acid (CDN Isotopes, Cat. # D-5089)
- 4-hydroxybenzoic-2,3,5,6-d4 acid (Sigma-Aldrich, Cat. # 662763)
- Leucine-enkephalin (Waters Corporation, Cat. # 186006013)
- 3-(trimethylsilyl)pripionic-*2,2,3,3-d_4* acid, sodium salt (Millipore Sigma, Cat. #269913)
- sodium acetate (Sigma-Aldrich Cat. # S8750)
- D-glucose (Fisher Chemical Cat. # D16-10)
- *β*-hydromuconic acid (Sigma-Aldrich, CAS: 4436-74-2)
- tri-n-butylamine (Sigma-Aldrich, CAS: 102-82-9)
- 4-oxoheptanedioic acid (Sigma-Aldrich, CAS: 502-50-1)
- sodium borohydride (Alfa Aesar, CAS: 16940-66-2)
- (R)-(−)-5-oxo-2-tetrahydrofurancarboxylic acid (Sigma-Aldrich Cat. # 310476)
- (S)-(+)-5-oxo-2-tetrahydrofurancarboxylic acid (Sigma-Aldrich Cat. # 301469)
- 1,2-diphenylethanol (Enamine, Cat. # EW300-55433)
- 4-propylphenol (Sigma-Aldrich, Cat. # P53802)
- acetophenone (Sigma-Aldrich, Cat. # A10701)
- a-methylbenzyl alcohol (Sigma-Aldrich, Cat. #13800)
- benzaldehyde (Sigma-Aldrich, Cat. # 418099)
- benzil (Alfa Aesar, Cat. #A12579)
- benzyl alcohol (Acros Organics, Cat. # 14839)
- benzyl phenyl ketone (TCI America Organic Chemicals, Cat. # B4035)
- bibenzyl (Sigma-Aldrich, Cat. # B33706)
- ethylbenzene (Sigma-Aldrich, Cat. # 296848)
- methyl benzoate (TCI America Organic Chemicals, Cat. # B0074)
- phenol (Sigma-Aldrich, Cat. # 185450)
- propiophenone (Sigma-Aldrich, Cat. # P51605)
- propylbenzene (Fluka Chemical Corporation, Cat. # 82119)
- sodium phosphate monobasic monohydrate (Sigma-Aldrich, Cat. S9638)
- potassium phosphate monobasic (Sigma-Aldrich, Cat. #P5655)
- sodium chloride (Sigma-Aldrich, Cat. #S9888)
- ammonium chloride (Sigma-Aldrich, Cat. #A9434)
- magnesium sulfate (Sigma-Aldrich, Cat. #M7506)
- calcium chloride dihydrate (Signa-Aldrich, Cat. #C7902)
- ferrous sulfate heptahydrate (Fisher Scientific, Cat. #M-4722)

Reaction Performance Testing

All reactions were performed on a Series 5000 Multiple Reactor System by Parr Instruments, which provides for six 75 mL (total volume) batch reactors operated in parallel with magnetic mixing and individual temperature control.

CAUTION: *the use of high pressures, O_2, and flammable solvents results in high explosion risk. Extreme care must be taken to ensure adequate barriers for protection, and to ensure that the concentration of O_2 in the headspace is maintained at a level where explosive mixtures do not result during heating or cooling.*

A typical experiment with a polymer feedstock consisted of filling a 316 stainless steel reactor with a 1" Teflon coated stir bar with 20 mL of glacial acetic acid, followed by the addition of cobalt (II) acetate, manganese (II) acetate, *N*-hydroxyphthalimide (NHPI), zirconium (IV) acetylacetonate (where used), and the polymer substrate. After the addition of all reactants, reactors were purged with ultra-high purity (UHP) helium atmosphere three times, before leak testing at 90 bar. Upon passing a leak test, reactors were charged with ultra-zero compressed air to the desired oxygen pressure (typically 38 bar air) and further diluted with UHP helium to ensure gaseous mixtures could never reach a flammable concentration (typically 80 bar total pressure). This determination was made using flammability limits (LOC (limiting oxygen concentration), LEL (lower explosion limit), UEL (upper explosion limit) and calculations of the headspace composition using Antione equation parameters obtained from the NIST database. Reactors were then heated to the desired temperatures for the desired duration. Reaction times listed in this work include the 30 minutes that it takes to reach the desired temperature. Upon completion, reactors were placed on ice and cooled to ~20 °C, after which they were depressurized, and reaction solutions were collected for analysis. Product mixtures directly from the catalytic reactions were filtered through 0.2 μm Nylon and diluted with THF prior to analysis. PET samples were first filtered to recover terephthalic acid solids, and the filtrate was collected, diluted, and submitted for analysis. The recovered solids were washed with 5 mL acetic acid, 5 mL acetone, dried overnight in a vacuum oven at 40 °C, and dissolved in dimethyl sulfoxide (DMSO) prior to dilution in tetrahydrofuran (THF) and subsequent analysis.

Reaction conditions for PS depolymerization as represented in Figure 2B:
Product concentrations were determined using high pressure liquid chromatography (HPLC) with diode array detection (DAD). Mol% carbon yields are calculated as a percentage of carbon in the quantified products relative to the carbon present in the repeating unit of the polymer starting material. Conditions: 280 kDa PS beads or 290 kDa EPS cup (350 mg, 168 mM repeating styrene unit), $Co(OAc)_2$ (13.6 wt%, 13.4 mM), $Mn(OAc)_2$ (13.3 wt%, 13.4 mM), NHPI (15.7 wt%, 16.8 mM), 8 bar O_2/72 bar N_2, 5.5 hr, 180 °C.

Reaction conditions for HDPE depolymerization as represented in Figure 2B:
Product concentrations were determined by ultra-high pressure liquid chromatography tandem mass spectrometry (UHPLC-MS/MS). Mol% carbon yields are calculated as a percentage of carbon in the quantified products relative to the carbon present in the repeating unit of the polymer starting material. Conditions: 54 kDa HDPE bead or 99 kDa milk bottle (350 mg, 1250 mM repeating ethylene unit), $Co(OAc)_2$ (9.7 wt%, 9.6 mM), $Mn(OAc)_2$ (9.5 wt%, 9.6 mM), NHPI (22.4 wt%, 24.0 mM), 8 bar O_2/72 bar N_2, 2.5 hr, 160 °C.

Reaction conditions for PET depolymerization as represented in Figure 2B:
Product concentrations were determined using UHPLC with DAD. Mol% carbon yields are calculated as a percentage of carbon in the quantified products relative to the carbon present in the

repeating unit of the polymer starting material. Conditions: PET (38 kDa PET powder, or 42 kDa PET soda bottle (350 mg, 83 mM repeating 2-hydroxyethyl terephthalic acid unit), $Co(OAc)_2$ (9.7 wt%, 9.6 mM), $Mn(OAc)_2$ (9.5 wt%, 9.6 mM), $Zr(acac)_4$ (6.7 wt%, 2.4 mM), NHPI (11.3 wt%, 12.1 mM), 1% H_2O (v/v), 8 bar O_2/72 bar N_2, 5.5 hr, 210 °C.

Reaction conditions for mixed PS + HDPE depolymerization as represented in Figure 2C:
PS and HDPE product concentrations were determined as described above. Mol% carbon yields are calculated as a percentage of carbon in the quantified products relative to the carbon present in the repeating unit of the polymer starting material. Catalyst wt% values are in relation to the total polymer content (mg PS + mg HDPE). Plastic content: 350 mg total plastic (175 mg 54 kDa HDPE bead or 99 kDa milk bottle (624 mM repeating ethylene unit), 175 mg 280 kDa PS beads or 290 kDa EPS cup (84 mM repeating styrene unit)), $Co(OAc)_2$ (6.8 wt%, 6.7 mM), $Mn(OAc)_2$ (6.7 wt%, 6.7 mM), NHPI (15.7 wt%, 16.8 mM), 8 bar O_2/72 bar N_2, 5.5 hr, 180 °C.

Reaction conditions for mixed PS + HDPE + PET depolymerization as represented in Figure 2C:
PS, HDPE, and PET product concentrations were determined as described above. Mol% carbon yields are calculated as a percentage of carbon in the quantified products relative to the carbon present in the repeating unit of the polymer starting material. Catalyst wt% values are in relation to the total polymer content (mg PS + mg HDPE + mg PET). Plastic content: 350 mg (117 mg PS (280 kDa PS beads or 290 kDa EPS cup, 56 mM repeating styrene unit), 117 mg HDPE (35 kDa HDPE beads or 99 kDa HPDE milk bottle (417 mM repeating ethylene unit), 117 mg PET (54 kDa PET powder or 42 kDa PET soda bottle (117 mg, 28 mM 2-hydroxyethyl terephthalic acid unit). $Co(OAc)_2$ (9.7 wt%, 9.6 mM), $Mn(OAc)_2$ (9.5 wt%, 9.6 mM), $Zr(acac)_4$ (6.7 wt%, 2.4 mM), NHPI (11.3 wt%, 12.1 mM), 1% H_2O (v/v), 8 bar O_2/72 bar N_2, 5.5 hr, 210 °C.

Synthesis of compounds for analytical standards
2-(5-oxo-tetrahydrofuran-2-yl)acetic acid (C_6-Lac): The synthesis of this compound was carried out as described previously (*33*). To 3.0 g (20.8 mmol) of *β*-hydromuconic acid was added 30 mg (0.162 mmol) tri-n-butylamine. Mixture was heated at 210 °C for 6.0 h under N_2 atmosphere, yielding the crude product. Product was purified using a Combiflash® NextGen 300+ instrument equipped with a silica RediSepRf column, with 5% CH_3OH in CH_2Cl_2 as the mobile phase.

3-(5-oxo-tetrahydrofuran-2-yl)propionic acid (C_7-Lac): The synthesis of this compound was carried out as described previously (*34*). 4-oxoheptanedioic acid (1.0 g, 5.74 mmol) was dissolved in dry THF (30 mL), and sodium borohydride (0.8 g, 24 mmol) was added. The mixture was stirred for 3 h at room temperature. The solvent was removed via rotary evaporation, 10 mL of 8 M HCl was added, and the reaction was left to stir for 10 min. The aqueous phase was extracted with CH_2Cl_2 (3 X 50 mL). 10 mL H_2O was added to increase solubility of borate salts in aqueous layer. The organic phase was collected and dried with Na_2SO_4, and the solvent was removed *via* rotary evaporation, yielding the crude product. The product was purified by dissolution in a minimal amount of Et_2O followed by evaporative crystallization.

4-hydroxyheptanedioic acid (C_7-ROLA): To an 8 mL screw cap vial equipped with a magnetic stir bar was added C_7-Lac (80 mg, 0.5 mmol), NaOH (60 mg, 1.5 mmol), and DI H_2O (1.0 mL). The reaction was left to stir sealed for 12 h, producing the ring-opened product.

Cryomilling of plastic beads to obtain powdered material
Samples were cryomilled using a Horiba Freezer Mill 6770. A 25mL 6751 polycarbonate cylinder grinding vial was fitted on one end with a steel plug, and a steel impact bar was inserted into the vial. The sample was placed into the vial and the open end was plugged with another steel plug.

The freezer mill reservoir was filled with liquid N_2, and the sample was introduced and allowed to pre-cool for 10 minutes. Then, the sample was ground at the highest grinding rate for two minutes, followed by cooling for two minutes. The grinding and cooling steps were performed two additional times for a total of seven steps in the method. The vial was allowed to thaw and the cryomilled sample was recovered.

Preparation of depolymerized plastics for bioconversion

Preparation of effluent from PS

To prepare depolymerized PS for bioconversion, the liquid reaction mixture from three individual reactions, each at 350 mg scale, was taken directly from the Parr reactors, combined in a 250 mL round-bottomed flask, and dried on a rotary evaporator for ~1 h with heating at 35 °C and 20 mbar, to remove the acetic acid solvent. Care must be taken to avoid removing benzoic acid through sublimation, which can be observed along the sides of the round-bottomed flask. To precipitate the metals, the partially dried substrate was weighed, added to water, and adjusted to pH 11.4-12.1 with 4 N NaOH, resulting in formation of a black precipitate, indicative of cobalt and manganese metal oxides. Achieving pH ~12 was targeted to fully precipitate the metals. The resulting suspension was filtered with a qualitative filter paper (Whatman Cat. 28310-026) which removed the black precipitate (**Figure S38**). To prepare the filtrate for bioconversion, the pH was adjusted to 7.4-8.0 with 37% (v/v) HCl and sterilized by vacuum filtration (0.2 µm, Nalgene Cat. 596-4520). Readjustment to neutral pH was done to minimize pH fluctuation of the media upon addition of the effluent solution. We note that M9 minimal medium is well buffered and therefore this step can be avoided if the cultivation media can tolerate the added effluent without affecting the pH. This solution contained primarily benzoic acid and small amounts of benzaldehyde (**Table S9** likely owing to non-enzymatic oxidative conversion of benzaldehyde to benzoate during the pH adjustment, as has been previously reported to occur in the presence of water and oxygen (*35*). Acetate was also present in the solution owing to pH adjustment of remaining acetic acid solvent. A representative filter cake of the precipitated metals contained 20.4 wt% Co and 18.8 wt% Mn as determined by ICP-OES. The effluent (filtrate) from PS beads contained 0.024 µM Mn and 0.076 µM Co; the effluent (filtrate) from EPS cups contained 0.022 µM Mn and 1.32 µM Co (**Table S12**).

For preparation of crude HDPE for bioconversion, the liquid reaction mixture from three individual reactions, each at 350 mg scale, was taken directly from the Parr reactors, combined in a 250 mL round-bottom flask, and dried on a rotary evaporator for ~1h with heating at 35 °C, at 20 mbar to recover the acetic acid solvent. To precipitate the metals, the crude solids were weighed, added to deionized water, and pH adjusted with 4 N NaOH to pH 11.8-12.0. Again, achieving pH ~12 was targeted to fully precipitate the metals. To recover the metal catalyst, the suspension was filtered twice with decreasing porosity (Whatman Cat. 28310-026, Fisher P4 09-803-67B). Notably, the precipitate particles were smaller than in the case of PS, and precipitate remained in suspension until 0.2 µm filtration (Nalgene Cat. 596-4520), after which the solution was sterilized and free of visible particles. The solution was not neutralized to prevent the precipitation of $>C_{10}$ dicarboxylates, which have low solubility in water unless the solution is highly alkaline (>pH 10). The solution was sterilized by 0.2 µm filtration (Nalgene Cat. 596-4520) after which it was free of visible particles (**Figure S38**). This sterile and solubilized effluent was added directly to M9 minimal media, which did not result in alkaline media and therefore was tolerated without further pH adjustment. C_4 through C_{22} dicarboxylates and acetate concentrations in the resulting solution were quantified to determine the volume needed in each shake flask cultivation. We also note that in all cases the effluent was added alongside additional media components, and therefore the

substrate concentrations (reported for every cultivation in **Supplemental Excel 1**) are lower than that reported in the effluent solution (reported in **Tables S9-11**) due to this dilution.

Preparation of effluent from mixed PS and HDPE

Effluent from mixed PS and HDPE was prepared for bioconversion in the same manner as described above. The resulting 0.2 μm vacuum-filtered solution contained benzoate, dicarboxylates (C_4-C_{18}), and acetate (**Table S10**). The effluent (filtrate) prepared from PS beads and HDPE beads contained 0.003 μM Mn and 3.58 μM Co; the effluent (filtrate) prepared from mixed post-consumer EPS cup and HDPE bottle contained 0.004 μM Mn and 4.56 μM Co (**Table S12**).

Preparation of effluent from mixed PS, HDPE, and PET

Effluent from PS, HDPE and PET was prepared for bioconversion in the same manner as described above. The resulting 0.2 μm vacuum filtered solution contained benzoate, terephthalate, dicarboxylates C_4-C_{18}, and acetate (**Table S11**). The effluent (filtrate) contained 0.004 μM Mn and 4.62 μM Co (**Table S12**).

Preparation of model substrates for bioconversion

To prepare a 100 mM benzoate stock, benzoic acid was added to deionized water and solubilized by slowly raising the pH to ~7.5 with 4 N NaOH. To prepare a 0.5 or 1.0 M acetate stock, sodium acetate was added to deionized water and solubilized by slowly lowering the pH to ~7.5 with acetic acid. To prepare a 2 M glucose stock, D-glucose was added to deionized water and stirred to solubilize. To prepare dicarboxylic acids for microbial cultivation, stocks of each compound were prepared either in DMSO or water. Succinic acid (C_4, 200 mM), glutaric acid (C_5, 200 mM), adipic acid (C_6, 200 mM), pimelic acid (C_7, 200 mM), suberic acid (C_8, 200 mM), azelaic acid (C_9, 200 mM), sebacic acid (C_{10}, 20 mM), undecanedioic acid (C_{11}, 20 mM), dodecanedioic acid ($C_{1,2}$ 20 mM), 1,11-undecanedicarboxylic acid (C_{13}, 20 mM), tetradecanedioic acid (C_{14}, 20 mM), 1,15-pentadecanedioic acid (C_{15}, 20 mM), hexadecanedioic acid (C_{16}, 20 mM), or heptadecanedioic acid (C_{17}, 20 mM) were utilized and added to deionized water and solubilized by slowly raising the pH to >8.5 (pH >12 for >C_{10} dicarboxylates) with 4 N NaOH or added to DMSO and vortexed to solubilize. The lactone acids (R)-(−)-5-oxo-2-tetrahydrofurancarboxylic acid, (S)-(+)-5-oxo-2-tetrahydrofurancarboxylic acid, 2-(5-oxotetrahydrofuran-2-yl)acetic acid (C_6-Lac), and 3-(5-oxo-tetrahydrofuran-2-yl)propionic acid (C_7-Lac) were added to DMSO in a known weight and vortexed to solubilize. The ring-opened lactone acid 4-hydroxyheptanedioic acid (C_7-ROLA) was prepared by adding 1 mL of water and adjusting to pH 9.21 with 4 N NaOH and 36% (v/v) HCl. All stocks were sterilized by 0.2 μm filtration prior to biological cultivations.

Bacterial strains and cultivation

For propagation of plasmids, chemically competent NEB® 5-alpha F'I^q *E. coli* was cultivated in Miller's LB supplemented with 50 μg/mL kanamycin (Kan) at 37 °C and 225 rpm. *Pseudomonas putida* KT2440 (ATCC® 47054) and derivative strains were cultivated in Miller's LB during strain construction and evaluated in M9 minimal medium (6.78 g/L Na_2HPO_4, 3 g/L KH_2PO_4, 0.5 g/L NaCl, 1 g/L NH_4Cl, 2 mM $MgSO_4$, 100 μM $CaCl_2$, and 18 μM $FeSO_4$), supplemented with carbon sources as indicated, at 30 °C and 225 rpm. Glycerol stocks were prepared at 20% (v/v) glycerol in LB, with Kan for *E. coli* stocks, and stored at -80 °C. For polyhydroxyalkanoate production, nitrogen-limited M9 minimal medium was provided as previously described (*36*).

Plasmid construction

All plasmid construction details can be found in **Table S5**, **Table S6, Table S7,** and **Table S8.** DNA constructs were synthesized by Twist Biosciences, and oligonucleotide primers were synthesized by Integrated DNA Technologies, unless otherwise indicated. DNA was amplified using polymerase chain reactions (PCRs) with Q5® Hot Start High-Fidelity 2X Master Mix for plasmid constructions or MyTaq™ Red Mix for colony PCRs. Plasmids were assembled using NEB® NEBuilder HiFi DNA Assembly Master Mix and assemblies were directly transformed into NEB® 5-alpha F'I^q *E. coli.* Correct plasmid assembly was confirmed with colony polymerase chain reaction (cPCR), then plasmid inserts were sequence confirmed with Sanger sequencing (GENEWIZ, Inc.).

Strain construction

All strain construction details can be found in **Table S5**, **Table S6, Table S7,** and **Table S8.** *Pseudomonas putida* KT2440 chromosomal deletions and integrations were conducted with the antibiotic/*sacB* method, as previously described (*37*). Briefly, electroporated cells were plated on LB+Kan_{50} selection plates, individual isolates were streaked again on LB+Kan_{50} selection plates, individual isolates were streaked onto YT+25% sucrose plates (10 g/L yeast extract, 20 g/L tryptone, 250 g/L sucrose, 18 g/L agar) for counter selection, and individual isolates were streaked again onto YT+25% sucrose plates. Removal of the plasmid backbone and complete segregation was confirmed by cPCR and an inability to grow on LB+Kan_{50}. Deletions were confirmed by cPCR. Integrations were confirmed by cPCR and Sanger sequencing of the integrated DNA (GENEWIZ, Inc.).

Microtiter plate cultivations

Precultures of *Pseudomonas putida* KT2440 or engineered derivatives were inoculated into Miller's LB from glycerol stocks, grown at 30 °C and 225 rpm overnight (~12 h), washed in 1X M9 salts, and inoculated into M9 minimal medium in triplicate with the supplemental carbon indicated in each individual experiment. Growth was measured in a BioscreenC® (Growth Curves, USA) as wideband absorbance (absorbance at 420-580 nm). Cells were cultivated in 200 µL volume in a Honeycomb 100-well plate at 30 °C with maximum orbital shaking. Recordings were made every 15 min.

Shake-flask cultivations

Precultures of *Pseudomonas putida* KT2440 or engineered derivatives thereof were prepared as described for microtiter plate cultivations. Cells were inoculated into M9 minimal medium in triplicate supplemented with the specified carbon source(s) at an OD_{600} of 0.1 in 125 mL baffled Erlenmeyer flasks with metal caps. Cultivations were performed at 30°C and 225 rpm in a benchtop incubator (0.75" orbital). Optical density at 600 nm (OD_{600}) was recorded to measure growth at a 1:10 or 1:20 dilution. To sample for metabolite analysis, 1 mL of culture was removed, centrifuged for 2 min at >18,000*g,* and filtered (0.2 µm syringe filter) into amber glass vials. Samples were stored at -20 °C prior to analysis.

Notably, upon addition of dicarboxylic acids with chain lengths above C_{12} to M9 minimal medium, white precipitate formed. The resulting complete media recipe was stirred until no further solubilization was visible (~ 3 h), then 0.2 µm filtered before inoculation and cultivation. Dicarboxylates were quantified at t_0 by sampling the inoculated culture (post-filtration) such that any removed, precipitated dicarboxylates were not accounted for in the analysis.

Characterization of HDPE products by high-resolution UHPLC-ES-MS/MS analysis

The HDPE sample was diluted 10 µL into 990 µL of 50:50 (v/v) water:methanol solution prior to injection. Characterization was performed on a Waters Acquity liquid chromatography system (UPLC H-class, Waters Corp.) using a Phenomenex Kinetex EVO C18 1.7 µm, 2.1 × 100 mm column at a constant flow rate of 0.3 mL/min, an injection volume of 10 µL, and column oven temperature of 30 ℃. The mobile phase solvents, which consisted of eluent (A) water modified with 0.1% formic acid (v/v), and eluent (B) acetonitrile modified with 0.1% formic acid (v/v), were used to form the following gradient for separation: 0-1 min hold at 95% A, and 11 min at 1% A, with a 2 min hold time before equilibrium. Leucine-enkephalin at 100 ng/mL in water/acetonitrile 50/50 (v/v) was infused post-column at 5 µL/min as an external reference for mass calibration.

Compounds were ionized by electrospray ionization post-column in negative-ion mode using a 1.9 kV spray voltage on a Waters Synapt G2-Si mass spectrometer. The desolvation and source temperatures were set to 450℃ and 120℃, respectively. Ions were scanned between a *m/z* range of 50-1200. Nitrogen was used for desolvation gas, sweep gas, and nebulizer gas, set at 800 L/hour, 10 L/hour, and 6.5 L/hour, respectively. Sampling cone, mobility extract, trap direct current (DC) bias, trap collision energy, and helium cell DC were set to 20, 6.9, 45, 4, and 50 V, respectively. The pressure in the helium cell and ion mobility cell were maintained using 180 and 90 mL/min gas flow, respectively. The traveling wave height and velocity were 40 V and 650 m/s, respectively. During LC-tandem mass spectrometry (MS/MS) analysis, ions with intensity over 1000 ion counts were isolated in the quadrupole and mass resolved by a time of flight at 50,000 full width half maximum. Tandem mass spectrometry of the isolated ions was achieved by accelerating the ions in the transfer with activation voltage of 20 V. Argon gas was introduced into the trap at 2 L/min to induce fragmentation. Waters MassLynx v4.1 and ORIGAMI were used for subsequent data analysis (*38*).

Quantitation of dicarboxylic acids from HDPE by UHPLC-ESI-MS/MS operating in multiple reaction monitoring (MRM) mode

Dicarboxylic acids carbon chain length C_3 to C_{22} were quantified by ultra-high performance liquid chromatography- tandem mass spectrometry (UHPLC-MS/MS). The high sensitivity and selectivity of the instrumentation enabled reliable quantitation of analytes in a complex mixture of products from oxidation catalysis.

Standard preparation

Unlabeled dicarboxylic acid standards were acquired commercially from Sigma Aldrich, Toronto Research Company Canada and Synthonix for all compounds (see *Chemicals* list, above) excluding heneicosanedioic acid (C_{21}) which is not commercially available and was quantified using the response from docosanedioic acid (C_{22}). Individual stock standards were prepared in tetrahydrofuran (THF) and then combined to make a working standard solution of 100 µg/mL. Dilutions were prepared from the working standard solution at concentrations ranging 0.5 µg/mL to 100 µg/mL for 8 calibration levels and a calibration verification standard at a concentration of 20 µg/mL. The following deuterated dicarboxylic acids were purchased from CDN Isotopes Inc to enable internal standard quantification: succinic-2,2,3,3-d_4 acid (C_4), pentanedioic-2,2,4,4-d_4 acid (C_5), hexanedioic-2,2,5,5-d_4 acid (C_6), and 1,12-dodecanedioic-2,2,11,11-d_4 acid (C_{12}). A stock solution of all internal standards (IS) was prepared in THF at a concentration of 500 µg/mL and spiked into standards and samples at a final concentration of 5 µg/mL.

Chromatography and mass spectroscopy

Samples and standards were analyzed using an Agilent 1290 series UHPLC system coupled to an Agilent 6470A triple quadrupole mass spectrometer. The mass spectrometer was equipped with dual Agilent jet stream electrospray ionization run in negative ion mode. Optimization of multiple reaction monitoring transitions for all compounds and internal standards was preformed prior to analysis. The quantifying and qualifying transitions and corresponding collision energies and fragmentor voltages are presented in **Table S2** to achieve reproducible and accurate quantitation of products. A volume of 0.5 µL of samples and standards were injected onto a Phenomenex Luna 2.5 µm, 2 × 100 mm C18(2)-HST column held at 40 °C. Separation was carried out utilizing mobile phases consisting of (A) 0.1% formic acid in water and (B) 0.1% formic acid in methanol at a constant flow rate of 0.5 mL/min. The following gradient was used for separation: 0-1.4 min A: 99% and B: 1% and then changed to A: 1% and B: 99% using a linear gradient until 10 min. This was held from 10 - 12 min before returning to the initial conditions at 12.1 min and held for a total run time of 15 min to allow for column equilibration. Parameters for the ESI source were optimized and set as follows; capillary voltage 3 kV, nozzle voltage 0 kV, drying gas temperature 300 °C, drying gas flow 7 L/min, sheath gas temperature 350 °C, sheath gas flow 11 L/min, and the ESI nebulizer gas was set to 35 psi. Analytes were quantified using internal standard curves using the closest carbon chain length IS for each analyte excluding C_{21} which was quantified from the response from C_{22}. Calibration curves had an r^2 coefficient of ≥ 0.995 with a quadradic curve fit. Data analysis was completed using Agilent MassHunter Quantitave Analysis (QQQ) software version B.08.00.

Quantitation of lactone acids by UHPLC-ESI-MS/MS

Lactone acids, specifically (R+S)-5-oxo-2-tetrahydrofurancarboxylic acid (C_5-Lac), 2-(5-oxo-tetrahydrofuran-2-yl)acetic acid (C_6-Lac), and 3-(5-oxo-tetrahydrofuran-2-yl)propionic acid (C_7-Lac) were quantified utilizing the same chromatographic and source parameters described above for quantitation of dicarboxylic acids with the optimized quantitative and qualitative transitions in **Table S4**. Samples and standards were diluted in acetic acid prior to analysis. Eight calibration standards ranging 0.5 µg/mL to 100 µg/mL were used to construct internal calibration curves using 4-hydroxybenzoic-2,3,5,6-d_4 acid as the internal standard. Internal calibration curves had an r^2 coefficient of ≥ 0.995 with a quadradic curve fit.

Quantitation of PS deconstruction products by HPLC-DAD

Quantification of products from PS depolymerization were performed utilizing an Agilent 1100 series high-performance liquid chromatography (HPLC) (Agilent Technologies, Santa Clara, CA) coupled with diode array detection (DAD) and a Phenomenex Luna C18 (2) 5 µm, 4.6 × 150 mm column (Torrance, CA) held at 60 °C. An injection volume of 10 µL was injected into a constant flow rate of 0.80mL/min composed of (A) 20 mM potassium phosphate monobasic buffer and (B) acetonitrile. The following gradient program was used to separate analytes of interest: initial to 2 min: A: 80%, B: 20%; 2-5 min ramp to A: 70%, B: 30%; 5-5.01 changed to A: 40%, B: 60% then isocratic to 11 min; 11-18 min ramp to A: 10%, B: 90%; 18-19 min return to A: 80%, B: 20% for a 25 min total run time. A standard was analyzed every 10-20 samples to verify calibration consistency and detector stability. Analytes monitored for were benzoic acid, benzaldehyde, phenol, benzyl alcohol, acetophenone, methyl benzoate, benzil, propiophenone, 4-propylphenol, 1,2-diphenylethanol, benzyl phenyl ketone, ethylbenzene, propyl benzene, and bibenzyl on DAD wavelength 210 nm with a linear quantitation range of 1 µg/mL to 100 µg/mL and an r^2 coefficient of ≥ 0.995.

Quantitation of terephthalic acid from PET depolymerization by UHPLC-DAD

Terephthalic acid was quantified as previously reported (*25*). Briefly, quantitation was achieved using UHPLC-DAD and chromatography was carried out using a gradient of 20 mM phosphoric acid and methanol on a C18 column.

Quantitation of β-ketoadipic acid, glucose, and acetic by HPLC

β-ketoadipic acid was analyzed as levulinic acid after hydrolysis was performed on the samples as previously described (*30*). Briefly, samples were analyzed post hydrolysis for levulinic acid by HPLC coupled with a refractive index detector (RID). Separation was carried out on a BioRad Aminex HPX-87H 9 μm, 7.8 × 300 mm column (BioRad) held at 55 °C run isostatically at 0.6 mL/min utilizing a mobile phase of 0.01 N sulfuric acid for a total run time of 27 min. Glucose and acetic acid were quantified using identical chromatographic conditions described previously (*30*) utilizing HPLC- RID.

To calculate molar β-ketoadipate yields in biological cultivations, the concentration of levulinic acid was first converted to millimolar using the molecular weight of levulinic acid. This was used as the millimolar concentration of β-ketoadipate (1:1 ratio). The millimolar concentration of β-ketoadipate was divided by the sum of the aromatic substrates; calculations were also performed to include aliphatic substrates for growth (see **Table S13**). To estimate total yields of β-ketoadipate from polymer feedstocks assuming no losses in the solubilization/filtration steps (see *Preparation of depolymerized plastics for bioconversion*), the mol% yield of aromatic constituents (benzoic acid and/or terephthalic acid) from deconstruction was multiplied by the molar β-ketoadipate yield from biological cultivations (**Table S14**).

Quantitation of polyhydroxyalkanoates by GC-MS

Medium chain length polyhydroxyalkanoates were analyzed as described previously (*36*). Briefly, lyophilized cell biomass was derivatized using BF_3/MeOH, subsequently washed with a series of dichloromethane and water washes and then dried and neutralized over Na_2SO_4 and Na_2CO_3. The resulting solutions containing hydroxyacid methyl esters (HAMEs) were filtered and quantified by GC-MS utilizing an Agilent DB-Wax column.

NMR analysis of lactone acids and 4-hydrox-dicarboxylic acid (ROLAs)

^{1}H Nuclear magnetic resonance (NMR) spectra of lactone acid standards and post-oxidation products were collected using a Bruker Ascend 300 MHz spectrometer. For this analysis, samples were prepared by dissolving ~20 mg of dried standard or oxidation products in 500 μL deuterium oxide. Chemical shifts for ^{1}H NMR spectra are reported in parts per million (ppm) using D_2O as a reference at 4.79 ppm (16 scans).

NMR spectra of metabolic ROLA and glucose experiments were collected on a Bruker Neo Avance 400 MHz equipped with a nitrogen-cooled Prodigy cryoprobe. Analysis of metabolite consumption was carried out using a "watergate" water suppression pulse sequence (*39*). For these samples, 100 μL of aqueous sample was added to a known mass (~500 μL) of deuterium oxide with 3 wt. % 3-(trimethylsilyl)pripionic-*2,2,3,3-d$_4$* acid, sodium salt for referencing. Pulse calibrations were performed on each sample prior to acquisition (16 scans) for water suppression optimization. All NMR analysis was carried out using Bruker TopSpin.

Metals quantitation

Metallic catalyst composition of the filter cake (see *Preparation of crude substrate for bioconversion*) was measured via ICP-OES (Agilent 5110 inductively coupled plasma-optical emission spectrometer). Initially, approximately 25 mg of each powder was weighed out and dissolved in 10 mL of concentrated HNO_3. This mixture was heated in a Teflon vessel at 200 °C

for 30 min in a microwave digestion system (CEM MARS5) operating at 1600 W. The digestate was filtered and diluted to 50 mL with DI water. A 5 mL aliquot of this solution was then combined with an additional 10 mL of concentrated HNO_3 and diluted again to 50 mL with DI water to produce a sample solution with appropriate concentrations for ICP-OES analysis. Calibration standards of the relevant elements (Co and Mn) were made at 1, 5, 10, 20, and 40 ppm in the same dilute HNO_3 matrix. Elemental concentrations were quantified after ICP-OES analysis using the following characteristic emission peaks: 238.892 nm (Co) and 294.921 nm (Mn).

ICP-MS analysis

An Agilent 7700x was used for ICP-MS analysis; both standard and collision gas cell modes were used and the operating mode with the lowest detection limit used for final analysis. Operating conditions were optimized to produce maximum elemental intensity by modifying the sample introduction rate and He flow in collision cell mode. Integration dwell times were 0.3 ms per reading with 3 replicates per sample. Intensity data were recorded and processed using Agilent MassHunter software. Instrument calibration was achieved by analysis of a blank and five calibration standards ranging from 0 – 100 ng/mL; calibration standard was a multicomponent standard purchased from High Purity Standards and used as received.

Gel permeation chromatography (GPC) analysis

Molecular weight analysis of PS and analysis of PS deconstruction products was performed using gel permeation chromatography (GPC) coupled with multi-angle light scattering (MALS) using an Infinity II 1260 HPLC system from Agilent. The HPLC stack was equipped with a degasser, vial sampler, and heated column compartment with one guard column and 3 PL gel mixed-B columns (purchased from Agilent) heated to 40 °C. The mobile phase used was HPLC-grade unstabilized THF purchased from Fisher running at a flow rate of 1 mL/min. The detectors used for GPC were a Wyatt Technology TrEX differential refractometer (RI), a Wyatt Technology Viscometer, and a Wyatt Technology miniDAWN Treos light scattering detector (MALS). A narrow molecular weight distribution polystyrene standard was used to normalize and align the detectors. A *dn/dc* value of 0.185 was used for all analyses. Effective separation of the polymer by size exclusion was evaluated during method development by a comparison of polymer molecular weight vs. retention time, which validates the presentation of GPC chromatograms using retention volume. All samples were prepared by taking post-reaction solutions directly from Parr reactors, followed by rotary evaporation to remove the acetic acid solvent, and drying in a vacuum oven for 12 h at 40 °C. The solids were then dissolved in THF at room temperature at concentrations between 3-4 mg/mL and filtered through a 0.2 μm syringe filter. All data were processed using Astra 8.2.

High-Temperature Gel permeation chromatography (HT-GPC) analysis

HT-GPC of HDPE and mixed HDPE + PS systems was performed using a Tosoh EcoSec HLC-8321 High Temperature GPC System with autosampler and a differential refractive index (DRI) detector. Temperature settings were as follows, solvent stocker at 40 °C, pump oven at 50 °C, column oven at 160 °C, RI detector at 160 °C, injector valve at 160 °C, and autosampler at 160 °C. The mobile phase used was 1,2,4-trichlorobenzene (TCB) (Fischer Scientific-HPLC Grade). The TCB solvent was used as received and no inhibitor was added. Sample columns were set to an operating flow rate of 1.0 mL/min and the reference column was set to an operating flow rate of 0.5 mL/min. A 300 μL sample loop was used for sample injection. Polymer separation was performed using four Tosoh TSKgel columns attached in the following order, 1 x TSKgel guard column HHR (30) HT2 7.5 mm I.D. x 7.5 cm. (PN 22891), 2 x TSKgel G2000 HHR (20) HT2 7.8

mm I.D. x 30 cm columns (PN 22890), and 1 x TSKgel GMH HR-H (S) HT2 7.8 mm I.D. x 30cm column (PN 22889). A 180-minute warm-up of the instrument at 10% flow rate was performed before analysis. Tosoh 10 mL high temperature sample vials with PTFE cap were used for sample preparation. 6-20 mg of sample were placed on a Tosoh high temperature 26 µm stainless steel mesh and the mesh was then folded around the sample. TCB solvent was then added to the vial to reach an end concentration of approximately 2 mg/mL. A 10.0 mm x 3.0 mm PTFE stir bar was placed in the vial and a Tosoh high temperature 30 mm square aluminum sheet was placed on the mouth of the vial, then covered by the PTFE lid. A Thermo Fischer Scientific Single-Block Reacti-Therm Module with heating and stirring was used to prep polymer samples. An 8-hole - (21 mm diameter x 45 mm deep) ThermoFischer heating block with custom machined fittings for the 10 mL vials was used with the Reacti-Therm module. The stirring level on the Reacti-Therm module was set to 3 and the temperature was set to 160 °C. The true temperature was tracked using a Traceable Platinum High-Accuracy Thermometer with Stainless-Steel Probe. The samples were then heated and stirred for 2 hours. Tosoh's Polystyrene-Quick Kit-M (PN 21916) was used to create the calibration curve. The calibration curve was verified using Tosoh polystyrene F-10 (106 kDa – PN 05210)) and F-20 (190 kDa – PN 05211) standards. All polystyrene standards were prepared without mesh at 1 mg/mL with no pre-heating or stirring. Run times for all standards and samples were 80 minutes. Eco-Sec 8321 software (Tosoh) was used to evaluate calibration curves and determine molecular weight and dispersity values. All polymer RI peaks were integrated in the range of when they first deviated from baseline to where the RI signal reached baseline signal again. Mark Houwink correction values were used to determine polyethylene molecular weight values (*40*). Mark Houwink values used for polystyrene were $K = 12.1 \times 10^{-5}$ dL/g and Alpha = 0.707. Mark Houwink values used for polyethylene were $K = 40.6 \times 10^{-5}$ dL/g and Alpha = 0.725.

Supplementary Text

PS and HDPE depolymerization by catalytic aerobic oxidation

Effect of reaction parameters on PS deconstruction

We explored temperature, reaction time, catalyst and initiator loading, O_2 pressure, and molecular weight (MW) as parameters that could influence radical oxidation reactions. While bromide-initiated reactions were primarily explored at 180 °C in previous work, we aimed to evaluate the effect of temperature when using NHPI as the initiator. We evaluated benzoic acid and benzaldehyde yields at 140-190 °C. A clear trend is observed, with an optimal temperature also determined to be 180 °C (**Figure S1a**). To gain an understanding of the depolymerization rate at 180 °C, a time course study (0.5-5.5 h) was performed to optimize the reaction duration (the reaction times indicated include the 30 minutes required for the reaction to reach the desired temperature) (**Figure S1b**). benzoic acid yields continued to slowly increase up to ~5.5 hours, so 5.5 hours was used as the reaction time for subsequent experiments.

A study of the effect of the concentration of NHPI (0-121 mM) on the oxidation of PS beads reveals a relatively minor effect on the product yields (**Figure S2a**). It is known that transition metal salts are capable of acting as initiators in aerobic oxidation reactions (*41*), though often high catalyst loadings are required (*13*). These results suggest that the metal salts may be responsible for generating initial radical species. Accordingly, varying the concentration of Co and Mn (0-19.2 mM) results in a much more pronounced effect on product yields (**Figure S2b-d**). At very high concentrations of Mn or Mn + Co, lower product yields are observed. This inhibition of autoxidation by transition metals at high concentrations has been examined previously and is

thought to result from decomposition of hydroperoxyl radical species, resulting in chain termination and inhibition (*42*).

Reactions were performed to determine the effect of the polymer molecular weight. Reactions using 35, 185, and 280 kDa standards revealed only slight differences in product yields (**Figure S3a**). This result suggests that the rapid depolymerization of the polymer under these conditions, as shown in **Figure S1b,** likely makes any effect of molecular weight insignificant under these conditions. Additionally, the effect of O_2 was probed, revealing a decrease in product yields as O_2 is reduced from 8 to 0 bar (**Figure S3b**), as would be expected under these conditions. This result confirms that care must be taken to avoid oxygen limitation and depletion of O_2 in solution. To further investigate mass transfer effects, PS beads were cryomilled to obtain a powder before use (**Figure S4**). These experiments showed increased product yields for the powder substrates, suggesting it is beneficial to increase the surface area of the material.

GPC traces taken over the duration of the reaction reveal a decrease in the polymer molecular weight starting at 1 hour and demonstrate that no polymer remains after the reaction is complete (**Figure S11**). These results also show an initial increase in polymer molecular weight before the depolymerization occurs, which may be due to initial cross-linking, or reactions at the polymer backbone resulting in the formation of oxygenated groups such as hydroperoxides, which facilitate the subsequent depolymerization. However, additional work will be required to confirm the nature of this initial MW increase, which is outside the scope of the current work and will be pursued in future efforts.

In addition to using extruded beads as our substrate, we also used a commercial PS substrate in the form of EPS cups. An initial temperature and time screen using a post-consumer EPS cup reveals similar trends compared to the PS beads (**Figure S5**), even in the presence of additives present in the commercial samples. The identity, composition, and effect of these additives on depolymerization of post-consumer substrates will be explored further in future work.

Effect of reaction parameters on HDPE deconstruction

After initial investigation of the reaction conditions for PS, we sought to explore the depolymerization of HDPE into dicarboxylic acids. There is a clear temperature dependence on these results, with a maximum at 150 °C, as shown in **Figure S6a**. Time course experiments reveal that HDPE depolymerization takes place much more rapidly than PS, achieving maximum achievable yields at around 1-1.5 hours (**Figure S6b**). There are several potential reasons that may contribute to faster depolymerization in HDPE relative to PS: firstly, defect sites in PE result in tertiary C-H bonds being present in the polymer, which may have a lower BDE and may serve as the initiation sites for radical species. Secondly, in HDPE autoxidation, it is known that intramolecular C-H abstraction can occur (*19*), increasing the reaction rate relative to PS, as intramolecular reactions are disfavored due to depolymerization due to steric hindrance. The exact nature of this difference will be explored in future work.

Varying the metal concentrations as shown in **Figure S7a-b** indicates a relatively minor role of the individual Co and Mn species on the product yields. The total metal concentration seemed to be more important, as shown in **Figure S7c**. For NHPI, however, a clear dependence is shown, where increasing NHPI concentrations result in both increased product yields and a selectivity for shorter-chain dicarboxylic acid products (**Figure S7d**).

The influence of the polymer molecular weight was examined, revealing little difference between a 125 kDa and 55 kDa plastic, both for conversion and selectivity (**Figure S8a**), suggesting that,

like in PS depolymerization, random chain scission is occurring. The O_2 dependence was evaluated (**Figure S8b**), again demonstrating impacts on both conversion and selectivity. As might be expected, increased oxygen levels resulted in a selectivity towards smaller-chain dicarboxylic acids, with no conversion occurring in the absence of O_2.

GPC analysis of the reaction mixture at different time points demonstrated a rapid depolymerization of HDPE (**Figure S12**) within the first 0.5 hours of the reaction and reveals that few, if any, oligomers are present in the oxidation mixture, even early in the reaction.

Under these conditions, overoxidation of the dicarboxylic acids into CO and CO_2 has been previously reported (*19*). For example, oxalic acid is known to readily degrade under these conditions and is not observed in any of our analyses. However, quantification of the CO and CO_2 generated from overoxidation of the polymer is challenging due to competing oxidation of the acetic acid solvent. A more thorough study of the relative oxidation of the polymer substrate relative to the acetic acid solvent will be explored in future work.

Of note is a second product series that was discovered using LC-MS, which were identified as lactone species (*vide infra*). Such species have been previously reported in the depolymerization of HDPE, though often as only minor products, and form via intramolecular reactions that occur during the depolymerization of the linear alkane chains (*43*). In our experiments, lactone acids accounts for a relatively small amount of products (**Figure S16**), but are notably the second most prevalent product series.

Effect of reaction parameters on PET deconstruction

We began by employing similar conditions that were favorable for PS oxidation and found that relatively low yields of terephthalic acid were produced. However, upon increasing the temperature to 210 °C, we obtained high product yields. The use of $Zr(acac)_4$ and small amounts of H_2O (1% v/v) to the reaction also resulted in slightly increased terephthalic acid yields. During these reactions, the terephthalic acid product precipitated out of solution due to its low solubility in acetic acid. These solids were recovered by filtration and were subsequently isolated and quantified. However, small amounts (<3%) of terephthalic acid remained in solution, which was quantified by HPLC. As was observed for PS and HDPE, minimal differences in product yields were found between depolymerization of the commercial resin and the post-consumer plastic bottle.

Effect of reaction parameters on mixed PS + HDPE and PS + HDPE + PET deconstruction

Once conditions favorable for the depolymerization of both PS and HDPE were identified, we sought to run oxidation reactions on mixed PS and HDPE substrates. As seen in the oxidation of each substrate in isolation, a clear temperature dependence is observed. PS depolymerization is favored at higher temperatures, whereas the HDPE product yields decreased as the temperature was increased from 160 °C to 185 °C (**Figure S18a-b**). Due to the increased yield of benzoic acid at 180 °C relative to 160 °C, and the relatively minor change in dicarboxylic acid yields from HDPE at 180 °C relative to 160 °C, 180 °C was selected as the temperature to perform oxidation reactions in this mixed system to maximize overall product yields. A time course study demonstrated that in the PS + HDPE system, PS depolymerization behaves much as it does in isolation, with increased times resulting in increased product yields. However, the situation is more complex for HDPE depolymerization, as a time course study at 170 °C revealed increased product yields over time, whereas the reaction at 180 °C resulted in decreasing product yields over the same timescale (**Figure S19a-b**). The best overall yields for PS depolymerization and HDPE

depolymerization products was at 5.5 hours, which was then used for subsequent experiments. These results suggest that there is still significant optimization needed in these mixed systems to obtain the correct conditions that maximize yields for both PS and HDPE depolymerization products, which could be further optimized by reactor engineering, and will be explored in subsequent studies.

When varying the metal concentrations for the PS + HDPE system, there appear to be inverse relationships between the metal concentrations and the PS and HDPE depolymerization yields, where higher metal concentrations result in higher PS depolymerization products and lower the dicarboxylic acid yields from HDPE depolymerization (**Figure S20a-d, Figure S21a-b**). However, as observed in the depolymerization of each substrate alone, increasing NHPI concentrations did not substantially impact the PS depolymerization, but affected HDPE product yields and selectivity towards smaller DCAs (**Figure S21c-d**). GPC analysis of the mixed PS plus HDPE case revealed that the MW increase observed for monolithic PS deconstruction was not observed in the mixed case, while HDPE was still rapidly deconstructed **(Figure S22**).

For the depolymerization of PS + HDPE + PET mixtures, the conditions were again dictated by the highest temperature required by one of the individual components, in this case PET. Reactions at 160 and 180 °C resulted in lower terephthalic acid yields from PET, similar benzoic acid yields from PS, and only moderately increased dicarboxylic acid yields from HDPE. However, increasing the temperature of the reaction to 210 °C resulted in increased terephthalic acid yields and similar yields of the products from the other plastics, resulting in an overall increase in total carbon yield. For that reason, 210 °C was selected as the optimal temperature for performing these reactions, though significant opportunities exist for further optimization of this system.

Identification of dicarboxylic and lactone acids series in HDPE reactions

The use of reverse phase chromatography with a linear mobile phase gradient led to a predictable elution pattern of compounds indicative of two main product series (**Figure S13a**). Additionally, the accurate high-resolution measured mass equated to the difference of $-CH_2$ between eluting peaks within each series (**Table S3**), suggesting there were two main homologous product series with extending chain length. Furthermore, tandem mass (MS/MS) data for each compound peak of a particular series presented similar fragmentation patterns indicating that each compound contained consistent functional groups. Ion mobility (IM) was also performed to obtain the drift time (DT) of the ionized compounds to confirm structural series from LC-MS/MS studies. In the plot of DT and *m/z* values, compounds with similar functional groups but varying chain lengths were observed within each series (*44*). Such trends were observed in the IM-MS spectrum (**Figure S13b**), which confirmed structural similarities of compounds within each main homologous series. From accurate MS data and further MS/MS analysis with validation from authentic standards, series 1 was identified as dicarboxylic acids and series 2 were identified as lactone acids.

The lactone acid series was initially identified by GC/MS fragmentation patterns and masses observed from high resolution LC-MS. Authentic standards for (R) and (S) stereoisomers of 5-oxo-2-tetrahydrofurancarboxylic acid (C_5-Lac) were purchased from Sigma and C_6-Lac and C_7-Lac were synthesized for verification of the series by both GC-MS and LC-MS/MS spectra and retention time (**Figure S14**). The lactone acid standards and HDPE samples were derivatized and run. **Figure S15b-c** illustrated the retention time match of the model compound standards with compounds in HDPE samples and identities were then verified by comparing fragmentation spectra. Further confirmation of the series as lactone acids was achieved with the C_7-Lac spectra in the sample and matched to the NIST library with quality match of 91. Standards and samples

were also analyzed by LC-MS/MS to verify compound species on a second analytical technique where matching retention time and MS/MS fragmentation was observed.

The *P. putida* base-strain RC026 catabolizes model compounds from PET and PS deconstruction

We sought to engineer a microbial strain capable of biologically funneling the intermediates derived from oxidative depolymerization of PS, HDPE, and PET. Based on preliminary data of the products released by oxidative depolymerization of these polymers, we initially targeted the following small molecules as model substrates for metabolic engineering efforts: for PS, benzoate; for HDPE, the 4-carbon dicarboxylate succinate (C_4), the 5-carbon dicarboxylate glutarate (C_5), and the 6-carbon dicarboxylate adipate (C_6); and for PET, terephthalate. Acetate was also included as a potential catabolite, as it would be present after pH neutralization of residual acetic acid solvent.

Recently, we engineered *Pseudomonas putida* KT2440 (hereafter *P. putida*) to utilize terephthalate as the sole carbon and energy source by heterologous expression of *tpaK,* encoding a terephthalate transporter from *Rhodococcus jostii* RHA1, and the terephthalate catabolic genes $tphA2_{II}A3_{II}B_{II}A1_{II,}$ encoding a terephthalate 1,2-dioxygenase and 1,2-dihydroxy-3,5-cyclohexadiene-1,4-dicarboxylate dehydrogenase from *Comamonas* sp. E6 (*25*). We additionally improved utilization of ethylene glycol by deleting *gclR,* encoding a transcriptional regulator, and overexpressing *glcDEFG,* encoding a glycolate oxidase (*25*). The strain harboring all of these modifications, RC026 (*P. putida* Δ*hsdMR*::P_{tac}:$tphA2_{II}A3_{II}B_{II}A1_{II\text{-}E6}$ *fpvA*:P_{tac}:$tpaK_{RHA1}$ P_{tac}:*glcDEFG:PP_3749* Δ*gclR*) utilized terephthalate and ethylene glycol as sole carbon and energy sources (*25*). Thus, we used RC026 as the base strain for further engineering.

To assess which compounds in our model mixed stream are catabolized by the base strain, we evaluated growth of RC026 on terephthalate, benzoate, and C_4, C_5, and C_6 dicarboxylates. Each compound was provided as the sole carbon and energy sources in M9 minimal medium at 5 mM concentration and growth was measured over time in a microtiter plate (**Figure S23a**). As expected, terephthalate, benzoate, and C_4 and C_5 dicarboxylates served as a sole carbon and energy source. However, no growth was observed on C_6 dicarboxylate as a sole carbon and energy source, and no additional growth was observed when supplemental acetate was provided (**Figure S23b**).

Expression of *dcaAKIJP* from *A. baylyi* enables growth on C_6, C_9, and C_{10} dicarboxylates as sole carbon and energy sources

To our knowledge, a catabolic pathway for each of the higher order ($\geq C_6$) dicarboxylates is not reported in *P. putida*. It is reported however, that utilization of C_6-C_{10} dicarboxylates is a unit characteristic, with organisms either able to utilize all acids in this carbon range or none (*45*). *P. putida* did not display growth on adipate (C_6), pimelate (C_7), suberate (C_8), azelate (C_9), or sebacate (C_{10}) dicarboxylates as sole carbon and energy sources (**Figure S24b**).

An extensive 1966 taxonomic characterization of pseudomonads found that none of the 41 *P. putida* strains screened could grow on dicarboxylic acids as the sole carbon and energy sources (*46*). Spontaneous mutants of *P. putida* have been reported to grow on C_6 dicarboxylate, but the nature of the mutations was never characterized (*47*). Dissimilation of the C_6 to C_{10} dicarboxylates series by β-oxidation was reported in a *Pseudomonas fluorescens* species in 1970 (*45*). Despite studying another species, and without high fidelity genetic tools to enable gene identification, Hoet and Stanier's seminal work (*45*) provides several key insights into the four key enzymatic steps involved in β-oxidation of higher order straight-chain dicarboxylates in a pseudomonad:

1) C_5 dicarboxylate metabolism proceeds through a separate biochemical pathway than C_6-C_{10} dicarboxylates,
2) two mechanisms for C_6 dicarboxylate activation to the CoA-ester (adipyl-CoA) are present (further examined in a companion paper, (*48*)),
3) at least one of the acyl-CoA transferases active on C_6 dicarboxylate can also recognize β-ketoadipate,
4) the same set of enzymes is active on the C_6-C_{10} dicarboxylates series, and
5) expression of the enzyme set is tightly regulated.

Still, it is unclear if odd-chain dicarboxylates (C_7, C_9, etc.) are shortened by one carbon unit to converge on a shared intermediate (e.g., β-ketoadipyl-CoA), or would yield glutarate or malonate before entering the corresponding catabolic pathways. Natively, succinate enters the TCA cycle directly, whereas glutarate conversion can occur via hydroxylation or glutaryl-CoA dehydrogenation (*49*).

Acinetobacter baylyi ADP1 (hereafter *A. baylyi*) has been reported to grow on C_6 dicarboxylate as the sole carbon and energy sources through a β-oxidation pathway (*27*). Indeed, in our experiments, *A. baylyi* grew on 15 mM C_4, C_6, C_7, C_8, C_9, and C_{10} but not C_5 dicarboxylates as sole carbon and energy sources (**Figure S24a**). The DcaP outer membrane porin and DcaK inner membrane MFS transporter import C_6 dicarboxylate from the extracellular milieu to the cytoplasm. Then, the acyl-CoA transferase DcaIJ converts C_6 to adipyl-CoA. Adipyl-CoA is converted to *trans*-2,3-dehydroadipyl-CoA by the acyl-CoA dehydrogenase, DcaA, and then to 3-hydroxyadipyl-CoA by the enoyl-CoA hydratase, DcaE. β-ketoadipyl-CoA is then formed by DcaH, the 3-hydroxyacyl-CoA dehydrogenase. Finally, the β-ketoadipyl-CoA thiolase, DcaF, converts β-ketoadipyl-CoA to acetyl-CoA and succinyl-CoA, which are further catabolized via the TCA cycle (**Figure S25**).

The phenylacetate (*paa*) pathway in *P. putida* has potential functional similarity to the *A. baylyi* pathway for β-oxidation of straight chain dicarboxylates, and we thus considered whether enzymes involved in fatty acid oxidation may recognize dicarboxylic, in addition to monocarboxylic, substrates. Specifically, we considered whether the following redundancies might exist:

1) PaaF, an enoyl-CoA hydratase/isomerase, or FadB, a fatty acid oxidation complex active towards crotonyl-CoA (a product in the glutaryl-CoA dehydrogenation pathway) could functionally replace DcaE,
2) PaaH, the 3-hydroxyacyl-CoA dehydrogenase, could functionally replace DcaH,
3) PaaJ, a 3-oxoadipyl-CoA/3-oxo-5,6-dehydrosuberyl-CoA thiolase (formerly referred to as PcaF), or PcaF-I, a β-ketoadipyl-CoA thiolase, could functionally replace PaaJ, and
4) PaaX, a DNA-binding transcriptional repressor, may act similarly to the homolog in *E. coli (29, 50)* by repressing expression of *paaF, paaH,* and *paaJ*.

Indeed, while this study was ongoing, Ackermann *et al.* reported these apparent redundancies listed as items (1), (2), and (3) in the list above and found they exist for the utilization of C_6 (*26*).

Considering these reports, we deleted *paaX* and heterologously expressed $dcaP_{ADP1}$, $dcaK_{ADP1}$, $dcaIJ_{ADP1}$, and $dcaA_{ADP1}$ to enable growth on higher order dicarboxylates as sole carbon and energy sources. High expression levels of transmembrane proteins can be detrimental to cell viability, so we designed and constructed two strains with two levels of transcriptional expression by utilizing two promoter strengths – high (P_{tac}) and low (P_{549}) – to drive *dcaKP* expression. First, we cloned

the entire *dcaAKIJP*$_{ADP1}$ operon from *A. baylyi* (*i.e.*, no codon optimization) and expressed with the strong and constitutive P_{tac} promoter from the Δ*paaX* chromosomal locus, generating strain AW061 (*P. putida* Δ*hsdMR*::P_{tac}:*tphA2*$_{II}$*A3*$_{II}$*B*$_{II}$*A1*$_{II}$ *fpvA*:P_{tac}:*tpaK* Δ*glcR* P_{tac}:*glcDEFG:PP_3749* Δ*paaX*::P_{tac}:*dcaAKIJP*). Second, we codon optimized each gene for expression in *P. putida*, designed synthetic RBSs for each gene, expressed *dcaAIJ* with P_{tac} from Δ*paaX*, and used the weaker P_{549} to express *dcaKP* from the *fpvA* locus, generating strain AW074 (*P. putida* Δ*hsdMR*::P_{tac}:*tphA2*$_{II}$*A3*$_{II}$*B*$_{II}$*A1*$_{II}$ *fpvA*:P_{tac}:*tpaK*:P_{549}:*dcaKP*^{CO} Δ*glcR* P_{tac}:*glcDEFG:PP_3749* Δ*paaX*::P_{tac}:*dcaAIJ*^{CO}).

AW061 displayed poor but increased growth on C_{10} and, to a lesser extent, C_6 and C_9 dicarboxylates (**Figure S24c**). AW074 displayed modest growth on C_6, C_9, and C_{10} dicarboxylates (**Figure S24d**). Interestingly, when 15 mM acetate was provided in addition to 15 mM C_6 dicarboxylate, growth of both AW061 and AW074 were improved beyond that observed for 15 mM acetate alone (**Figure S26**). Together, these results demonstrate that heterologous expression of the *dcaAKIJP*$_{ADP1}$ genes is sufficient to enable growth on C_6, C_9, and C_{10} dicarboxylates by *P. putida*, and further suggests that tuning expression levels is critical for efficient growth on C_6 dicarboxylate as the sole carbon and energy source.

Deletion of *psrA* improves utilization of mixed dicarboxylates

We next evaluated utilization of C_4 through C_{14} dicarboxylates in a mixture more representative of a depolymerized HDPE stream which contains primarily C_4-C_6 but quantified up to C_{22} dicarboxylates**.** Evaluations were performed in baffled shake flasks with M9 minimal medium supplemented with ~1 mM of C_4 through C_{14} dicarboxylates along with 8 mM acetate to represent residual acetic acid solvent, and samples were taken over time to measure growth and substrate utilization.

Dicarboxylate concentrations were stable over time in non-inoculated controls (**Figure S27a**). In AW074 cultivations, utilization of C_4, C_5, C_8, C_9, and C_{10} dicarboxylates began first, followed by C_6, C_7, C_{11}, C_{12}, and C_{13} dicarboxylates (**Figure S27b**). At 48 h of cultivation, at which point all dicarboxylates except C_6, C_{12}, C_{13}, and C_{14} were depleted, no further utilization occurred. Interestingly, C_7 and C_8 dicarboxylates did not support AW074 growth as sole carbon and energy sources, yet were utilized efficiently in a C_4-C_{14} mixture, suggesting select dicarboxylates may activate the catabolic pathways required for utilization of a broader range.

In comparing AW061 to AW074, it was unclear whether the improved C_6 utilization was due to (a) expression of codon optimized genes with synthetic ribosome binding sites, or (b) lower expression of *dcaKP*. We considered whether a strain with optimized expression (codon optimized genes with synthetic ribosome binding sites) driven by P_{tac} would outperform AW074. To evaluate this, we constructed AW128 (*P. putida* Δ*hsdMR*::P_{tac}:*tphA2*$_{II}$*A3*$_{II}$*B*$_{II}$*A1*$_{II}$ *fpvA*:P_{tac}:*tpaK* Δ*glcR* P_{tac}:*glcDEFG:PP_3749* Δ*paaX*::P_{tac}:*dcaAKIJP*^{CO}) and evaluated utilization of mixed dicarboxylates. Utilization of mixed dicarboxylates by AW128 was similar to AW074; however, more C_6, C_{12}, C_{13}, and C_{14} were utilized, albeit incompletely (**Figure S28c**). These data suggest that high expression of an optimized cassette resulted in slightly improved dicarboxylate utilization compared to non-optimized and low transmembrane expression, but did not resolve the suspected repression.

To identify additional genetic targets to improve dicarboxylate utilization, we considered whether learnings from fatty acid catabolism could be applied towards dicarboxylate catabolism as dicarboxylate acids differ from unsaturated fatty acids only in the terminal carboxylic acid group

that could be considered an "R" group (**Figure S25**). Thompson *et al*. utilized random barcode transposon sequencing to identify critical genes in the catabolism of fatty acids and fatty alcohols by *P. putida* (*28*). By analyzing the Thompson *et al.* dataset, we saw that PP_2173 – a FadB homolog – was critical for utilization of fatty acids of several chain lengths. PsrA has been reported to be a repressor of β-oxidation pathways in *P. putida* (*51*), including PP_2173 and potentially others. Therefore, we hypothesized that deletion of *psrA* would improve utilization of mixed dicarboxylates.

To test this hypothesis, we deleted *psrA* in AW074, generating strain AW160 (*P. putida* Δ*hsdMR*::P_{tac}:*tphA2*$_{II}$*A3*$_{II}$*B*$_{II}$*A1*$_{II}$ *fpvA*:P_{tac}:*tpaK*:P_{549}:*dcaKP*^{CO} Δ*glcR* P_{tac}:*glcDEFG:PP_3749* Δ*paaX*::P_{tac}:*dcaAIJ*^{CO} Δ*psrA*) and AW128, generating strain AW162 (*P. putida* Δ*hsdMR*::P_{tac}:*tphA2*$_{II}$*A3*$_{II}$*B*$_{II}$*A1*$_{II}$ *fpvA*:P_{tac}:*tpaK* Δ*glcR* P_{tac}:*glcDEFG:PP_3749* Δ*paaX*::P_{tac}:*dcaAKIJP*^{CO} Δ*psrA*). We evaluated utilization of mixed dicarboxylates as before. Both AW160 and AW162 displayed a striking increase in dicarboxylate utilization, with each dicarboxylate above C_5 being utilized more rapidly (**Figure S28d-e**), and with AW162 utilizing all the provided dicarboxylates completely and within 29 h. This demonstrates that deletion of *psrA* improves catabolism of mixed C_4-C_{14} dicarboxylates, suggesting that PsrA is a negative regulator of genes involved in dicarboxylate utilization, including at a minimum FadB activity on dehydro-CoA-esters. Given that the initiation and termination of dicarboxylates differs across chain lengths, the possibilities exist that either a presently undiscovered regulator controls the timing of dicarboxylate utilization in *P. putida* or the *A. baylyi* DcaK and DcaP transport system or DcaA and DcaIJ enzymes exhibit substrate preferences that underly the phenomenon.

Evaluation of two additional dicarboxylate engineering targets

Two additional genetic targets were pursued after analyzing the RB-TnSeq data from Thompson *et al*. (*28*). First, the methylcitrate cycle (MCC) was shown to be critical for growth on odd-chain fatty acids. Two of the MCC enzymes, MmgF and PrpC, are expressed in a single operon. The GnuR repressor (PP_3415) is predicted to repress expression of the *mmgF* and *prpC* containing operon. We thus hypothesized that deletion of *gnuR* would improve utilization of odd-chain dicarboxylates. Second, PP_0370 – a FadE homolog – was shown to be preferred for acyl-CoA dehydrogenation of C_6-C_8 fatty acids, but the regulation of *PP_0370* expression is not reported to our knowledge. So, we hypothesized that constitutive overexpression of *PP_0370* would improve utilization of C_6-C_8 dicarboxylates. To evaluate these hypotheses, we deleted *gnuR* and overexpressed *PP_0370* using the P_{14d} promoter (*52*) in strain AW162, individually and in combination, resulting in the following strains:

- AW170 (*P. putida* Δ*hsdMR*::P_{tac}:*tphA2*$_{II}$*A3*$_{II}$*B*$_{II}$*A1*$_{II}$ *fpvA*:P_{tac}:*tpaK* Δ*glcR* P_{tac}:*glcDEFG:PP_3749* Δ*paaX*::P_{tac}:*dcaAKIJP*^{CO} Δ*psrA* Δ*gnuR*),
- AW177 (*P. putida* Δ*hsdMR*::P_{tac}:*tphA2*$_{II}$*A3*$_{II}$*B*$_{II}$*A1*$_{II}$ *fpvA*:P_{tac}:*tpaK* Δ*glcR* P_{tac}:*glcDEFG:PP_3749* Δ*paaX*::P_{tac}:*dcaAKIJP*^{CO} Δ*psrA* P_{14d}:*PP_0370*), and
- AW179 (*P. putida* Δ*hsdMR*::P_{tac}:*tphA2*$_{II}$*A3*$_{II}$*B*$_{II}$*A1*$_{II}$ *fpvA*:P_{tac}:*tpaK* Δ*glcR* P_{tac}:*glcDEFG:PP_3749* Δ*paaX*::P_{tac}:*dcaAKIJP*^{CO} Δ*psrA* Δ*gnuR* P_{14d}:*PP_0370*).

We again evaluated growth of each strain in M9 minimal medium supplemented with C_4 through C_{10} dicarboxylates individually in microtiter plates. Growth rates on C_4 and C_5 were similar for all tested strais; however, AW170, AW177, and AW179 displayed worse or no growth on C_6-C_{10} dicarboxylates as compared to AW162 (**Figure S28**). However, both modifications (Δ*gnuR* and

P_{14d}:*PP_0370*) resulted in improved growth on C_9 and C_{10} dicarboxylates compared to AW128, which does not include the Δ*psrA* modification.

We then evaluated growth and substrate utilization in cultivations with mixed C_4-C_{14} dicarboxylates in shake flasks with or without acetate supplementation by wild-type *P. putida*, AW162, and AW179 (**Figure S29, Figure S30, Figure S31**). Again, metabolite concentrations in non-inoculated controls were stable over time (**Figure S29a-b**). Wild-type *P. putida* utilized C_4 and C_5 dicarboxylates quickly and completely; C_{13} and C_{14} dicarboxylate concentrations decreased more than in the non-inoculated controls, especially in cultivations with acetate supplementation, indicating basal catabolic activity by the wild-type strain. Interestingly, dicarboxylate utilization dynamics were very similar between AW162 and AW179. These data demonstrate that Δ*gnuR* and P_{14d}:*PP_0370* have a negligible effect of dicarboxylate utilization when provided in a mixture, but a negative effect on growth on individual C_6, C_7, C_8, C_9, and C_{10} dicarboxylates. Together, these data disprove our hypotheses that deletion of *gnuR* would improve growth on odd-chain dicarboxylates (e.g., C_7, C_9) and overexpression of *PP_0370* would improve growth on C_6-C_8 dicarboxylates, so these genetic modifications were not pursued further.

P. putida does not grow on HDPE-derived lactone acid or ring-opened lactone acid species (ROLAs)

Oxidative depolymerization of HDPE generates small molecules primarily consisting of dicarboxylates, but also small amount of lactone acid product. To determine if the lactone acid compounds inhibit growth of *P. putida*, we cultivated AW162 in M9 minimal medium supplemented with 5 mM glucose plus 5 mM of (*R*)-(−)-5-oxo-2-tetrahydrofurancarboxylic acid (*R*-C_5-Lac) or (*S*)-(+)-5-oxo-2-tetrahydrofurancarboxylic acid (*S*-C_5-Lac) (**Figure S32a-b**). Lactone acids were provided in DMSO, such that a final concentration of 0.5% (v/v) DMSO was provided to each culture. A 5 mM glucose plus 0.5% (v/v) DMSO control was additionally run. AW162 growth was not inhibited by 5 mM of either *R*-C_5-Lac or *S*-C_5-Lac (**Figure S32d**).

To determine if the lactone compounds are catabolized as sole carbon and energy sources, we cultivated AW162 in M9 minimal medium supplemented with 5 mM *S*-C_5-Lac or *R*-C_5-Lac. Additionally, cultivations were run in 5 mM of in-house synthesized C_6-Lac and C_7-Lac. No growth was observed on any of the lactone compounds as a sole carbon and energy source (**Figure S32e-f**). This demonstrates that while the lactone acids do not inhibit growth, they also do not support growth at 5 mM concentrations.

Upon treatment with base (e.g., NaOH), as is done in the preparation of deconstructed polymers for microbial cultivations (explained in following sections), the lactone acid species ring-open to form 4-hydroxy-dicarboxylic acids, abbreviated ROLAs for ring-opened lactone acid (**Figure S33**). We additionally considered whether *P. putida* could utilize the ROLAs, or if growth was inhibited by these chemicals. To test this, a C_7 lactone acid was ring-opened by treatment with NaOH (see *Materials and Methods*) into a C_7 ROLA. The ROLA solution was diluted further in deionized water and pH adjusted to 9.21 with NaOH and HCl. To determine if the C_7 ROLA was utilized by *P. putida*, we cultivated wild-type and AW162 in M9 minimal medium supplemented with 5 mM of the C_7 ROLA solution with or without 5 mM glucose. NMR analysis of the C_7 ROLA peak in initial and final timepoints showed no utilization (**Figure S34**). These data demonstrate that *P. putida* does not utilize C_7 ROLA as a sole carbon and energy source, or in the presence of glucose.

Trace catalyst and initiator do not inhibit cell growth

We additionally considered whether engineering tolerance to trace amounts of catalyst or initiator would be necessary. Considering the extent to which cobalt and manganese were removed as salts after NaOH-mediated precipitation, we compared the growth of AW061 in an equimolar mixture of model compounds anticipated to be in a mixed plastics depolymerization stream with or without the addition of trace catalyst. Specifically, we added 1 mM of the initiator NHPI and catalysts cobalt (II) acetate and manganese (II) acetate, each, to M9 minimal medium supplemented with 5 mM of benzoate, terephthalate, acetoxyacetate (potentially formed from PET or acetic acid oxidation), glycolate, formate (an acetic acid decomposition product), and C_4, C_5, and C_6 dicarboxylates. NHPI is only marginally soluble in water at 1 mM, and partially crashed out of solution raising the absorbance. Nonetheless, growth was observed by AW061 cultivations in the presence of NHPI, cobalt (II) acetate, and manganese (II) acetate (**Figure S35**).

To further discern the effect of residual metal catalysts (Co and Mn) on bacterial growth, we evaluated AW162 in M9 minimal medium supplemented with 10 mM glucose and cobalt acetate (Co-Ace) or manganese acetate (Mn-Ace) from 0.5 mM to 100 mM, greater than 20-fold the concentrations observed in effluent solutions (**Table S12**). In the absence of additional Co-Ace or Mn-Ace (on 10 mM glucose alone), AW162 displayed a growth rate of 0.82 ± 0.14 h^{-1}. Growth rate was reduced in the presence of Co-Ace, with a rate of 0.47 ± 0.11 h^{-1} observed in the presence of 100 mM Co-Ace (**Figure S36a-b**). Lag phase was extended at higher Co-Ace concentrations, increasing from 4.85 ± 0.1 h without any Co-Ace to 9.33 ± 0.41 h in the presence of 100 mM Co-Ace (**Figure S36c**). Growth rate was less affected – or even slightly improved – in the presence of Mn-Ace: a rate of 1.26 ± 0.05 h^{-1} was observed in the presence of 100 mM Mn-Ace (**Figure S36d-e**). Lag phase was unaffected by Mn-Ace (**Figure S36f**). Given that <5 mM Co and <0.02 mM Mn were observed in the effluent solutions (**Table S12**), this data suggests that the metals retained in the biological cultivations do not substantially affect strain viability, and that concentrations could be increased 20-fold without encountering acute cytotoxicity.

AW162 grows on effluent from mixed PS and PE

Effluent from mixed PS plus HDPE contained benzoate, dicarboxylates C_4 through C_{18}, and acetate (**Table S10**). Non-inoculated and AW162 cultivations were run in shake flasks with M9 minimal medium supplemented with either effluent from mixed HDPE beads and PS beads, effluent from mixed post-consumer HDPE bottle and EPS cup, or commercial C_4-C_{18} dicarboxylates, benzoate, and acetate in roughly similar concentrations. Metabolite concentrations were stable over time in non-inoculated controls (**Figure S39**). AW162 cultivations in mixed model substrates simultaneously utilized benzoate, dicarboxylates, and acetate with all substrates depleted by 24 h (**Figure S39b**). AW162 cultivations in effluent from mixed HDPE and PS beads displayed similar utilization and growth as in the mixed model substrates, utilizing the benzoate, dicarboxylates, and acetate simultaneously and completely by 12 h (**Figure S39d**), while utilization of effluent from post-consumer HDPE bottle plus EPS cup occurred more slowly and incompletely and exhibited poor growth (**Figure S39f**). Notably, visible precipitation was observed upon addition of the effluent from post-consumer HDPE bottle plus EPS cup to M9 minimal medium; it is unknown if this precipitation contributed to the ~12 h lag phase observed in these cultivations.

AW162 grows on effluent from mixed PS and PE

*Here, we refer to the aqueous solution prepared from deconstructed polymers (detailed in Materials and Methods, and **Figure S38**) as the "effluent", where the prefix "mixed" and conjunction "and" indicates polymers that were deconstructed in the same reactor.*

Effluent from mixed PS and HDPE contained benzoate, C_4 through C_{18} dicarboxylates, and acetate (**Table S10**). Non-inoculated and AW162 cultivations were run in shake flasks with M9 minimal medium supplemented with either effluent from mixed HDPE beads and PS beads, effluent from mixed post-consumer HDPE bottle and EPS cup, or commercial C_4-C_{18} dicarboxylates, benzoate, and acetate in roughly similar concentrations. Metabolite concentrations were stable over time in non-inoculated controls (**Figure S39a, c, e**). AW162 cultivations in mixed model substrates simultaneously utilized benzoate, dicarboxylates, and acetate with all substrates depleted by 24 h (**Figure S39b**). AW162 cultivations in effluent from mixed HDPE beads and PS beads displayed similar utilization and growth as in the mixed model substrates, utilizing the benzoate, dicarboxylates, and acetate simultaneously and completely by 12 h (**Figure S39d**). Utilization of effluent from a post-consumer HDPE bottle and EPS cup occurred more slowly and incompletely and exhibited poor growth (**Figure S39f**). Notably, visible precipitation was observed upon addition of the effluent from mixed post-consumer HDPE bottle and EPS cup to M9 minimal medium. Considering the lag phase was only observed in instances of precipitated media (**Figure S39**), we submit that the precipitated media provoked a ~12 h lag phase.

AW307 converts intermediates in the effluent from mixed PS and HDPE to β-ketoadipate

We next explored the possibility of converting benzoate to β-ketoadipate. β-ketoadipate can be polymerized with hexamethylenediamine to form a performance-advantaged nylon material (*24*). In this way, we sought to convert aromatic constituents to β-ketoadipate to enable upcycling to a performance-advantaged nylon. To do this, we first constructed a strain of *P. putida* capable of accumulating β-ketoadipate. Natively, benzoate is catabolized via the β-ketoadipate pathway such that deletion of *pcaIJ,* encoding a 3-oxoadipate CoA-transferase, enables accumulation of β-ketoadipate from aromatic carbon sources that converge at protocatechuate or catechol (*24, 25*). *PcaIJ* was deleted in AW162, generating strain AW307 (*P. putida* Δ*hsdMR*::P_{tac}:*tphA2*$_{II}$*A3*$_{II}$*B*$_{II}$*A1*$_{II\text{-}E6}$ *fpvA*:P_{tac}:*tpaK*$_{RHA1}$ Δ*glcR* P_{tac}:*glcDEFG:PP_3749* Δ*paaX*::P_{tac}:*dcaAKIJP*$_{ADP1}^{CO}$ Δ*psrA* Δ*pcaIJ*).

AW307 was cultivated in M9 minimal medium supplemented with model mixed substrates (benzoate, C_4-C_{18} dicarboxylates, and acetate), effluent from mixed PS beads and HDPE beads, or effluent from mixed post-consumer EPS cup and HDPE bottle. AW307 produced 1.01 ± 0.11 mol β-ketoadipate per mol benzoate from commercial mixed benzoate, C_4-C_{18} dicarboxylates, and acetate at 12 h of cultivation despite incomplete utilization of the dicarboxylates (**Figure S43a**). β-ketoadipate concentrations unexpectedly decreased at later time-points, suggesting DcaIJ may exhibit some activity on β-ketoadipate. It is unclear why AW307 cultivations did not fully utilize C_6 and C_7 dicarboxylates here, whereas AW162 cultivations completely and simultaneously utilized all dicarboxylates – including C_6 and C_7 dicarboxylates – when provided in the same concentrations. A possible explanation is that PcaIJ is partially active on C_6 and C_7 dicarboxylates, such that the deletion of *pcaIJ* in AW307 was detrimental. AW307 produced 0.81 ± 0.07 mol β-ketoadipate per mol benzoate from intermediates in the effluent from mixed PS beads and HDPE beads (**Figure S43b**), again with incomplete utilization of C_6 and C_7 dicarboxylates. Despite a longer lag phase, AW307 cultivations produced 0.85 ± 0.05 mol β-ketoadipate per mol benzoate from intermediates in the effluent from mixed post-consumer EPS cups and HDPE bottle (**Figure S43**). Together, this demonstrates conversion of intermediates in the effluent from PS to β-ketoadipate with cellular energy supported by effluent from HDPE at theoretical or near-theoretical molar yield.

AW162 grows on effluent from mixed PS, HDPE, and PET

We next tested if engineered *P. putida* could grow on effluent from mixed PS, HDPE, and PET, which contained benzoate, terephthalate, C_4-C_{18} dicarboxylates, and acetate (**Table S11**). AW162 was engineered to catabolize terephthalate by heterologous expression of the *tpaK* transporter from *R. jostii* RHA1 and *tphA2*$_{II}$*A3*$_{II}$*B*$_{II}$*A1*$_{II}$ catabolic cluster, encoding a terephthalate 1,2-dioxygenase and DCD dehydrogenase, from *Comamonas* sp. E6 (*25*).

Non-inoculated or AW162 cultivations in shake flasks with M9 minimal medium supplemented with either a model mixture of C_4-C_{18} dicarboxylates, benzoate, terephthalate, and acetate or effluent from mixed PS, HDPE, and PET were performed. Substrate concentrations were stable in non-inoculated controls (**Figure S40a, c**). AW162 grew on the model mixture of benzoate, terephthalate, acetate, and C_4-C_{18} dicarboxylates (**Figure S40b**), as well as effluent from mixed PS, HDPE, and PET (**Figure S40d**) with simultaneous utilization of benzoate, terephthalate, all dicarboxylates, and acetate.

While *N*-hydroxyphthalimide, the catalytic initiator, is not present in effluent streams, phthalate – the product of *N*-hydroxyphthalimide hydrolysis – and isophthalate – a comonomer of PET – are present (**Figure S37a**). No utilization of either phthalate or isophthalate was observed by AW162 or AW307 cultivations in effluent from mixed PET, HDPE, and PS (**Figure S37b-c**). Thus, future work will involve targeting conversion of carbon present in the effluent streams that is not directly derived from the polymers (*e.g.,* degraded initiator, additives, dyes, comonomers, etc.

AW307 converts intermediates in the effluent from mixed PS + HDPE + PET to β-ketoadipate

Next, we sought to convert intermediates in effluent from mixed PS, HDPE, and PET to β-ketoadipate. AW307 was cultivated in M9 minimal medium supplemented with either a model mixture (benzoate, terephthalate, C_4-C_{18} dicarboxylates, and acetate) or effluent from mixed PS, HDPE, and PET. We hypothesized that benzoate and terephthalate would be converted to β-ketoadipate while the dicarboxylic acids and acetate would serve as an energy source for cellular growth and maintenance (**Figure S44a**). AW307 cultivations produced β-ketoadipate at 0.73 ± 0.01 mol/mol yields from benzoate and terephthalate in model mixtures of benzoate, terephthalate, dicarboxylates and acetate (**Figure S44b**). In the first prepared effluent from mixed PS, HDPE, and PET, AW307 cultivations produced β-ketoadipate at 0.76 ± 0.08 mol/mol yields from benzoate and terephthalate (**Figure S44c**). Later, after optimization of PET deconstruction had been conducted, this experiment was repeated: in this second batch of prepared effluent from mixed PS, HDPE, and PET, AW307 cultivations produced β-ketoadipate at 0.71 ± 0.10 mol/mol yields from benzoate and terephthalate (**Figure S44d-e**).

We next considered the carbon yield to the β-ketoadipate over the entire process. HDPE, PS, and PET were supplied at equal weights in the deconstruction step. Given this, the following describes the flow of carbon across the entire process, visualized in the Sankey diagram presented in **Figure S45**. On a carbon basis: 20% of HDPE was converted to dicarboxylates, which were utilized for cellular growth and energy; 63% of PS was converted to benzoate, and 64% of PET carbon was converted to terephthalate; at a molar yield of 0.71 ± 0.10 mol/mol, 57% of the carbon in benzoate (one CO_2 released) and terephthalate (two CO_2 released) were converted to β-ketoadipate. Thus, from the starting mixed HDPE beads, PS beads, and PET powder, 25.5% of the carbon was upcycled to β-ketoadipate.

AW162 converts intermediates in the from effluent from mixed PS and HDPE to polyhydroxyalkanoates

P. putida natively produces polyhydroxyalkanoates from acetyl-CoA under conditions of limiting nitrogen (*23*). Thus, we sought to produce polyhydroxyalkanoates from effluent from mixed PS and HDPE as an illustrative product from carbon sources in both plastic feedstocks (i.e., benzoate from PS and dicarboxylates from HDPE) without additional engineering. We point the reader to several recent reviews covering means and approaches to increase polyhydroxyalkanoate yields in bacteria and *P. putida* (*23*) but note that we did not engage in optimization work as polyhydroxyalkanoates were only to be an illustrative product from HDPE, PS, and PET.

AW162 was first cultivated in nitrogen limited M9 minimal medium supplemented with either a model mixture of substrates (commercial benzoate, C_4-C_{18} dicarboxylates, and acetate), effluent from mixed HDPE beads and PS beads, or effluent from mixed post-consumer HDPE bottle and EPS cup. Cultivations were inoculated at OD_{600} of 0.05 in 300 mL of media in 1 L baffled shake flasks. At 48 h in the commercial model mixture, AW162 had entered stationary phase (**Figure S41a**) and was harvested for polyhydroxyalkanoates analysis. AW162 produced 2.41 ± 0.58 mg polyhydroxyalkanoates, consisting of 30 ± 2% HAME-8, 60 ± 0% HAME-10 and 10 ± 2% HAME-12 (**Figure S41a**).

AW162 was also cultivated in nitrogen limited M9 minimal medium supplemented with effluent from mixed HDPE beads and PS beads, or effluent from mixed post-consumer HDPE bottle and EPS cup. These substrates precipitated out of the nitrogen-limited M9 minimal medium upon addition, which was not observed in the prior experiments done with nitrogen replete M9 minimal medium. After 48 h, no growth was observed in either the effluent from mixed PS beads and HDPE beads nor the effluent from mixed post-consumer HDPE bottle and EPS cup. Therefore, fresh AW162 preculture was added to these cultivations such that the OD_{600} was 0.2 in 50 mL cultivations in 250 mL flasks (as opposed to 300 mL in 1 L, as was done with the model mixture). AW162 growth was observed after addition of the second inoculum, and cultivations were harvested 44 h later (93 h after the first inoculum) (**Figure S41b-c)**. Considering the concentration of substrates quantified (dicarboxylates, benzoate, and acetate) were similar in the model commercial mixture and effluent from polymers, this suggests that an additional stress, perhaps due to the precipitation of the substrates, may have been present in the effluent from polymers that stymied growth of a low-density cultivation. In AW162 cultivations in effluent from mixed HDPE beads and PS beads, all substrates except C_6 dicarboxylates were simultaneously utilized during cell growth (**Figure S41b**). Polyhydroxyalkanoates were produced (0.13 ± 0.02 mg) with a distribution of 33% HAME-10 and 67% HAME-12 (**Figure S42**). In AW162 cultivations in effluent from mixed post-consumer HDPE bottle and EPS cup, polyhydroxyalkanoates were produced to a similar level (0.13 ± 0.02 mg) and HAME distribution (34% HAME-10 and 66% HAME-12) (**Figure S41c**). Together, these data demonstrate bioconversion of intermediates in effluent from mixed plastics (PS and HDPE) to the bioplastic polyhydroxyalkanoate with similar yield and HAME distribution observed from beads as from post-consumer items (HDPE bottle plus EPS cup).

Abbreviations
BDE: bond dissociation energy
CsiD: glutarate dioxygenase
LhgO: (S)-2-hydroxyglutarate oxidase
AscA-I: acetyl-CoA synthetase
GcdH: glutaryl-CoA dehydrogenase
ETF_{ox}: oxidized electron transfer flavoprotein

ETF_{red}: reduced electron transfer flavoprotein
FadB: fatty acid oxidation complex, α component
Hbd: 3-hydroxybutyryl-CoA dehydrogenase
FadBA: type II 3-hydroxyacyl-CoA dehydrogenase
BktB: β-ketothiolase BktB
YqeF: acetyl-CoA acetyltransferase
GlcDEF: glycolate oxidase
Gcl: glyoxylate carboligase
TCA cycle: tricarboxylic acid cycle; or, citric acid cycle; or, Krebs cycle; or, Szent-Gyorgyi-Krebs cycle
$DcaP_{ADP1}$: Probable outer membrane porin for adipate in *Acinetobacter* sp. strain ADP1
$DcaK_{ADP1:}$ Probable inner membrane transporter for adipate in *Acinetobacter* sp. strain ADP1
$DcaIJ_{ADP1:}$ CoA-transferase active on adipate in *Acinetobacter* sp. strain ADP1
$DcaA_{ADP1:}$ Acyl-CoA dehydrogenase active on adipate in *Acinetobacter* sp. strain ADP1
PaaF: enoyl-CoA hydratase/isomerase
PaaH: 3-hydroxyacyl-CoA dehydrogenase PaaH
PaaJ: 3-oxoadipyl-CoA/3-oxo-5,6-dehydrosuberyl-CoA thiolase
PcaF-I: beta-ketoadipyl-CoA thiolase
CoA: coenzyme A
NAD^+: nicotinamide adenine dinucleotide oxidized
NADH: nicotinamide adenine dinucleotide reduced
BenK: benzoate MFS transporter
BenABC: benzoate 1,2-dioxygenase
BenD: 1,6-dihydroxycyclohexa-2,4-diene-1-carboxylate dehydrogenase
CatA: catechol 1,2-dioxygenase
CatB: muconate cycloisomerase 1
CatC: muconolactone delta-isomerase
PcaD: 3-oxoadipate enol-lactonase
PcaIJ: 3-oxoadipate CoA-transferase
DCD: 1,2-dihydroxy-3,5-cyclohexadiene-1,4-dicarboxylate
TPA: terephthalate or terephthalic acid
MHET: 2-hydroxyethyl terephthalic acid
$TpaK_{RHA1}$: MFS superfamily TPAtransporter from *Rhodococcus jostii* RHA1
$TphA1A2A3_{E6}$: TPA 1,2-dioxygenase from *Comamonas* sp. E6
$TphB_{E6}$: DCD dehydrogenase from *Comamonas* sp. E6
PcaHG: protocatechuate 3,4-dioxygenase
PcaB: 3-carboxy-cis,cis-muconate cycloisomerase
PcaC: 4-carboxymuconolactone decarboxylase
ATP: adenosine 5′-triphosphate
ADP: adenosine diphosphate
EM: extracellular milieu
OM: outer membrane
IM: inner membrane
DCA: dicarboxylic acid
C_4 DCA: succinic acid, or butanedioic acid
C_5 DCA: glutaric acid, or pentanedioic acid

C_6 DCA: adipic acid, or hexanedioic acid
C_7 DCA: pimelic acid, or heptanedioic acid
C_8 DCA: suberic acid, or octanedioic acid
C_9 DCA: azelaic acid, or nonanedioic acid
C_{10} DCA: sebacic acid, or decanedioic acid
C_{11} DCA: undecanedioic acid
C_{12} DCA: dodecanedioic acid
C_{13} DCA: brassylic acid, or tridecanedioic acid
C_{14} DCA: tetradecanedioic acid
C_{15} DCA: 1,15-pentadecanedioic acid
C_{16} DCA: thapsic acid, or hexadecanedioic acid
C_{17} DCA: heptadecanedioic acid
C_{18} DCA: octadecanedioic acid
C_{19} DCA: nonadecanedioic acid
C_{20} DCA: eicosanedioic acid
C_{21} DCA: heneicosanedioic acid
C_{22} DCA: phellogenic acid, or docosanedioic acid
AA: acetate
BA: benzoate
PS: polystyrene
HDPE: high density polyethylene
PE: polyethylene
PET: polyethylene terephthalate
ROLA: ring-opened lactone acid
PHA: polyhydroxyalkanoate
cPCR: colony PCR
NMR: nuclear magnetic resonance
IRMS: isotope ratio mass spectrometry
UHPLC: Ultra-high pressure liquid chromatography
HPLC: high pressure liquid chromatography
DAD: diode array detection
ESI: electrospray ionization
LC: liquid chromatography
MRM: multiple reaction monitoring
GC: gas chromatography
MS: mass spectrometry
MS/MS: tandem mass spectrometry
IS: internal standard
TCD: thermal conductivity detector
ICP-OES: inductively coupled plasma optical emission spectroscopy
ICP-MS: inductively coupled plasma mass spectrometry
GPC: gel permeation chromatography
MALS: multi-angle light scattering
RI: refractive index
NHPI: *N*-hydroxyphthalimide
UHP: Ultra-high purity

LOC: limiting oxygen concentration
LEL: lower explosion limit
UEL: upper explosion limit
DMSO: dimethyl sulfoxide
THF: tetrahydrofuran
UV: ultraviolet
DCW: dry cell weight

Supplementary Figures

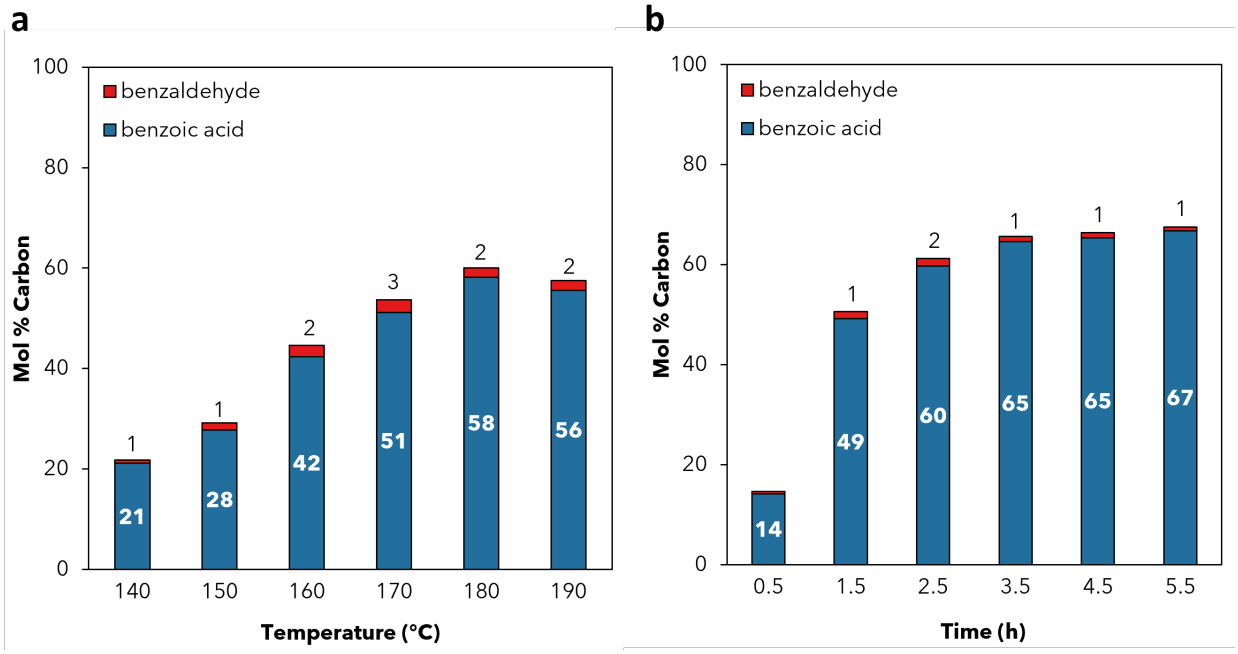

Figure S1. Effect of (a) temperature and (b) time on deconstruction of PS beads.
Product concentrations determined using HPLC with DAD. Mol% carbon yields are calculated as a percentage of carbon in the quantified products relative to the carbon present in the repeating unit of the polymer starting material. Conditions: (**a**) Temperature screen: 280 kDa PS beads (500 mg, 240 mM repeating styrene unit), $Co(OAc)_2$ (6.8 wt%, 9.6 mM), $Mn(OAc)_2$ (6.7 wt%, 9.6 mM), NHPI (15.7 wt%, 24.1 mM), 8 bar O_2/72 bar He, 5.5 hr, 140-190 °C. (**b**) Time screen: 280 kDa PS beads (350 mg, 170 mM repeating styrene unit), $Co(OAc)_2$ (13.6 wt%, 13.4 mM), $Mn(OAc)_2$ (13.3 wt%, 13.4 mM), NHPI (15.7 wt%, 16.8 mM), 8 bar O_2/72 bar He, 0.5-5.5 hr, 180 °C.

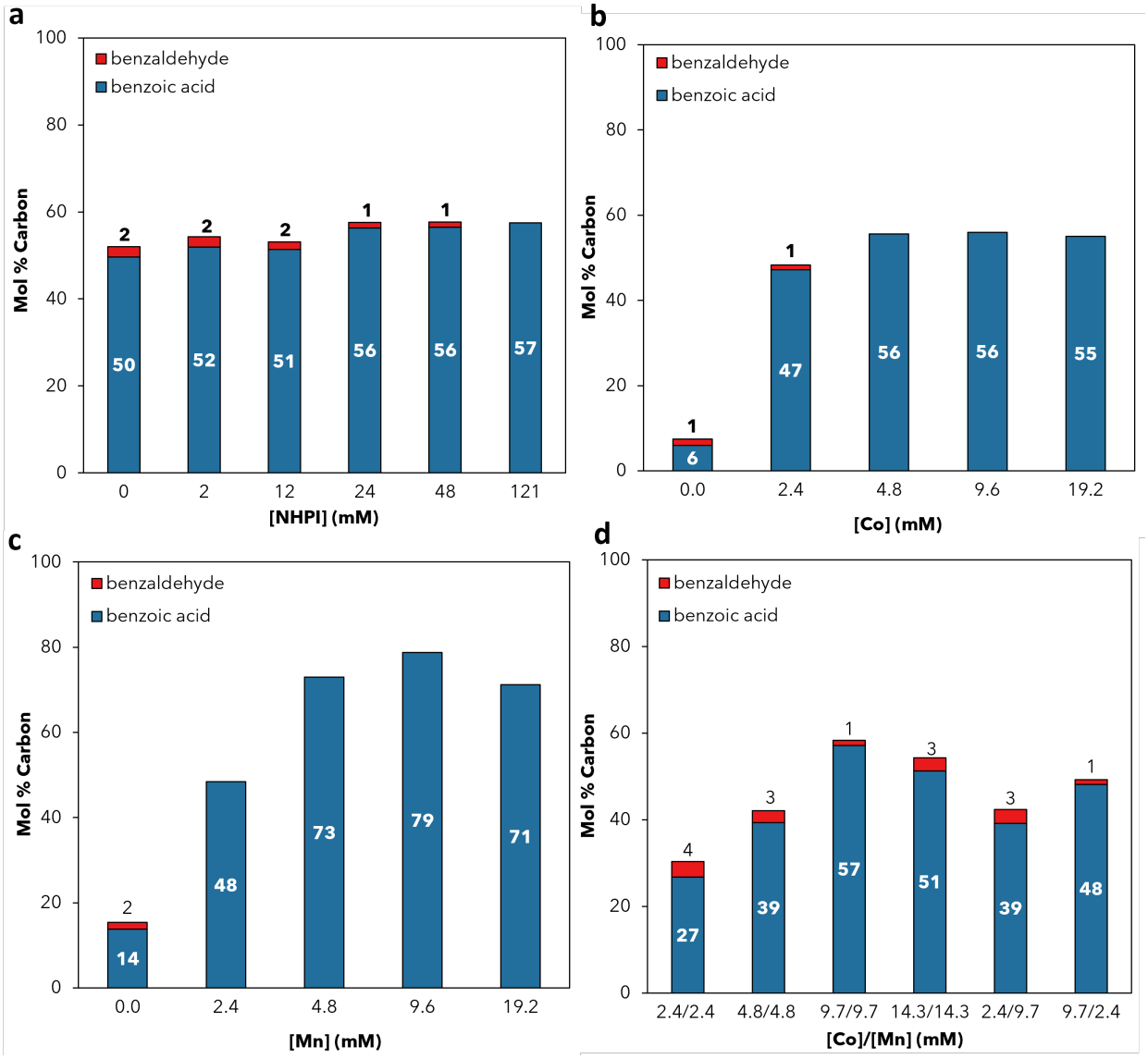

Figure S2. Dependence of (a) [NHPI], (b) [Co], (c) [Mn], and (d) [Co] & [Mn] on deconstruction of PS beads.

Product concentrations determined using HPLC with DAD. Mol% carbon yields are calculated as a percentage of carbon in the quantified products relative to the carbon present in the repeating unit of the polymer starting material. Conditions: (**a**) NHPI concentration screen: 280 kDa PS beads (500 mg, 240 mM repeating styrene unit), $Co(OAc)_2$ (6.8 wt%, 9.6 mM), $Mn(OAc)_2$ (6.7 wt%, 9.6 mM), NHPI (0.0-78.7 wt%, 0.0-120.7 mM), 8 bar O_2/72 bar He, 5.5 hr, 180 °C. (**b**) $Co(OAc)_2$ concentration screen: 280 kDa PS beads (350 mg, 170 mM repeating styrene unit), $Co(OAc)_2$ (0.0-38.7 wt%, 0.0-38.3 mM), $Mn(OAc)_2$ (9.5 wt%, 9.6 mM), NHPI (22.5 wt%, 24.1 mM), 8 bar O_2/72 bar He, 5.5 hr, 180 °C. (**c**) $Mn(OAc)_2$ concentration screen: 280 kDa PS beads (350 mg, 170 mM repeating styrene unit), $Co(OAc)_2$ (9.7 wt%, 9.6 mM), $Mn(OAc)_2$ (0.0-38.1 wt%, 0.0-38.5 mM), NHPI (22.5 wt%, 24.1 mM), 8 bar O_2/72 bar He, 5.5 hr, 180 °C. (**d**) $Co(OAc)_2$ and $Mn(OAc)_2$ screen: 280 kDa PS beads (500 mg, 240 mM repeating styrene unit), $Co(OAc)_2$ (1.7-17.0 wt%, 2.4-24.0 mM), $Mn(OAc)_2$ (1.7-16.6 wt%, 2.4-24.0 mM), NHPI (15.7 wt%, 24.1 mM), 8 bar O_2/72 bar He, 5.5 hr, 180 °C.

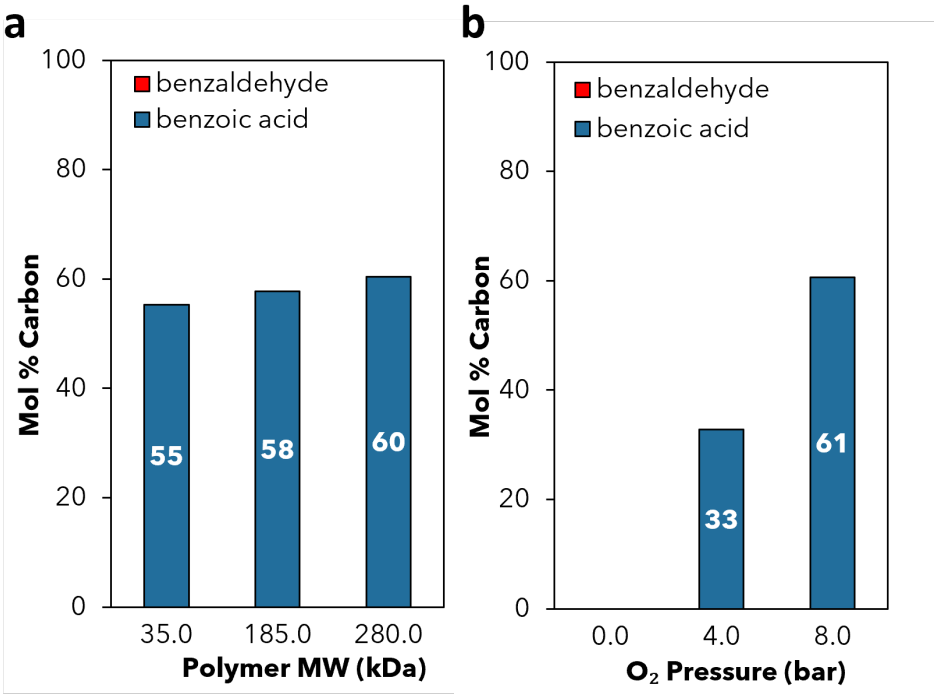

Figure S3. Effect of (a) PS MW and (b) O_2 pressure.
Product concentrations determined using HPLC with DAD. Mol% carbon yields are calculated as a percentage of carbon in the quantified products relative to the carbon present in the repeating unit of the polymer starting material. Conditions: (**a**) PS molecular weight effect: 280 kDa, 185 kDa, and 35 kDa PS beads (500 mg, 240 mM repeating styrene unit), $Co(OAc)_2$ (6.8 wt%, 9.6 mM), $Mn(OAc)_2$ (6.7 wt%, 9.6 mM), NHPI (15.7 wt%, 24.1 mM), 8 bar O_2/72 bar He, 5.5 hr, 180 °C. (**b**) Oxygen pressure effect: 280 kDa PS beads (500 mg, 240 mM repeating styrene unit), $Co(OAc)_2$ (6.8 wt%, 9.6 mM), $Mn(OAc)_2$ (6.7 wt%, 9.6 mM), NHPI (15.7 wt%, 24.1 mM), 8, 4, or 0 bar O_2/72, 76, or 80 bar He, 5.5 hr, 180 °C.

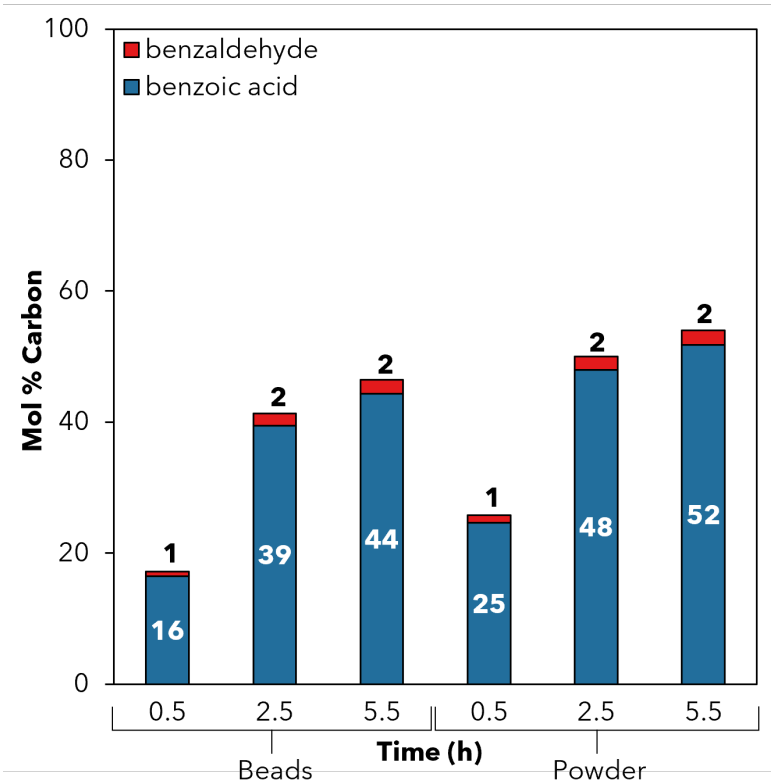

Figure S4. Oxidation of **commercial resin** PS and powder.
Product concentrations determined using HPLC with DAD. Mol% carbon yields are calculated as a percentage of carbon in the quantified products relative to the carbon present in the repeating unit of the polymer starting material. Beads were cryomilled to obtain powders before reaction. Conditions: 280 kDa PS beads or cryomilled powder (500 mg, 240 mM repeating styrene unit), $Co(OAc)_2$ (5.9 wt%, 8.4 mM), $Mn(OAc)_2$ (5.8 wt%, 8.4 mM), NHPI (13.7 wt%, 21.0 mM), 8 bar O_2/72 bar He, 5.5 hr, 180 °C.

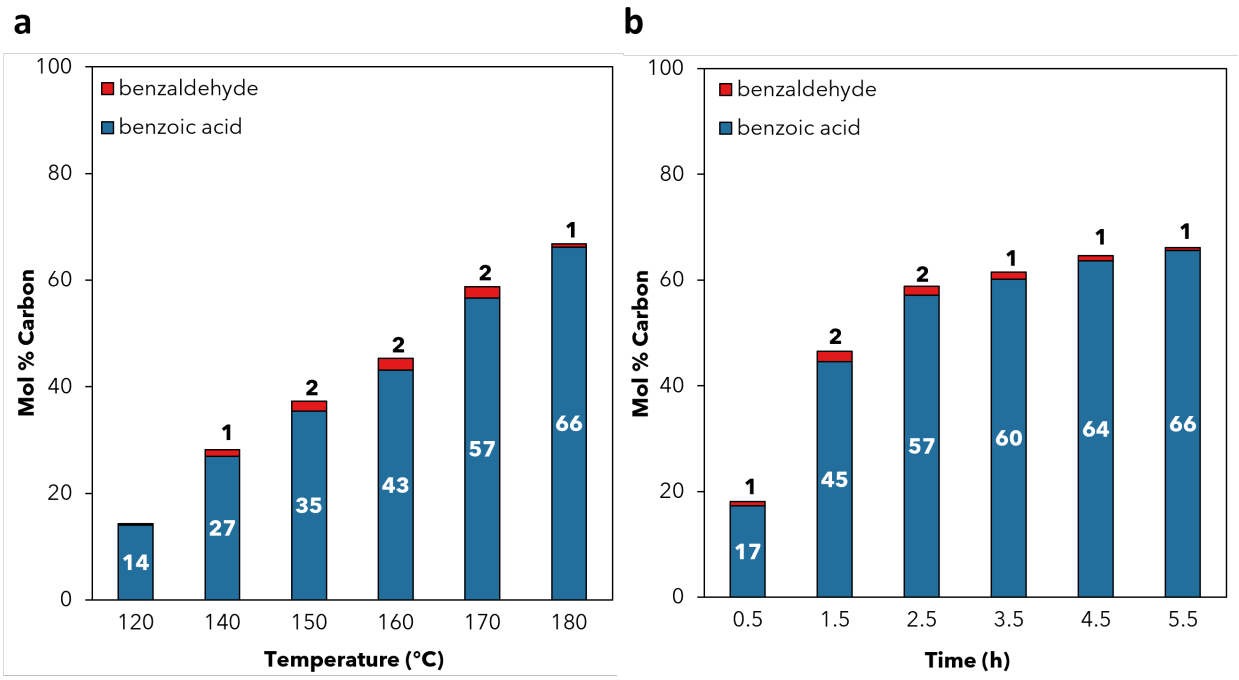

Figure S5. Effect of temperature and time on deconstruction of a post-consumer EPS cup. Product concentrations determined using HPLC with DAD. Mol% carbon yields are calculated as a percentage of carbon in the quantified products relative to the carbon present in the repeating unit of the polymer starting material. Conditions: (**a**) Temperature screen: 290 kDa EPS cup (500 mg, 240 mM repeating styrene unit), $Co(OAc)_2$ (6.8 wt%, 9.6 mM), $Mn(OAc)_2$ (6.7 wt%, 9.6 mM), NHPI (15.7 wt%, 24.1 mM), 8 bar O_2/72 bar He, 5.5 hr, 120-180 °C. (**b**) Time screen: 280 kDa PS beads (500 mg, 240 mM repeating styrene unit), $Co(OAc)_2$ (6.8 wt%, 9.6 mM), $Mn(OAc)_2$ (6.7 wt%, 9.6 mM), NHPI (15.7 wt%, 24.12 mM), 8 bar O_2/72 bar He, 0.5-5.5 hr, 180 °C.

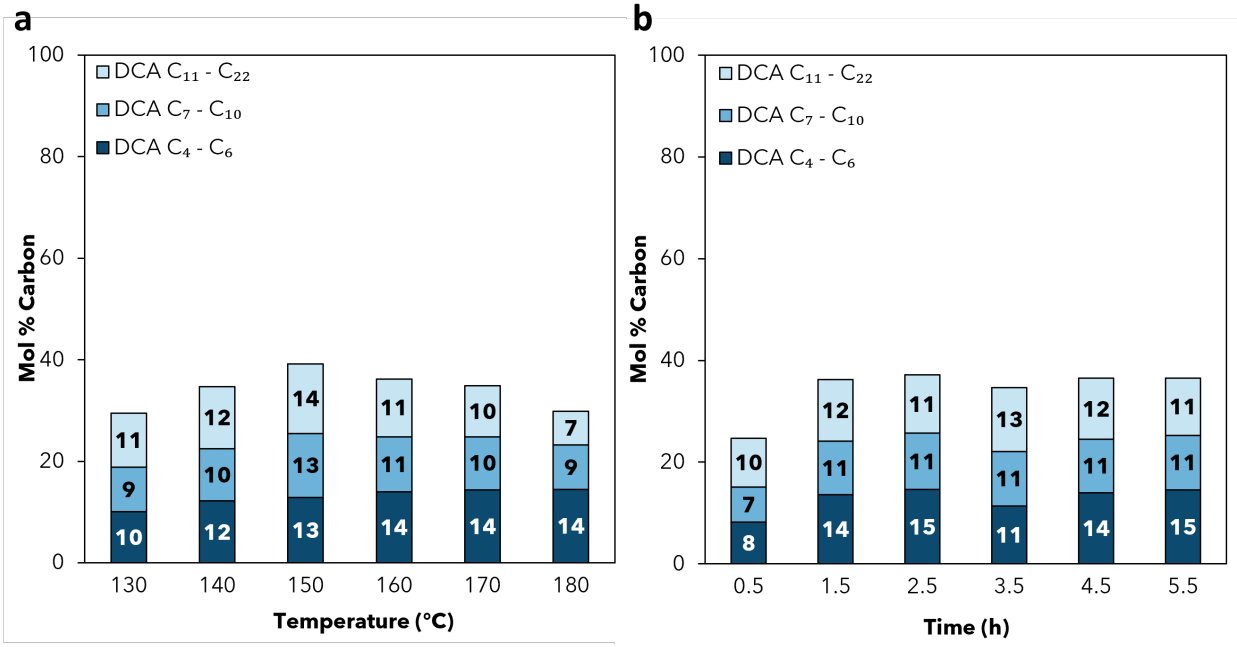

Figure S6. Effect of (a) temperature and (b) time on deconstruction of HDPE beads. Dicarboxylic acid (DCA) product concentrations (C_4-C_{22}) determined using UHPLC-MS/MS. Mol% carbon yields are calculated as a percentage of carbon in the quantified products relative to the carbon present in the repeating unit of the polymer starting material. Conditions: (**a**) Temperature screen: 54 kDa HDPE bead (350 mg, 1250 mM repeating ethylene unit), $Co(OAc)_2$ (9.7 wt%, 9.6 mM), $Mn(OAc)_2$ (9.5 wt%, 9.6 mM), NHPI (22.4 wt%, 24.0 mM), 8 bar O_2/72 bar He, 2.5 hr, 130-180 °C. (**b**) Time screen: 54 kDa HDPE bead (350 mg, 1250 mM repeating ethylene unit), $Co(OAc)_2$ (9.7 wt%, 9.6 mM), $Mn(OAc)_2$ (9.5 wt%, 9.6 mM), NHPI (22.4 wt%, 24.0 mM), 8 bar O_2/72 bar He, 0.5-5.5 hr, 160 °C.

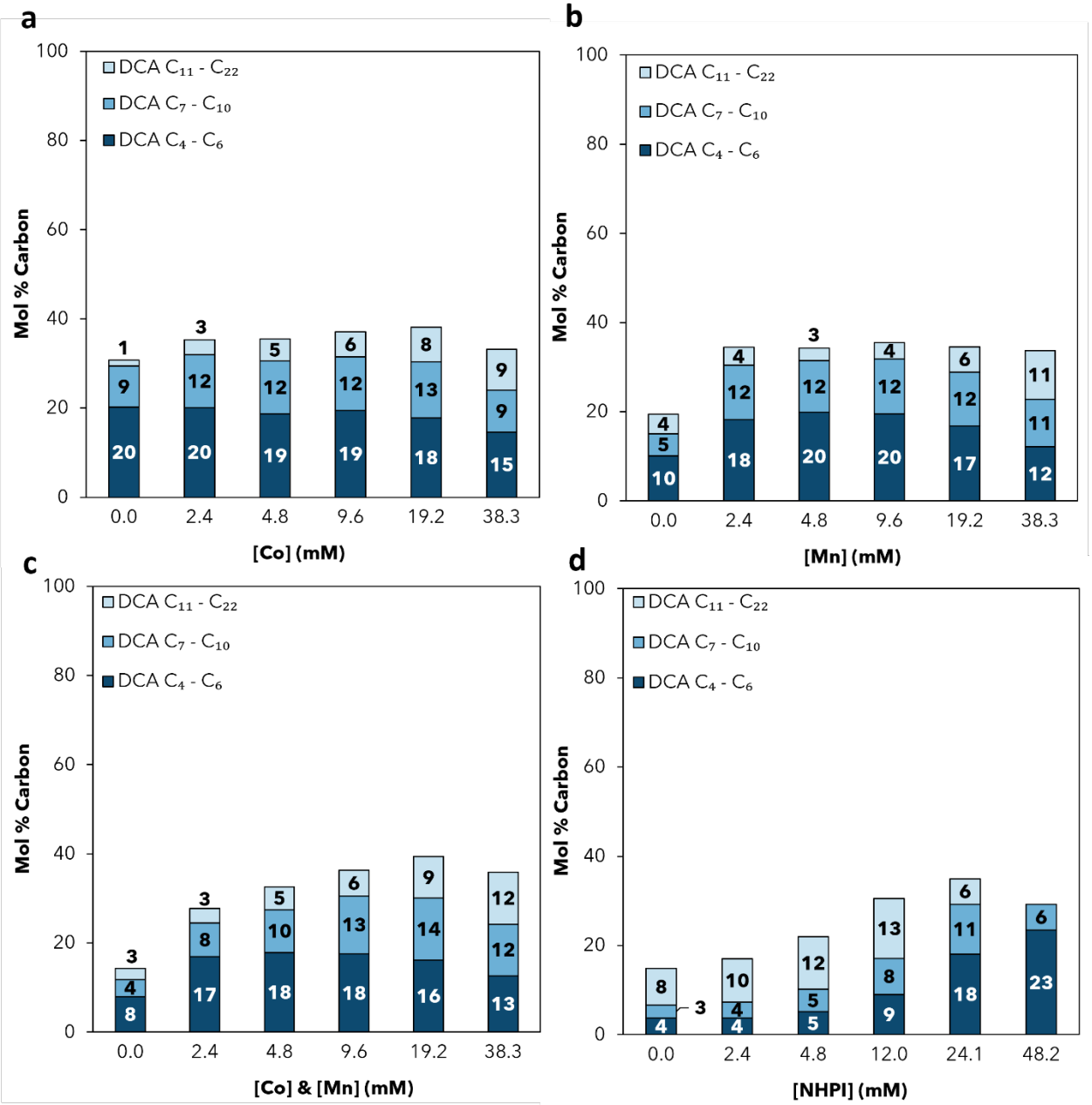

Figure S7. Dependence of (a) [Co], (b) [Mn], (c) [NHPI] and (c) [Co] & [Mn] on depolymerization of HDPE beads.

Dicarboxylic acid (DCA) product concentrations (C_4-C_{22}) determined using UHPLC-MS/MS. Mol% carbon yields are calculated as a percentage of carbon in the quantified products relative to the carbon present in the repeating unit of the polymer starting material. Conditions: (**a**) $Co(OAc)_2$ concentration screen: 54 kDa HDPE bead (200 mg, 710 mM repeating ethylene unit), $Co(OAc)_2$ (0.0-67.8 wt%, 0.0-38.3 mM), $Mn(OAc)_2$ (16.7 wt%, 9.6 mM), NHPI (39.2 wt%, 24.0 mM), 8 bar O_2/72 bar He, 2.5 hr, 160 °C. (**b**) $Mn(OAc)_2$ concentration screen: 54 kDa HDPE bead (200 mg, 710 mM repeating ethylene unit), $Co(OAc)_2$ (17.0 wt%, 9.6 mM), $Mn(OAc)_2$ (0.0-66.6 wt%, 0.0-38.5 mM), NHPI (39.2 wt%, 24.0 mM), 8 bar O_2/72 bar He, 2.5 hr, 160 °C. (**c**) $Co(OAc)_2$ and $Mn(OAc)_2$ screen: 54 kDa HDPE bead (200 mg, 710 mM repeating ethylene unit), $Co(OAc)_2$ (0.0-67.8 wt%, 0.0-38.3 mM), $Mn(OAc)_2$ (0.0-66.6 wt%, 0.0-38.5 mM), NHPI (39.2 wt%, 24.0 mM),

8 bar O_2/72 bar He, 2.5 hr, 160 °C. (**d**) NHPI concentration screen: 54 kDa HDPE bead (200 mg, 710 mM repeating ethylene unit), $Co(OAc)_2$ (17.0 wt%, 9.6 mM), $Mn(OAc)_2$ (16.7 wt%, 9.6 mM), NHPI (0.0-78.7 wt%, 0.0-48.2 mM), 8 bar O_2/72 bar He, 2.5 hr, 160 °C.

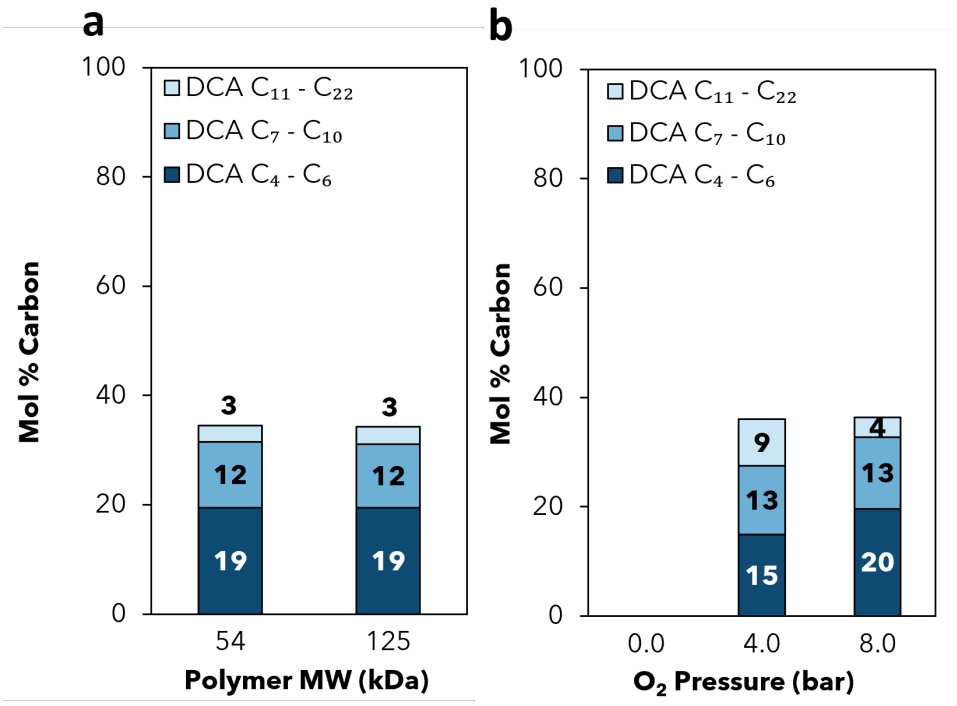

Figure S8. Effect of (a) HDPE MW and (b) O_2 pressure on deconstruction of HDPE. Dicarboxylic acid (DCA) product concentrations (C_4-C_{22}) determined using UHPLC-MS/MS. Mol% carbon yields are calculated as a percentage of carbon in the quantified products relative to the carbon present in the repeating unit of the polymer starting material. Conditions: (**a**) HDPE molecular weight effect: 125 kDa and 54 kDa HDPE beads (200 mg, 710 mM repeating ethylene unit), $Co(OAc)_2$ (17.0 wt%, 9.6 mM), $Mn(OAc)_2$ (16.7 wt%, 9.6 mM), NHPI (39.4 wt%, 24.1 mM), 8 bar O_2/72 bar He, 5.5 hr, 160 °C. (**b**) Oxygen pressure effect: 54 kDa HDPE beads (200 mg, 710 mM repeating ethylene unit), $Co(OAc)_2$ (17.0 wt%, 9.6 mM), $Mn(OAc)_2$ (16.7 wt%, 9.6 mM), NHPI (39.4 wt%, 24.1 mM), 0-8 bar O_2/72 bar He, 2.5 hr, 160 °C.

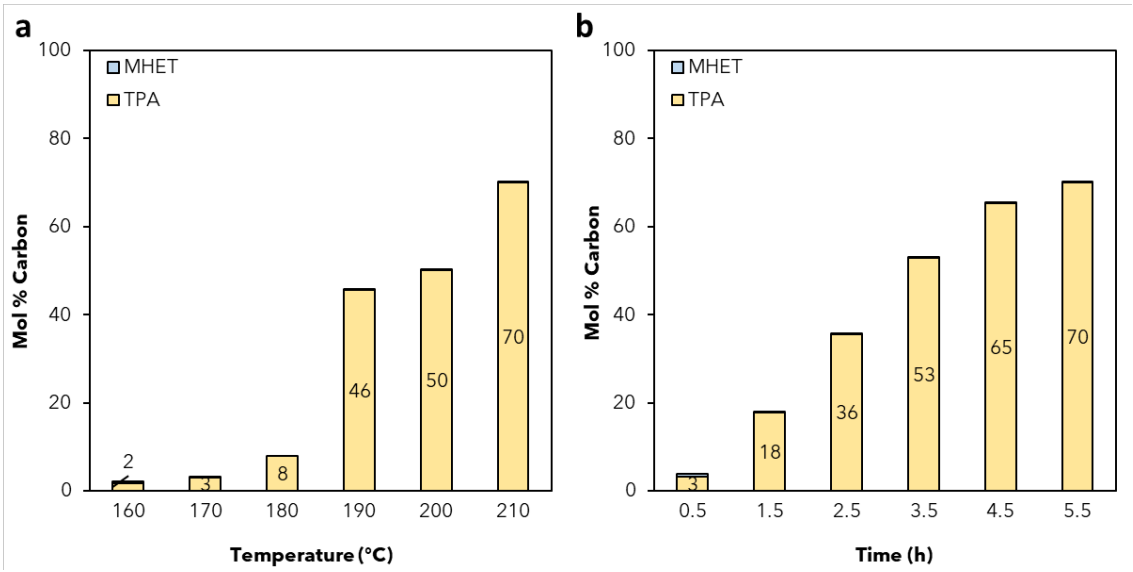

Figure S9. Effect of (a) temperature and (b) time on deconstruction of PET powder.

Terephthalic acid (TPA) and 2-hydroxyethyl terephthalic acid (MHET) product concentrations determined using UHPLC with DAD. Mol% carbon yields are calculated as a percentage of carbon in the quantified products relative to the carbon present in the repeating unit of the polymer starting material. Conditions: (**a**) Temperature effect: 38 kDa PET powder (350 mg, 83 mM repeating 2-hydroxyethyl terephthalic acid unit), $Co(OAc)_2$ (9.7 wt%, 9.6 mM), $Mn(OAc)_2$ (9.5 wt%, 9.6 mM), $Zr(acac)_4$ (6.7 wt%, 2.4 mM), NHPI (11.3 wt%, 12.1 mM), 1% H_2O (v/v), 8 bar O_2/72 bar N_2, 5.5 hr, 160-210 °C. (**b**) Time effect: 38 kDa PET powder (350 mg, 83 mM repeating 2-hydroxyethyl terephthalic acid unit), $Co(OAc)_2$ (9.7 wt%, 9.6 mM), $Mn(OAc)_2$ (9.5 wt%, 9.6 mM), $Zr(acac)_4$ (6.7 wt%, 2.4 mM), NHPI (11.3 wt%, 12.1 mM), 1% H_2O (v/v), 8 bar O_2/72 bar N_2, 0.5-5.5 hr, 210 °C.

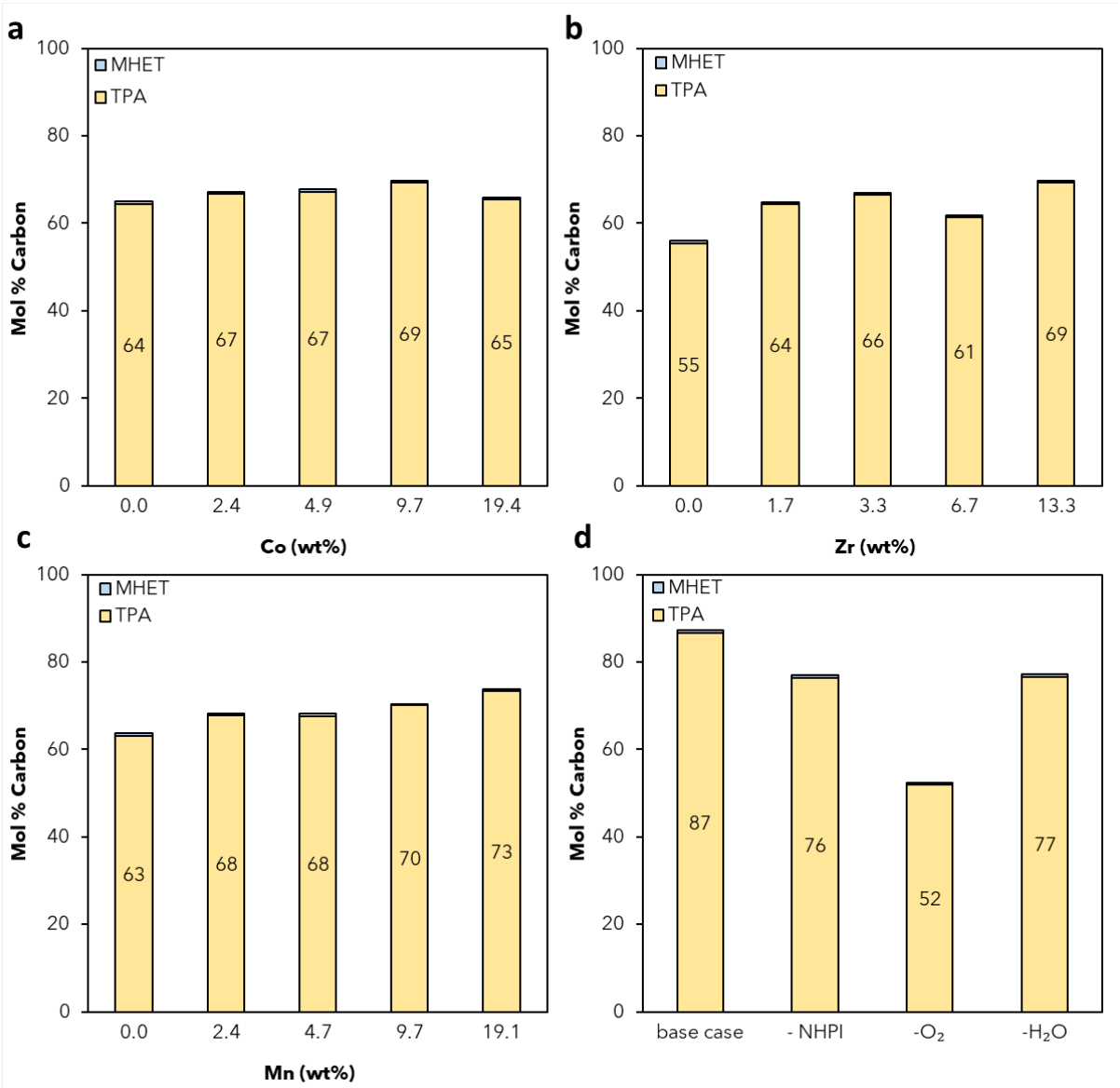

Figure S10. Dependence of (a) [Co], (b) [Mn], (c) [Zr], and (d) additional controls on depolymerization of PET powder.

Terephthalic acid (TPA) and 2-hydroxyethyl terephthalic acid (MHET) product concentrations determined using UHPLC with DAD. Mol% carbon yields are calculated as a percentage of carbon in the quantified products relative to the carbon present in the repeating unit of the polymer starting material. Conditions: (**a**) [Co] effect: 38 kDa PET powder (350 mg, 83 mM repeating 2-hydroxyethyl terephthalic acid unit), $Co(OAc)_2$ (0-19.1 wt%, 0-19.2 mM), $Mn(OAc)_2$ (9.5 wt%, 9.6 mM), $Zr(acac)_4$ (6.7 wt%, 2.4 mM), NHPI (11.3 wt%, 12.1 mM), 1% H_2O (v/v), 8 bar O_2/72 bar N_2, 5.5 hr, 210 °C. (**b**) [Zr] effect: 38 kDa PET powder (350 mg, 83 mM repeating 2-hydroxyethyl terephthalic acid unit), $Co(OAc)_2$ (9.7 wt%, 9.6 mM), $Mn(OAc)_2$ (9.5 wt%, 9.6 mM), $Zr(acac)_4$ (0-13.3 wt%, 0-4.7 mM), NHPI (11.3 wt%, 12.1 mM), 1% H_2O (v/v), 8 bar O_2/72 bar N_2, 5.5 hr, 210 °C. (**c**) [Mn] effect: 38 kDa PET powder (350 mg, 83 mM repeating 2-hydroxyethyl terephthalic acid unit), $Co(OAc)_2$ (9.7 wt%, 9.6 mM), $Mn(OAc)_2$ (0-19.1 wt%, 0-19.3 mM), $Zr(acac)_4$ (6.7 wt%, 2.4 mM), NHPI (11.3 wt%, 12.1 mM), 1% H_2O (v/v), 8 bar O_2/72 bar N_2, 5.5

hr, 210 °C. (**d**) effect of several controls relative to "base case" with the standard conditions of: 38 kDa PET powder (350 mg, 83 mM repeating 2-hydroxyethyl terephthalic acid unit), $Co(OAc)_2$ (9.7 wt%, 9.6 mM), $Mn(OAc)_2$ (9.5 wt%, 9.6 mM), $Zr(acac)_4$ (6.7 wt%, 2.4 mM), NHPI (11.3 wt%, 12.1 mM), 1% H_2O (v/v), 8 bar O_2/72 bar N_2, 5.5 hr, 210 °C. -NHPI, -O_2, and -H_2O represent these conditions in the absence of each of these components, respectively.

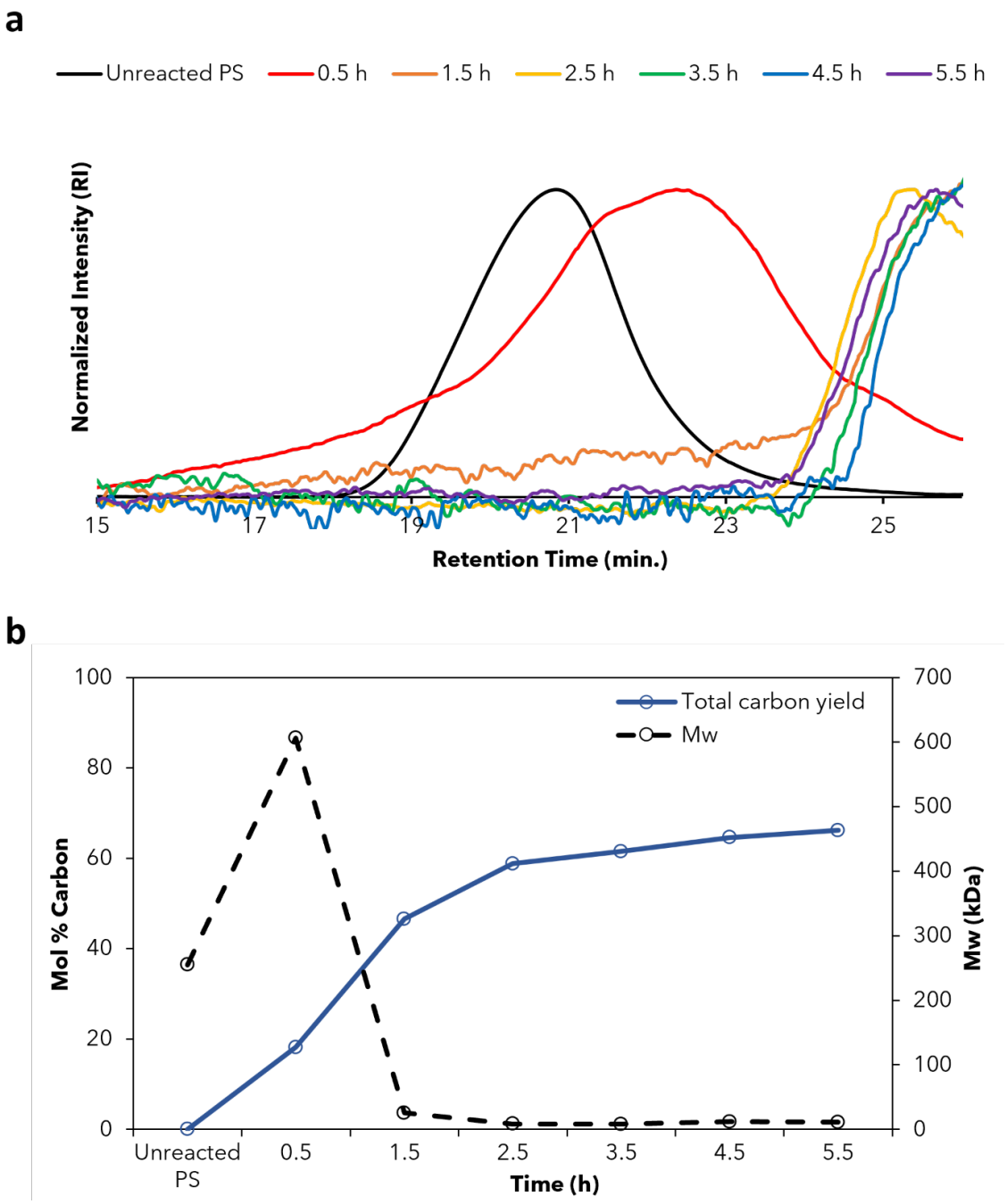

Figure S11. GPC traces over time during the deconstruction of PS beads.
Quantified product yields are shown in **Figure S1b**. SEC-MALS GPC was performed using RI and MALS dual-detection at 40 °C with THF as solvent. Reaction conditions: 280 kDa PS beads (350 mg, 170 mM repeating styrene unit), $Co(OAc)_2$ (13.6 wt%, 13.4 mM), $Mn(OAc)_2$ (13.3 wt%, 13.4 mM), NHPI (15.7 wt%, 16.8 mM), 8 bar O_2/72 bar He, 0.5-5.5 hr, 180 °C. (**a**) GPC traces at varying time points, revealing decreased molecular weight over time as the PS is depolymerized. An increase in the RT at 0.5 h suggests that polymer crosslinking occurs at early timescales. (**b**) Graphical representation of the MW measured by GPC relative to the product yields quantified by HPLC with UV detector.

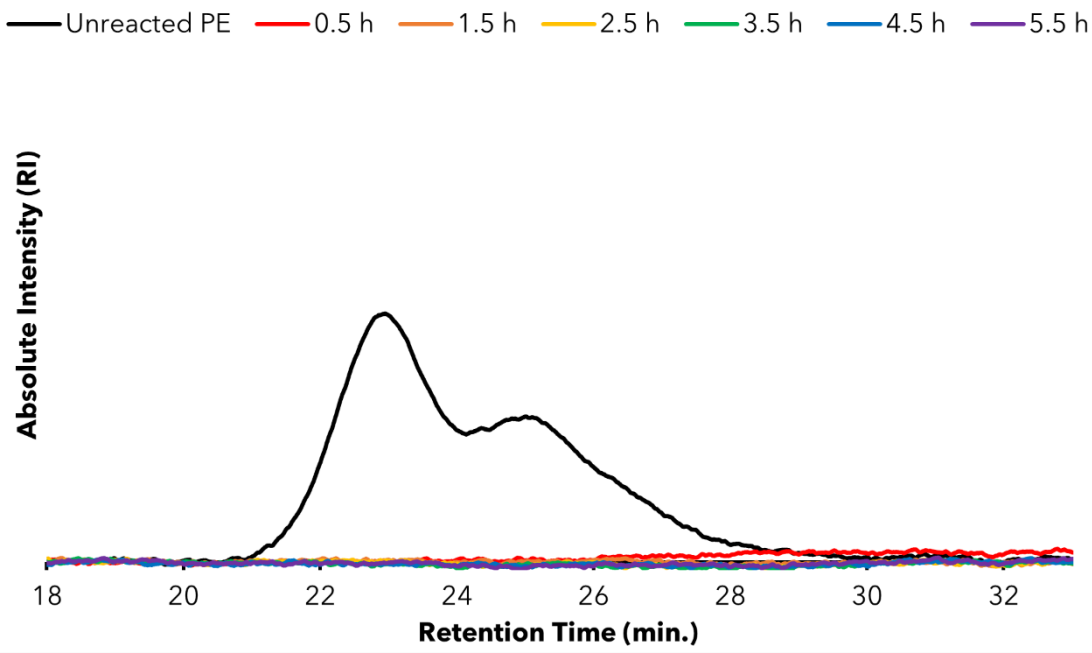

Figure S12. GPC chromatograms for deconstruction of HDPE at different reaction times. HT-GPC was performed at 160 °C using a DRI detector and trichlorobenzene as solvent, calibrated to PS standards. Reaction conditions: 54 kDa HDPE bead (350 mg, 1250 mM repeating ethylene unit), $Co(OAc)_2$ (9.7 wt%, 9.6 mM), $Mn(OAc)_2$ (9.5 wt%, 9.6 mM), NHPI (22.4 wt%, 24.0 mM), 8 bar O_2/72 bar He, 0.5-5.5 hr, 160 °C.

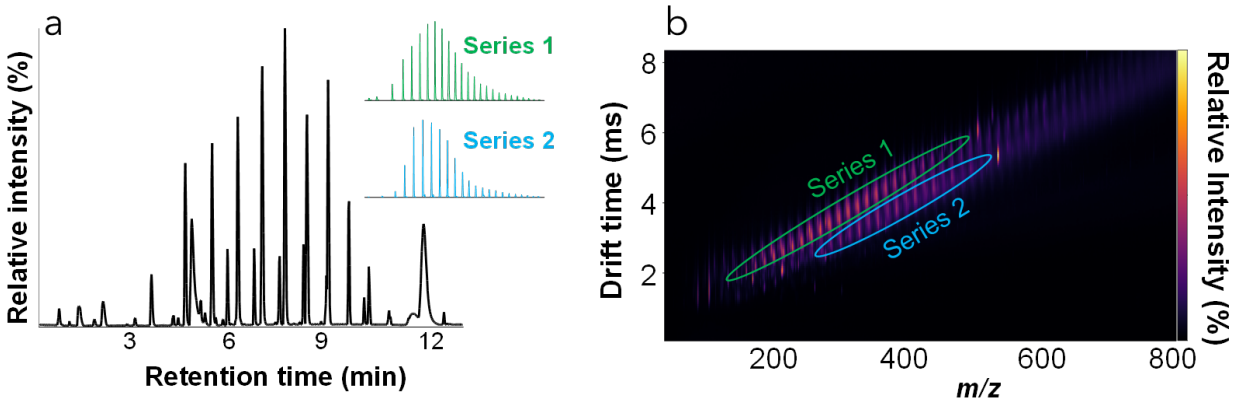

Figure S13. TIC and IMS of homologous series resulting from HDPE autoxidation.
(**a**) Total ion chromatogram of products with insets showing extracted ion chromatograms of two separate homologous compound series, where Series 1 is the dicarboxylic acids and Series 2 is the lactone acids. (**b**) Ion mobility (IMS) spectra confirming each main series structurally differed from each other, but that there were structural similarities within each homologous series, where Series 1 is the dicarboxylic acids and Series 2 is the lactone acids.

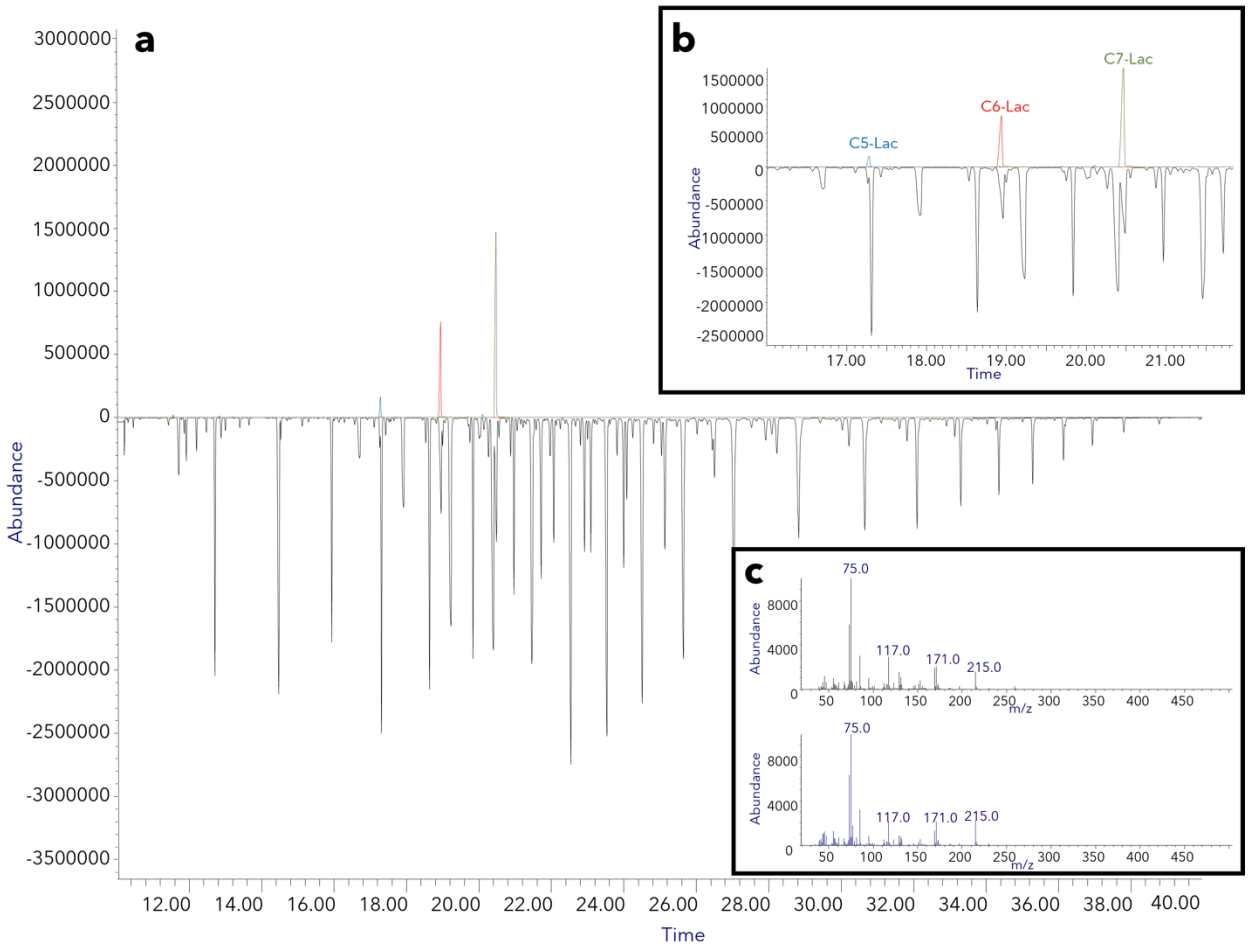

Figure S14. Ion chromatographs of lactone acid standards.
(**a**) Overlaid and inverted extracted ion chromatograms of lactone acid standards (top) and deconstructed HDPE sample (bottom) of m/z 116.7 to 117.7. (**b**) Zoomed-in image from (a) of retention time region containing lactone acids carbon length C_5-C_7. (**c**) Mass spectra of reference from NIST 2017 library of compound 3-(5-oxo-tetrahydrofuran-2-yl)propionic acid, trimethylsilyl (TMS) derivative (bottom blue spectra) and spectra from deconstructed HDPE sample from the retention time 20.467min (C_7-Lac region).

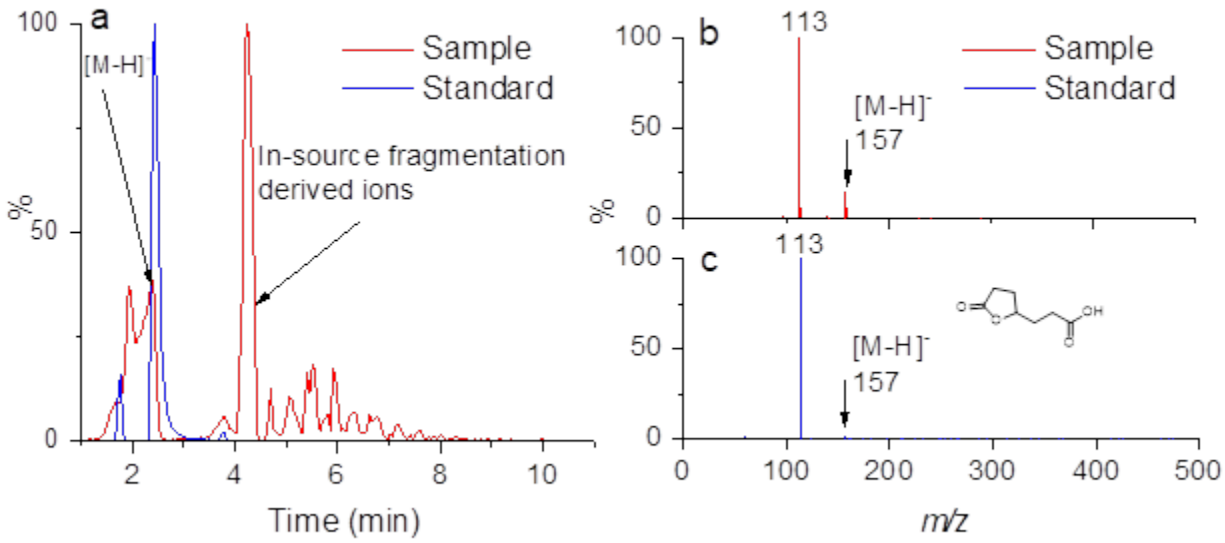

Figure S15. Extracted ion chromatograms for HDPE samples.
(**a**) Extracted ion mass chromatogram overlay of *m/z* 157 from HDPE post-catalysis sample and the corresponding model compound standard. (**b**) MS/MS spectrum of compound *m/z* 157 from HDPE sample. (**c**) MS/MS spectrum of the model compound standard with known structure of C_7-Lac.

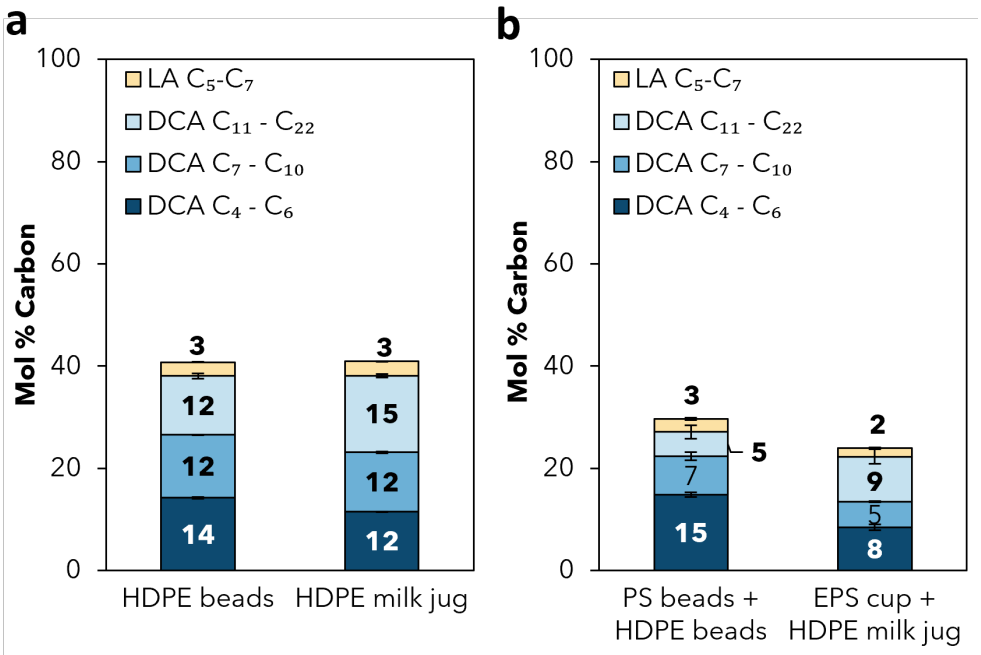

Figure S16. Lactone acid and dicarboxylic acid analysis for (a) HDPE reactions and (b) PS + HDPE reactions.

Dicarboxylic acid and lactone acid product concentrations determined using UHPLC-MS/MS. Mol% carbon yields are calculated as a percentage of carbon in the quantified products relative to the carbon present in the repeating unit of the polymer starting material. Catalyst wt% values are in relation to the total polymer content (mg PS + mg HDPE). (**a**) Plastic content: 350 mg (54 kDa HDPE bead or post-consumer HDPE bottle, 1250 mM repeating ethylene unit), $Co(OAc)_2$ (9.7 wt%, 9.6 mM), $Mn(OAc)_2$ (9.5 wt%, 9.6 mM), NHPI (22.4 wt%, 24.0 mM), 8 bar O_2/72 bar He, 2.5 hr, 160 °C. Error bars indicate standard deviation from triplicate trials. (**b**) Plastic content: 350 mg plastic (175 mg 280 kDa PS bead or EPS cup, 84 mM repeating styrene unit; 175 mg 54 kDa HDPE bead or HDPE bottle, 624 mM repeating ethylene unit), $Co(OAc)_2$ (9.7 wt%, 9.6 mM), $Mn(OAc)_2$ (9.5 wt%, 9.6 mM), NHPI (22.4 wt%, 24.0 mM), 8 bar O_2/72 bar He, 2.5 hr, 160 °C. Error bars indicate standard deviation from triplicate trials.

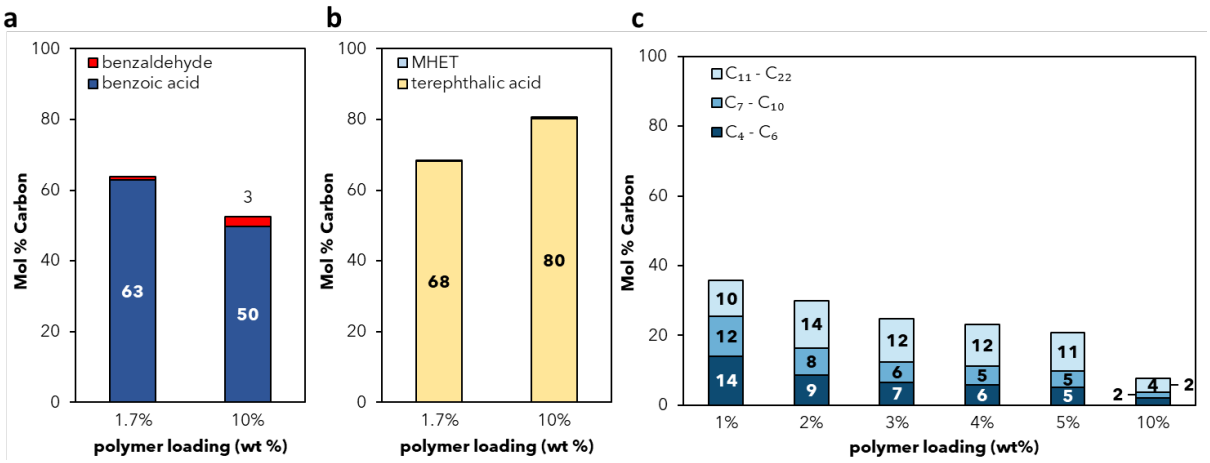

Figure S17. Scale-up experiments for (a) PS, (b) PET, and (c) HDPE.
Conditions: (**a**) PS degradation. Product concentrations determined using HPLC with DAD. Mol% carbon yields are calculated as a percentage of carbon in the quantified products relative to the carbon present in the repeating unit of the polymer starting material. 280 kDa PS beads (500 mg or 2,100 mg, 240 mM or 1,000 mM repeating styrene unit), $Co(OAc)_2$ (34 mg, 9.6 mM), $Mn(OAc)_2$ (33 mg, 9.6 mM), NHPI (39 mg, 24.1 mM). Reactions were pressurized with 8 bar O_2/72 bar N_2 for 3.5 hr at 180 °C, after which they were cooled for 30 min, pressure was outgassed, and reactors were re-pressurized with 8 bar O_2/72 bar N_2. This process was repeated 3X for a total reaction time of 10.5 h reaction time. (**b**) PET degradation. Terephthalic acid (TPA) and 2-hydroxyethyl terephthalic acid (MHET) product concentrations determined using UHPLC with DAD. Mol% carbon yields are calculated as a percentage of carbon in the quantified products relative to the carbon present in the repeating unit of the polymer starting material. 38 kDa PET powder (350 mg or 2,100 mg, 83 mM or 500 mM repeating 2-hydroxyethyl terephthalic acid unit), $Co(OAc)_2$ (34 mg, 9.6 mM), $Mn(OAc)_2$ (33 mg, 9.6 mM), $Zr(acac)_4$ (23 mg, 2.4 mM), NHPI (39 mg, 12.1 mM), 1% H_2O (v/v) at 210 °C. Reactions were pressurized with 8 bar O_2/72 bar N_2 for 3.5 hr at 180 °C, after which they were cooled for 30 min, pressure was released, and reactors were re-pressurized with 8 bar O_2/72 bar N_2. This process was repeated 3X for a total reaction time of 10.5 h reaction time. (**c**) Dicarboxylic acid (DCA) product concentrations (C_4-C_{22}) determined using UHPLC-MS/MS. Mol% carbon yields are calculated as a percentage of carbon in the quantified products relative to the carbon present in the repeating unit of the polymer starting material. 125 kDa HDPE beads (1% = 210 mg, 2% = 420 mg, 3% = 630 mg, 4% = 840 mg, 5% = 1,050 mg, 10% = 2,100 mg), $Co(OAc)_2$ (34 mg, 9.6 mM), $Mn(OAc)_2$ (33 mg, 9.6 mM), NHPI (39 mg, 12.1 mM), 8 bar O_2/72 bar He, 2.5 hr, 160 °C.

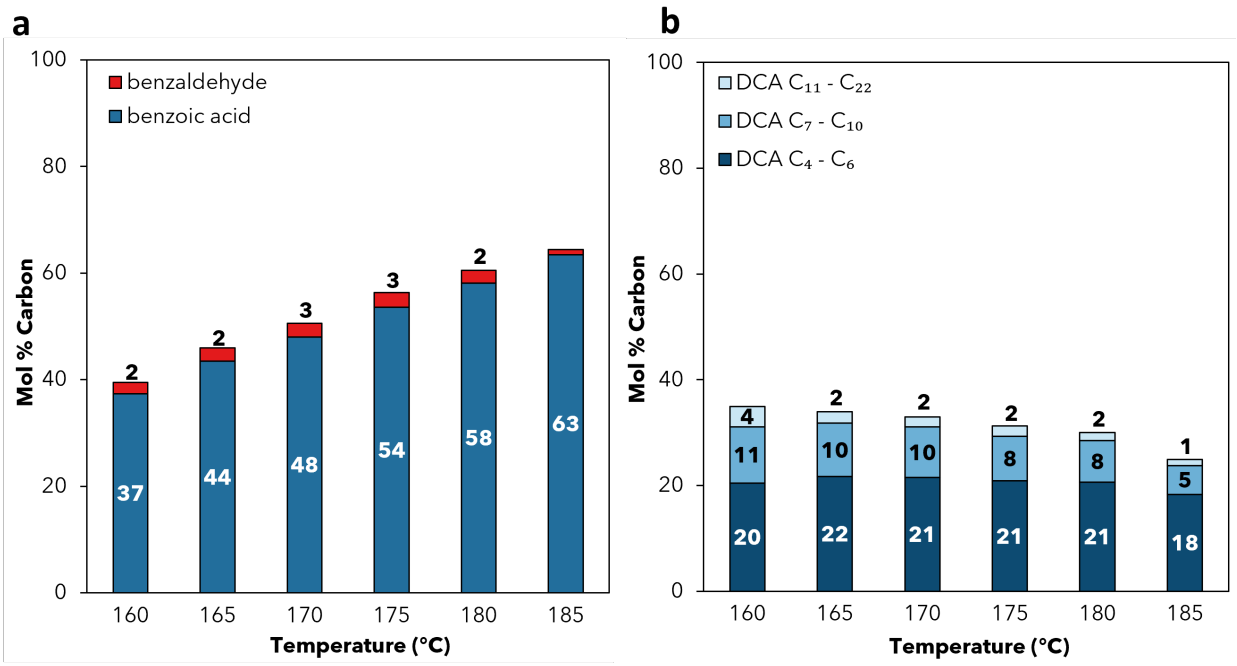

Figure S18. Effect of temperature on deconstruction of mixed PS and HDPE beads. Benzoic acid and benzaldehyde product concentrations from PS were determined using HPLC with DAD, and dicarboxylic acid (DCA) product concentrations (C_4-C_{22}) from HDPE were determined using UHPLC-MS/MS. Mol% carbon yields are calculated as a percentage of carbon in the quantified products relative to the carbon present in the repeating unit of the polymer starting material. Catalyst wt% values are in relation to the total polymer content (mg PS + mg HDPE). Plastic loading 350 mg (100 mg of 54 kDa HDPE beads, 890 mM repeating ethylene unit; 250 mg of 280 kDa PS beads, 120 mM repeating styrene unit), $Co(OAc)_2$ (9.7 wt%, 9.6 mM), $Mn(OAc)_2$ (9.5 wt%, 9.6 mM), NHPI (22.5 wt%, 24.1 mM), 8 bar O_2/72 bar He, 5.5 hr, 160-185 °C. Yields of (**a**) PS-derived products and (**b**) HDPE-derived products.

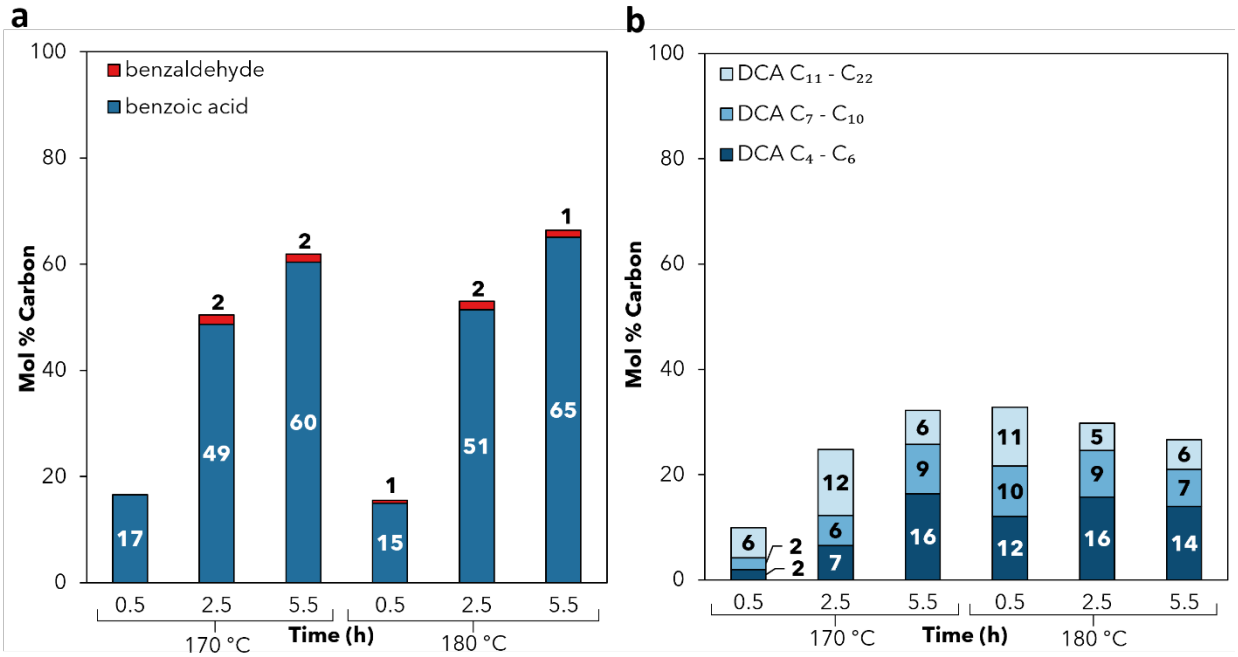

Figure S19. Effect of reaction time on deconstruction of mixed PS and HDPE beads. Benzoic acid and benzaldehyde product concentrations from PS were determined using HPLC with DAD, and dicarboxylic acid (DCA) product concentrations (C_4-C_{22}) from HDPE were determined using UHPLC-MS/MS. Mol% carbon yields are calculated as a percentage of carbon in the quantified products relative to the carbon present in the repeating unit of the polymer starting material. Catalyst wt% values are in relation to the total polymer content (mg PS + mg HDPE). Plastic loading 350 mg (100 mg of 54 kDa HDPE beads, 890 mM repeating ethylene unit; 250 mg of 280 kDa PS beads, 120 mM repeating styrene unit), $Co(OAc)_2$ (9.7 wt%, 9.6 mM), $Mn(OAc)_2$ (9.5 wt%, 9.6 mM), NHPI (22.5 wt%, 24.1 mM), 8 bar O_2/72 bar He, 0.5-5.5 hr, 170 or 180 °C. Yields of (**a**) PS-derived products and (**b**) HDPE-derived products.

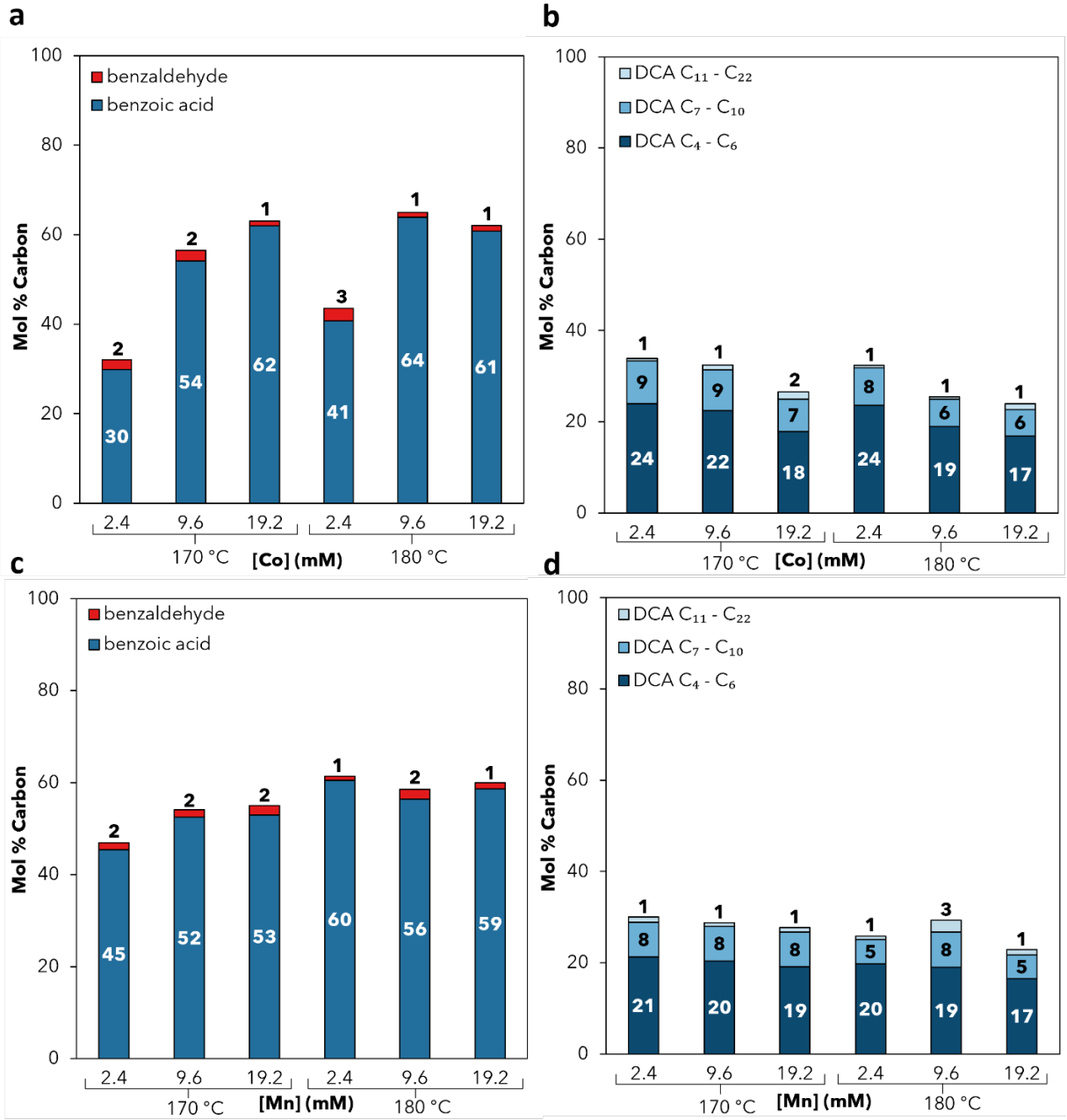

Figure S20. Effect of $Co(OAc)_2$ and $Mn(OAc)_2$ concentrations on deconstruction of mixed PS and HDPE beads.

Benzoic acid and benzaldehyde product concentrations from PS were determined using HPLC with DAD, and dicarboxylic acid (DCA) product concentrations (C_4-C_{22}) from HDPE were determined using UHPLC-MS/MS. Mol% carbon yields are calculated as a percentage of carbon in the quantified products relative to the carbon present in the repeating unit of the polymer starting material. Catalyst wt% values are in relation to the total polymer content (mg PS + mg HDPE). Plastic loading 350 mg (100 mg of 54 kDa HDPE beads, 890 mM repeating ethylene unit; 250 mg of 280 kDa PS beads, 120 mM repeating styrene unit), $Co(OAc)_2$ (2.4-19.4 wt%, 2.4-19.2 mM), $Mn(OAc)_2$ (2.4-19.0 wt%, 2.4-19.2 mM), NHPI (22.5 wt%, 24.1 mM), 8 bar O_2/72 bar He, 5.5hr, 170 or 180 °C. Yields of (**a, c**) PS-derived products and (**b, d**) HDPE-derived products.

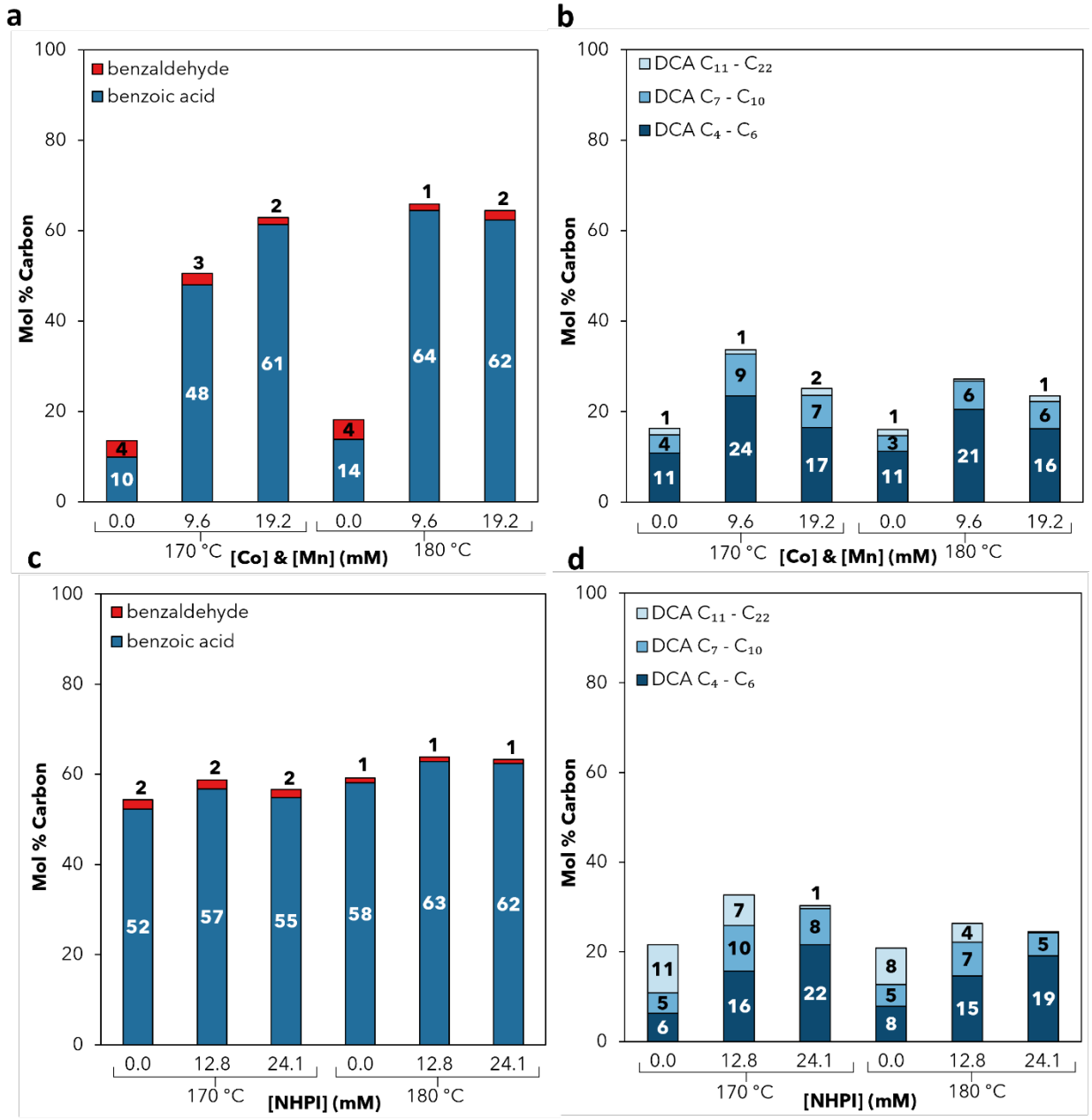

Figure S21. Effect of $Co(OAc)_2$ and $Mn(OAc)_2$ concentrations on deconstruction of mixed PS and HDPE beads.

Benzoic acid and benzaldehyde product concentrations from PS were determined using HPLC with DAD, and dicarboxylic acid (DCA) product concentrations (C_4-C_{22}) from HDPE were determined using UHPLC-MS/MS. Mol% carbon yields are calculated as a percentage of carbon in the quantified products relative to the carbon present in the repeating unit of the polymer starting material. Catalyst wt% values are in relation to the total polymer content (mg PS + mg HDPE). Plastic loading 350 mg (100 mg of 54 kDa HDPE beads, 890 mM repeating ethylene unit; 250 mg of 280 kDa PS beads, 120 mM repeating styrene unit), $Co(OAc)_2$ (2.4-19.4 wt%, 2.4-19.2 mM), $Mn(OAc)_2$ (2.4-19.0 wt%, 2.4-19.2 mM), NHPI (0-22.5 wt%, 0-24.1 mM), 8 bar O_2/72 bar He, 5.5 hr, 170 or 180 °C. Yields of (**a, c**) PS-derived products and (**b, d**) HDPE-derived products.

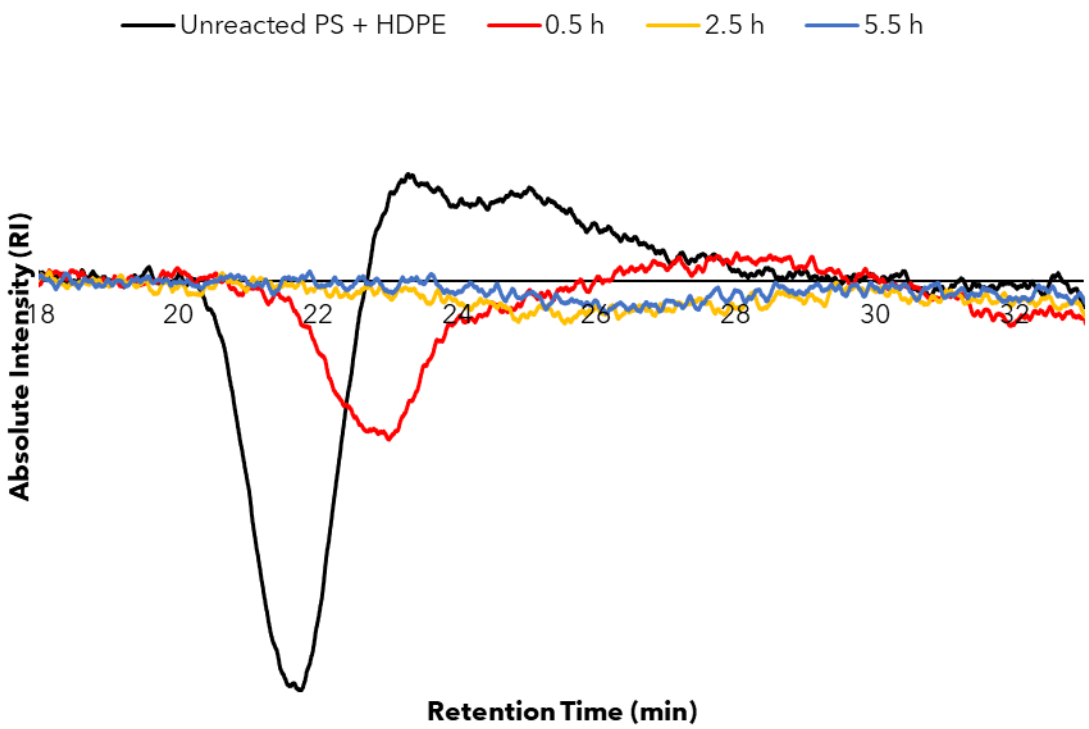

Figure S22. GPC chromatograms for depolymerization of mixed PS and HDPE at different reaction times.

HT-GPC traces were measured at 160 °C using a DRI detector using trichlorobenzene as solvent and compared to known PS standards. Under these conditions, PS presents as a negative peak and HDPE as a positive peak. Conditions: Plastic loading 350 mg (100 mg of 54 kDa HDPE beads, 890 mM repeating ethylene unit; 250 mg of 280 kDa PS beads, 120 mM repeating styrene unit), $Co(OAc)_2$ (9.7 wt%, 9.6 mM), $Mn(OAc)_2$ (9.5 wt%, 9.6 mM), NHPI (22.5 wt%, 24.1 mM), 8 bar O_2/72 bar He, 0.5-5.5 hr, 170 °C.

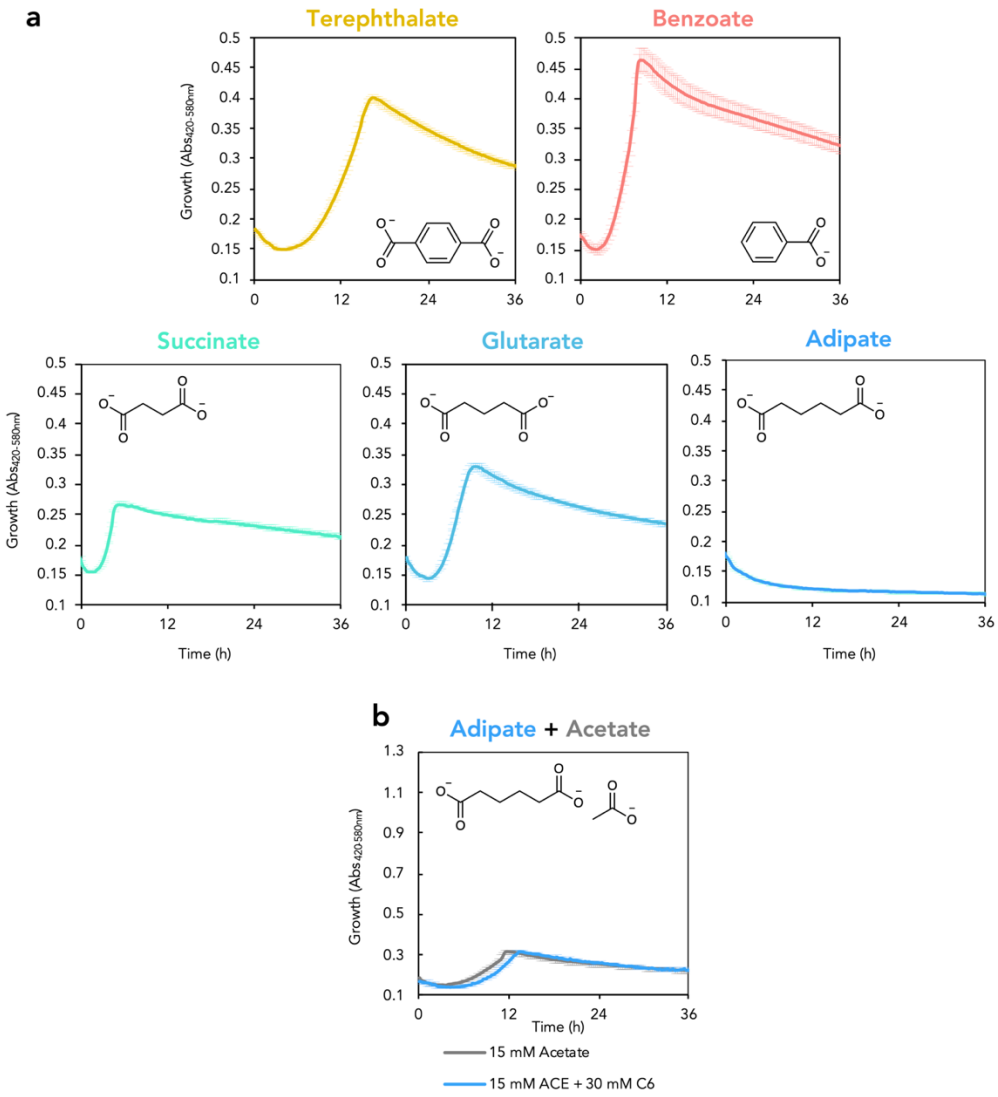

Figure S23. Growth of strain RC026 on model compounds predicted to be released by oxidative deconstruction of PET, PS, and HDPE.
(**a**) RC026 was cultivated in M9 minimal medium supplemented with 5 mM of each specified compound individually. (**b**) RC026 was cultivated in M9 minimal medium supplemented with 15 mM acetate or 15 mM acetate and 30 mM of adipate. Wideband absorbance (420-580 nm) was monitored in a BioscreenC®. n=3; average ± standard deviation. The RC026 genotype is provided in **Table S6**.

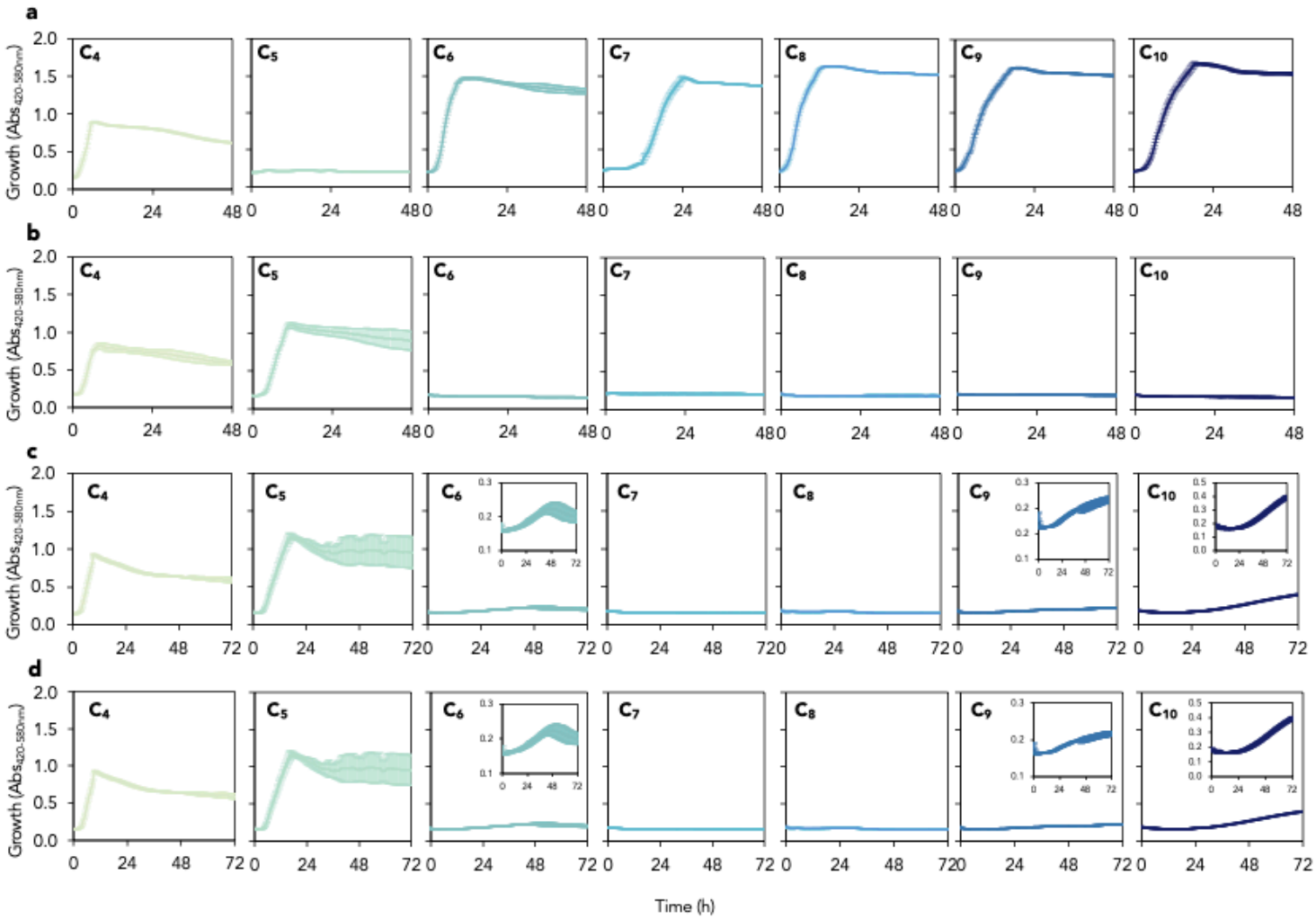

Figure S24. Growth of wild-type and engineered strains on C_4 through C_{10} dicarboxylates as sole carbon and energy sources. Growth of (**a**) *A. baylyi,* (**b**) wild-type *P. putida,* (**c**) AW061, and (**d**) AW074 on C_4 through C_{10} dicarboxylates individually as the sole carbon and energy source. Strains were cultivated in M9 minimal medium supplemented with 15 mM of each specified compound individually. Wideband absorbance (420-580 nm) was monitored in a BioscreenC®. n=3; average ± standard deviation. C_4, succinate; C_5, glutarate; C_6, adipate; C_7, pimelate; C_8, suberate; C_9, azelate; C_{10}, sebacate. Strain genotypes are provided in **Table S6**.

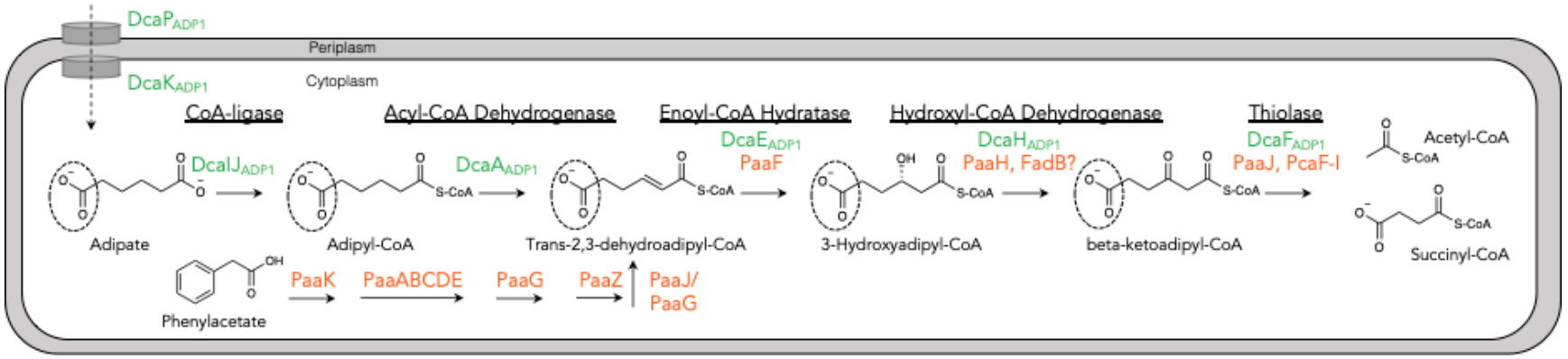

Figure S25. Proposed metabolic pathway for catabolism of adipate and phenylacetate by a metabolically engineered *P. putida* strain.

Orange text indicates enzymes encoded by genes native to *P. putida*. Green text indicates proteins/enzymes encoded by genes native to *A. baylyi*. The proposed spatial localization is indicated by the ovals indicating extracellular, periplasmic, and cytoplasmic space. Dashed circles indicate potential R groups (e.g., potential activity on compounds of a different chain length).

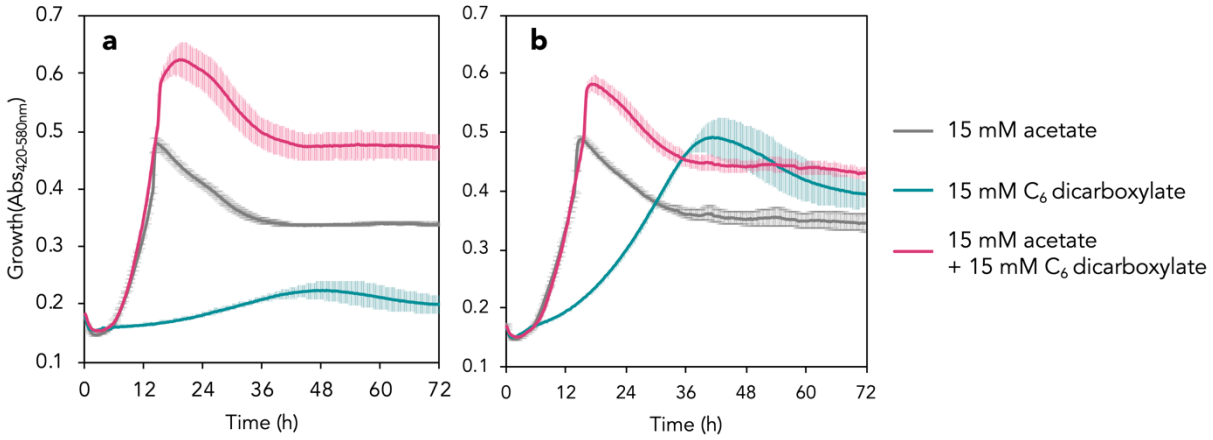

Figure S26. Growth of engineered *P. putida* on C_6 dicarboxylate with or without acetate. Growth of (**a**) AW061 and (**b**) AW074 on 15 mM acetate, 15 mM C_6 dicarboxylate, or 15 mM acetate plus 15 mM C_6 dicarboxylate. Strains were cultivated in M9 minimal medium supplemented with the specified compound(s). Wideband absorbance (420-580 nm) was monitored in a BioscreenC®. n=3; average ± standard deviation. Strain genotypes are provided in **Table S6**.

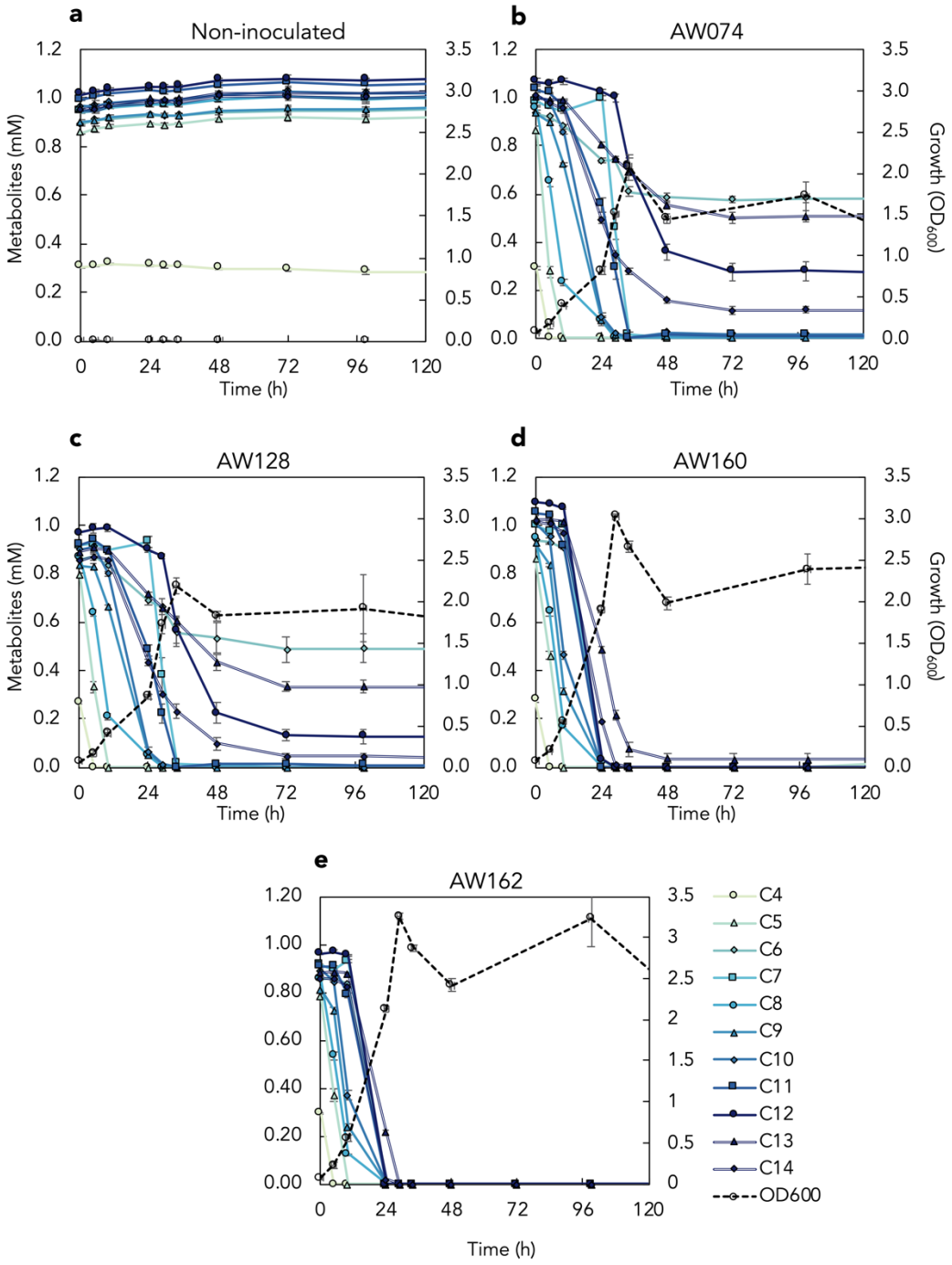

Figure S27. Utilization of mixed dicarboxylates by engineered *P. putida*.
Cultivation of (**a**) non-inoculated, (**b**) AW074, (**c**) AW128, (**d**) AW160 and (**c**) AW162 in M9 minimal medium supplemented with 8 mM acetate and the depicted concentrations of dicarboxylates C_4 through C_{14}. Cultivations were performed in shake flasks. n=3; average ± standard deviation. Strain genotypes are provided in **Table S6**. C_4, succinate; C_5, glutarate; C_6, adipate; C_7, pimelate; C_8, suberate; C_9, azelate; C_{10}, sebacate; C_{11}, undecanedioate; C_{12}, dodecanedioate; C_{13}, tridecanedioate; C_{14}, tetradecanedioate; OD600, optical density measured at 600 nm.

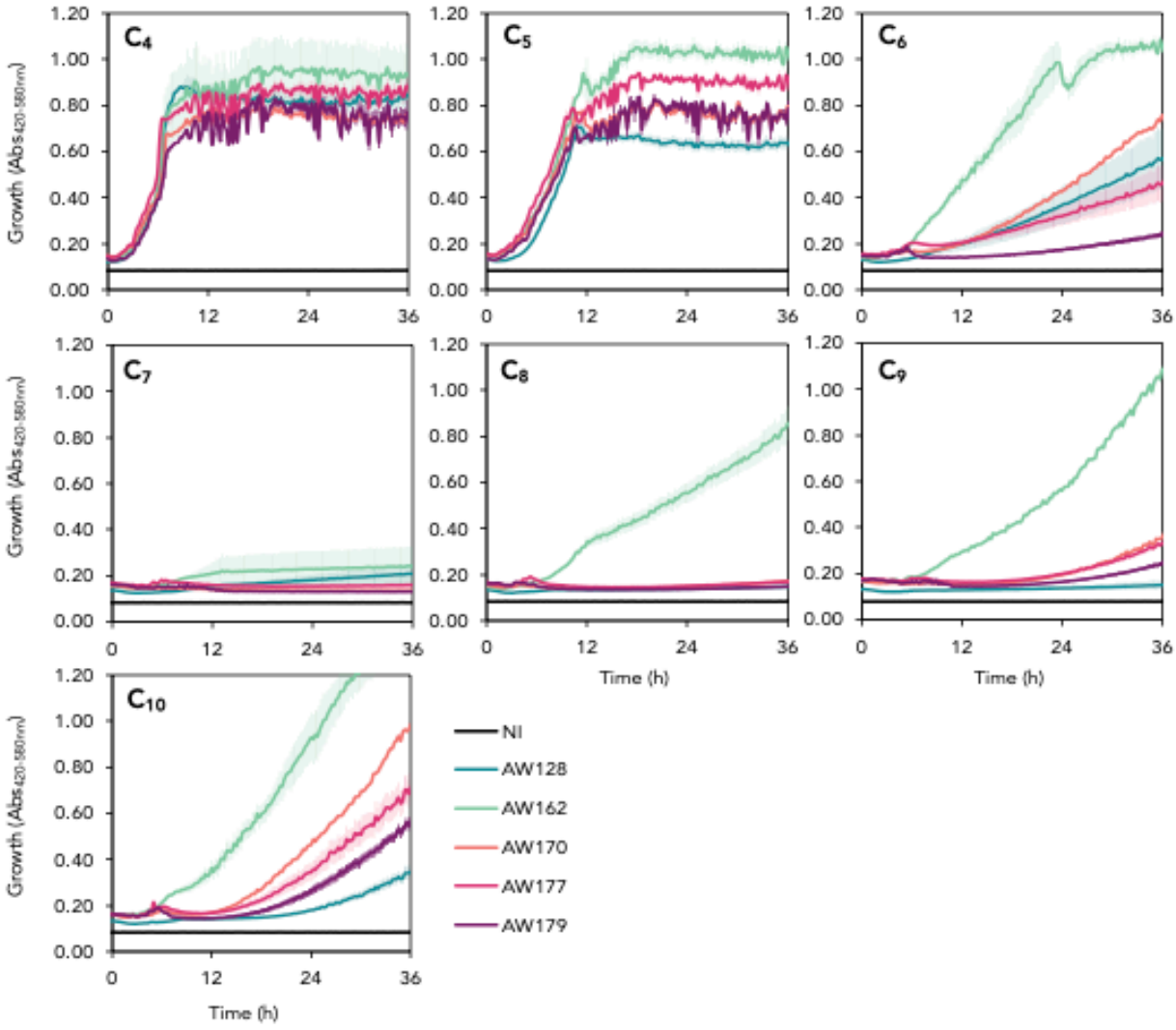

Figure S28. Growth of engineered *P. putida* strains on C_4 through C_{10} dicarboxylates individually.

Non-inoculated (NI) controls, AW128, AW170, AW162, AW177, or AW179 was cultivated in M9 minimal medium supplemented with 10 mM of each dicarboxylate. Wideband absorbance (420-580 nm) was monitored in a BioscreenC®. n=3; average ± standard deviation. Strain genotypes are provided in in **Table S6**. C_4, succinate; C_5, glutarate; C_6, adipate; C_7, pimelate; C_8, suberate; C_9, azelate; C_{10}, sebacate.

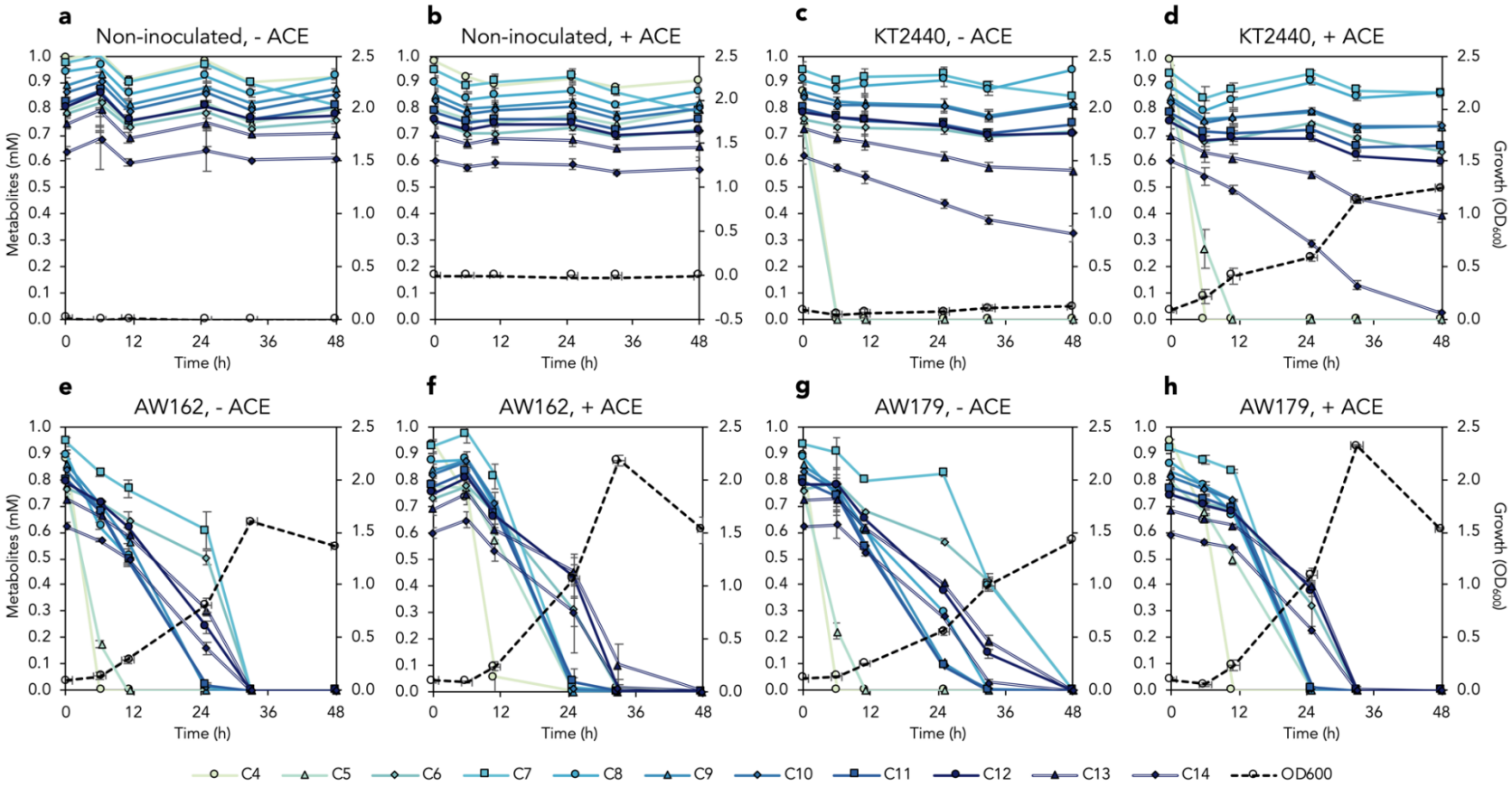

Figure S29. Growth and utilization of mixed C_4 through C_{14} dicarboxylates without or with acetate by wild-type or engineered *P. putida*.

Cultivations were performed in M9 minimal medium supplemented with ~1 mM each of C_4, C_5, C_6, C_7, C_8, C_9, C_{10}, C_{11}, C_{12}, C_{13}, and C_{14} dicarboxylates of (**a**) non-inoculated controls, (**c**) wild-type *P. putida*, (**e**) AW162, and (**g**) AW179. Cultivations were performed in M9 minimal medium supplemented with ~1 mM of C_4, C_5, C_6, C_7, C_8, C_9, C_{10}, C_{11}, C_{12}, C_{13}, and C_{14} dicarboxylates plus 20 mM acetate and fed to 20 mM acetate at 24 h of (**b**) non-inoculated controls, (**d**) wild-type *P. putida*, (**f**) AW162, and (**h**) AW170. n=3; average ± standard deviation. Strain genotypes are provided in **Table S6**. C_4, succinate; C_5, glutarate; C_6, adipate; C_7, pimelate; C_8, suberate; C_9, azelate; C_{10}, sebacate; C_{11}, undecanedioate; C_{12}, dodecanedioate; C_{13}, tridecanedioate; C_{14}, tetradecanedioate..

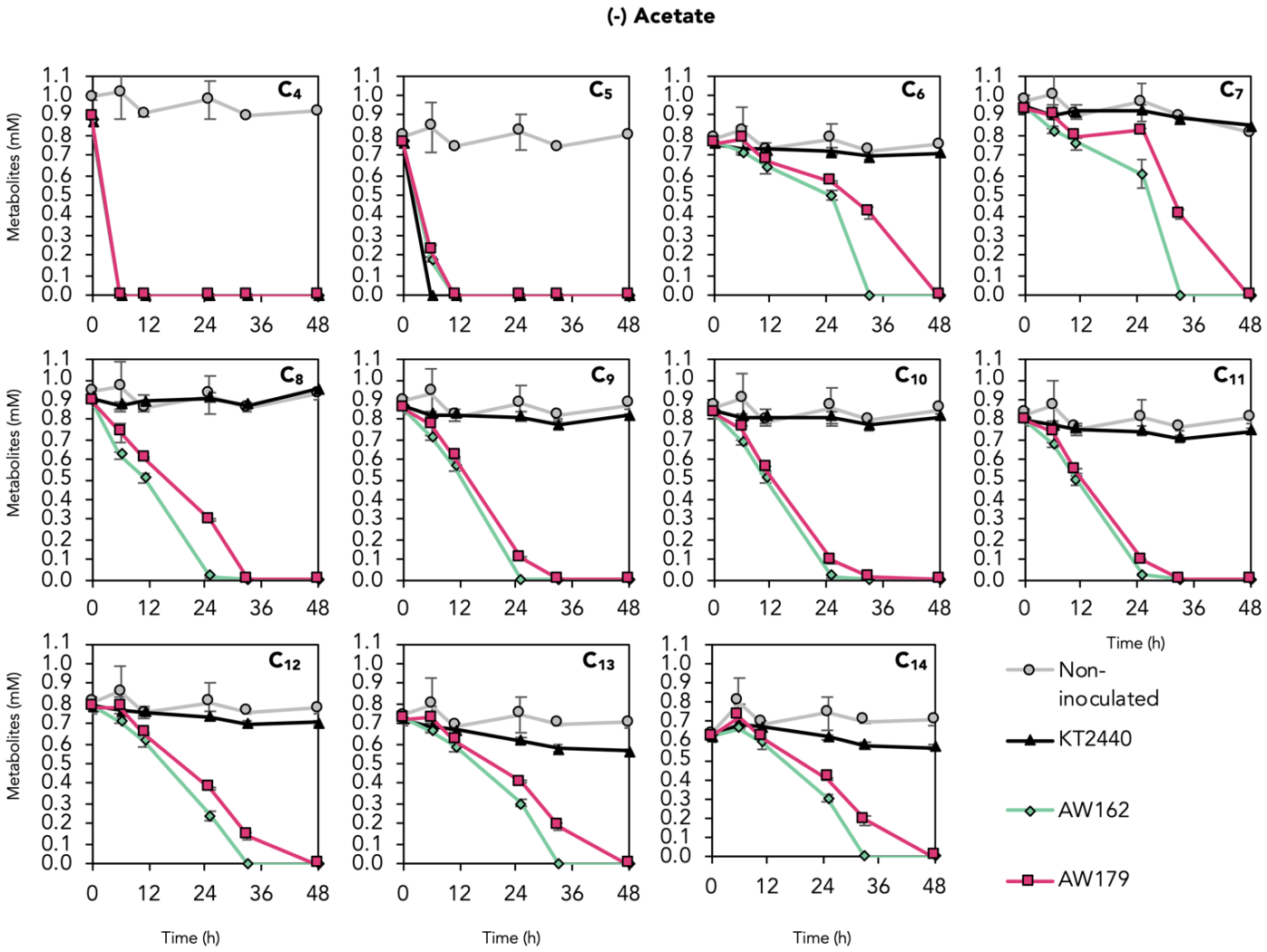

Figure S30. Utilization of mixed C_4 through C_{14} dicarboxylates without acetate supplementation.
Each dicarboxylate is plotted individually for non-inoculated, wild-type *P. putida*, AW162, and AW179 cultivations. See **Figure S29** for additional information and growth data. n=3; average ± standard deviation. Strain genotypes are provided in **Table S6**. C_4, succinate; C_5, glutarate; C_6, adipate; C_7, pimelate; C_8, suberate; C_9, azelate; C_{10}, sebacate; C_{11}, undecanedioate; C_{12}, dodecanedioate; C_{13}, tridecanedioate; C_{14}, tetradecanedioate.

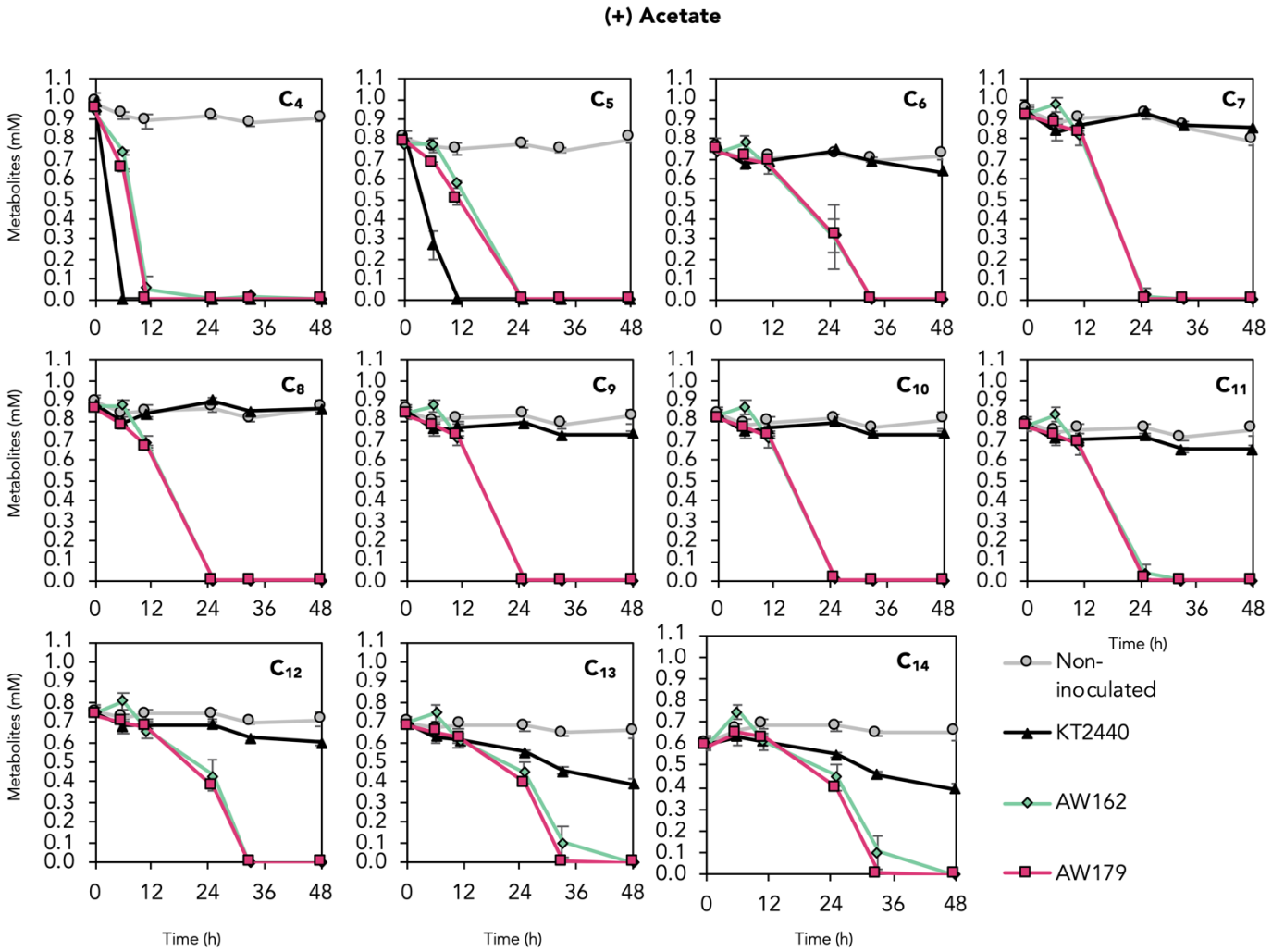

Figure S31. Utilization of mixed C_4 through C_{14} dicarboxylates with acetate supplementation.
Each dicarboxylate is plotted individually for non-inoculated, wild-type *P. putida*, AW162, and AW179 cultivations. See **Figure S29** for additional information and growth data. n=3; average ± standard deviation. Strain genotypes are provided in **Table S6**. C_4, succinate; C_5, glutarate; C_6, adipate; C_7, pimelate; C_8, suberate; C_9, azelate; C_{10}, sebacate; C_{11}, undecanedioate; C_{12}, dodecanedioate; C_{13}, tridecanedioate; C_{14}, tetradecanedioate.

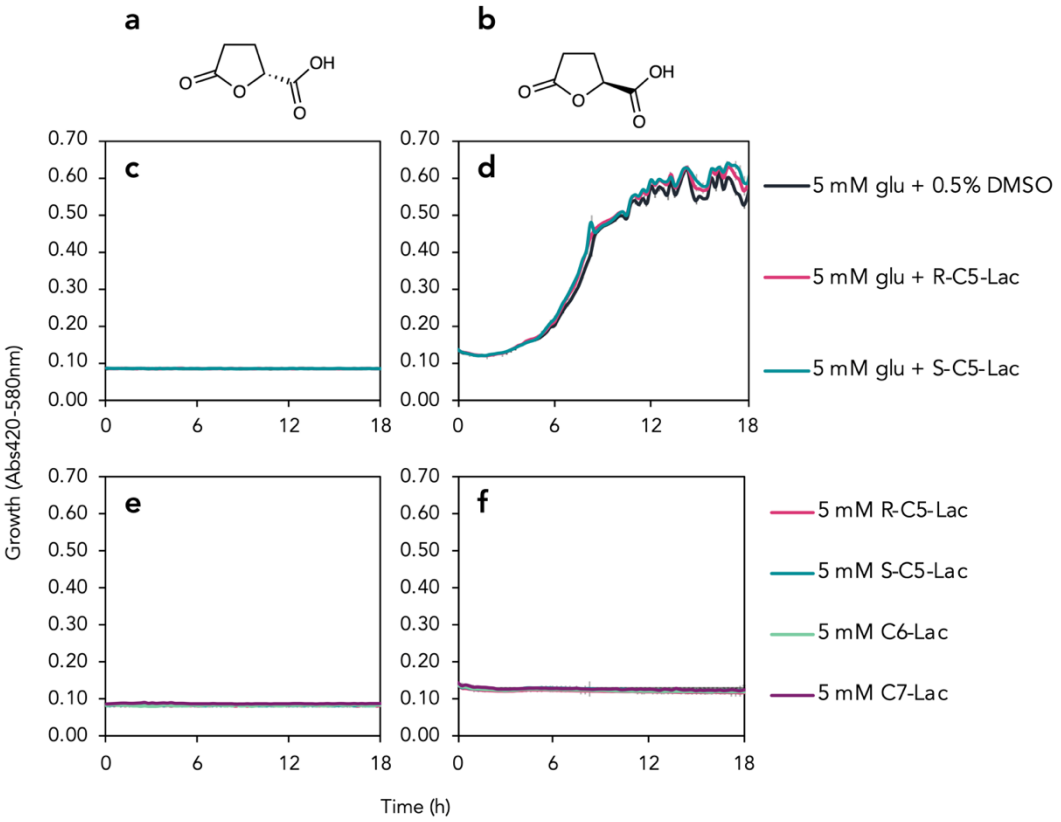

Figure S32. Growth of *P. putida* AW162 on HDPE-related lactone compounds.
Structure of (**a**) *R*-C_5-Lac ((*R*)-(−)-5-oxo-2-tetrahydrofurancarboxylic acid) and (**b**) *S*-C_5-Lac ((*S*)-(+)-5-oxo-2-tetrahydrofurancarboxylic acid) compounds. Cultivation of (**c**) non-inoculated controls or (**d**) AW162 in M9 minimal medium supplemented with 5 mM glucose (glu) plus 0.5% (v/v) DMSO, 5 mM glu plus 5 mM *R*-C_5-Lac, or 5 mM glu plus 5 mM *S*-C_5-Lac. Cultivation of (**e**) non-inoculated control or (**f**) AW162 in 5 mM *R*-C_5-Lac, *S*-C_5-Lac, C_6-Lac, or C_7-Lac as a sole carbon and energy source. Wideband absorbance (420-580 nm) was monitored in a BioscreenC®. n=3; average ± standard deviation. Strain genotypes are provided in **Table S6**.

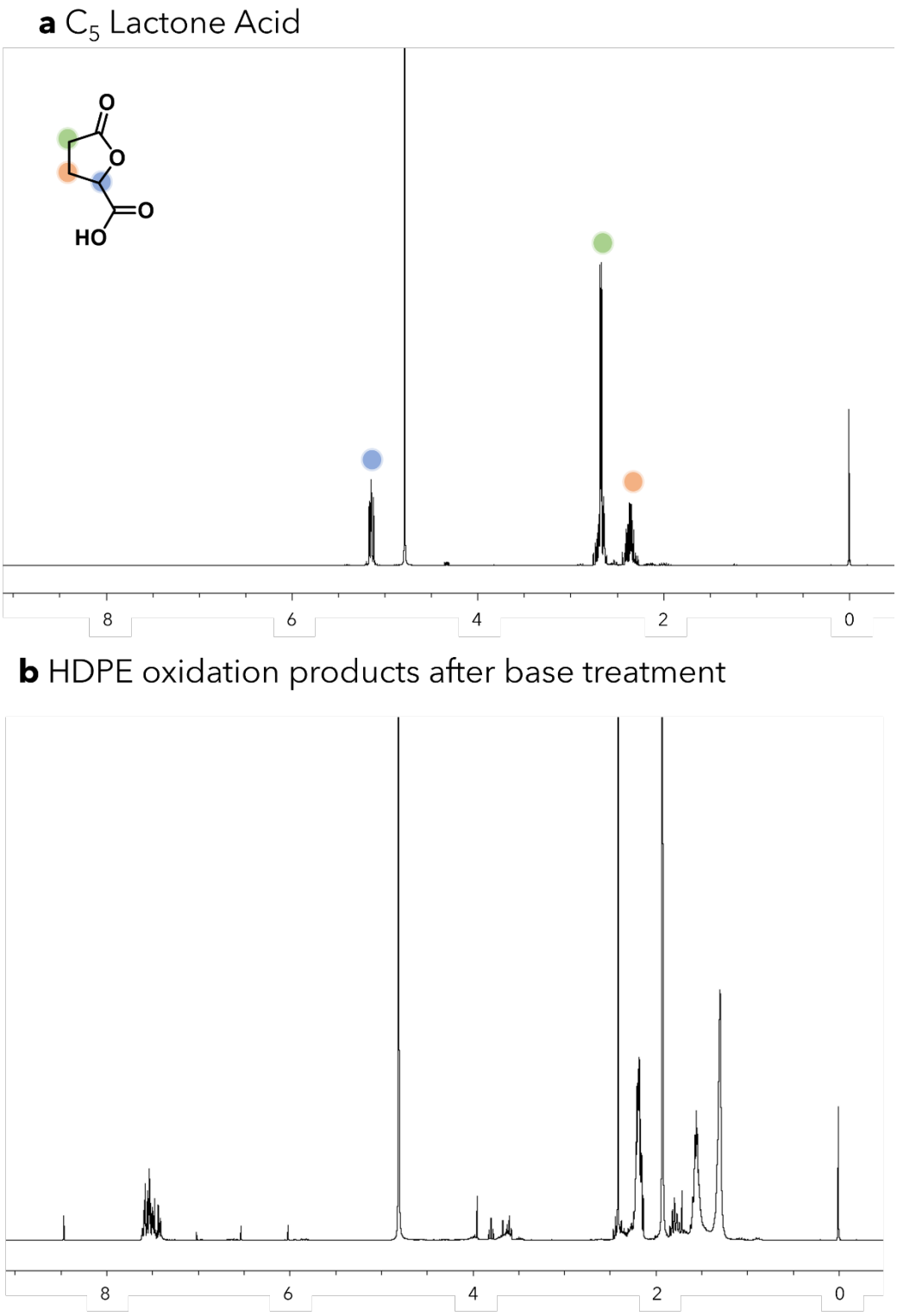

Figure S33. ^{1}H NMR spectra of (S)-(+)-5-oxo-2-tetrahydofurancarboxylic acid and base-treated HDPE products.
(**a**) *R*-C_5-Lac and (**b**) HDPE oxidation products after base treatment in D_2O. Oxidation products post-treatment with base do not show any remaining lactone presence.

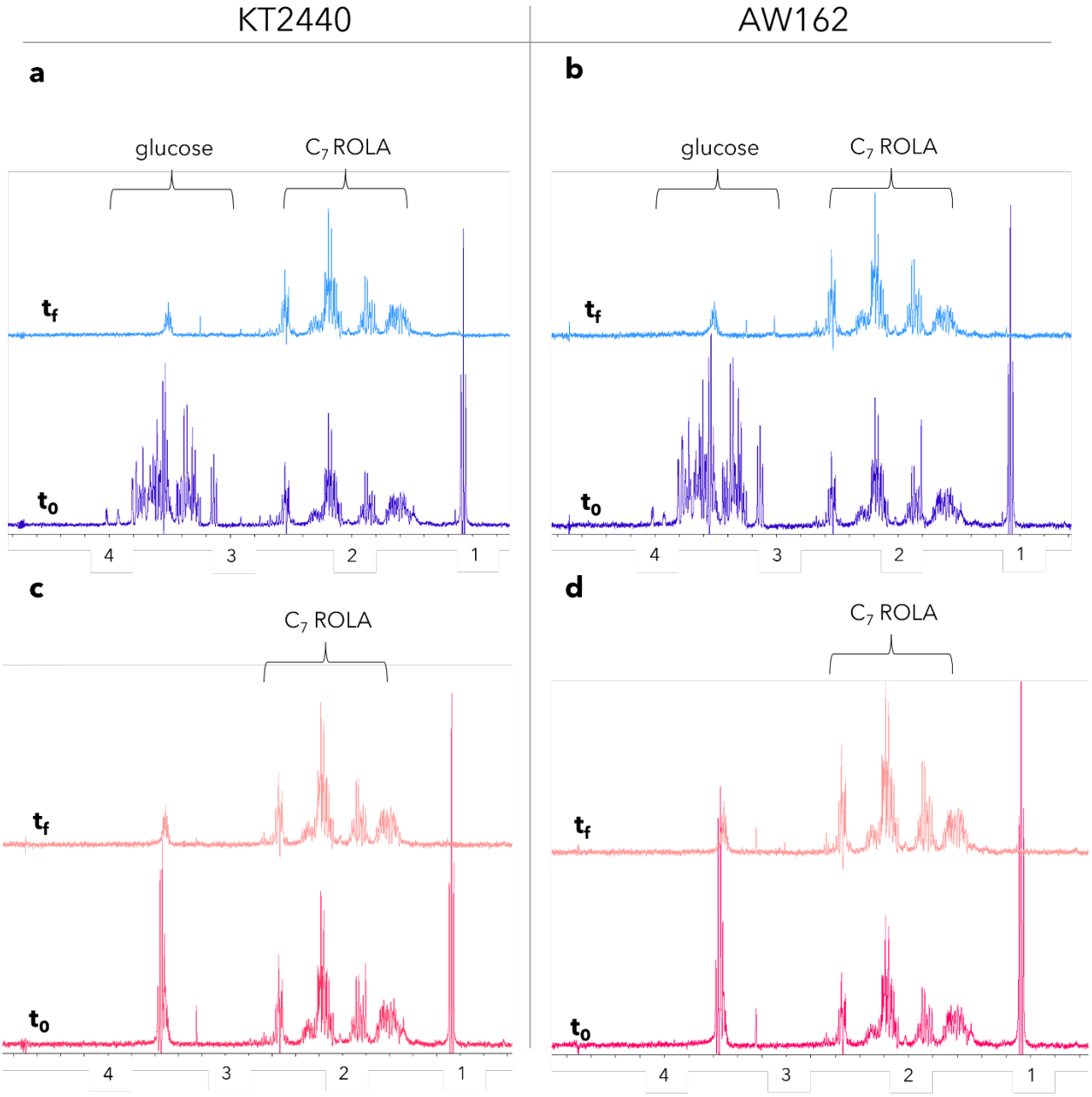

Figure S34. Cultivation and ^{1}H NMR spectra of wild-type and engineered *P. putida* on a C_7 ring-opened lactone acid (ROLA).

^{1}H NMR spectra of pre- (t_0) and post- (t_f) metabolism of C_7 ring-opened lactone acid (C_7 ROLA) or glucose using (**a, c**) wild-type or (**b, d**) AW162. Metabolism of mixed glucose and C_7 ROLA substrates (**a** and **c**) shows complete glucose consumption and no C_7 ROLA consumption. Metabolism of C_7 ROLA as the sole substrate (**b** and **d**) shows no consumption of the C_7 ROLA.

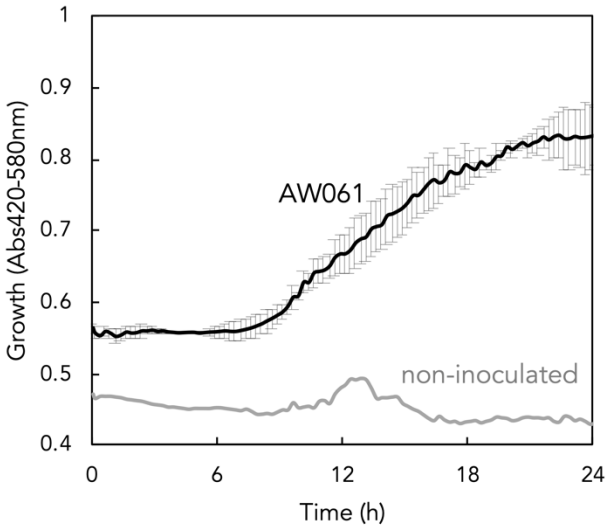

Figure S35. Growth of engineered *P. putida* in the presence of catalyst and initiator.
Growth of AW061 or non-inoculated control in M9 minimal medium supplemented with 1 mM NHPI, 1 mM $Co(OAc)_2$, 1 mM $Mn(OAc)_2$, and 5 mM each of benzoate, terephthalate, acetoxyacetate, glycolate, formate, succinate, glutarate, and adipate each. Wideband absorbance (420-580 nm) was monitored in a BioscreenC®. n=3; average ± standard deviation. Strain genotypes are provided in **Table S6**.

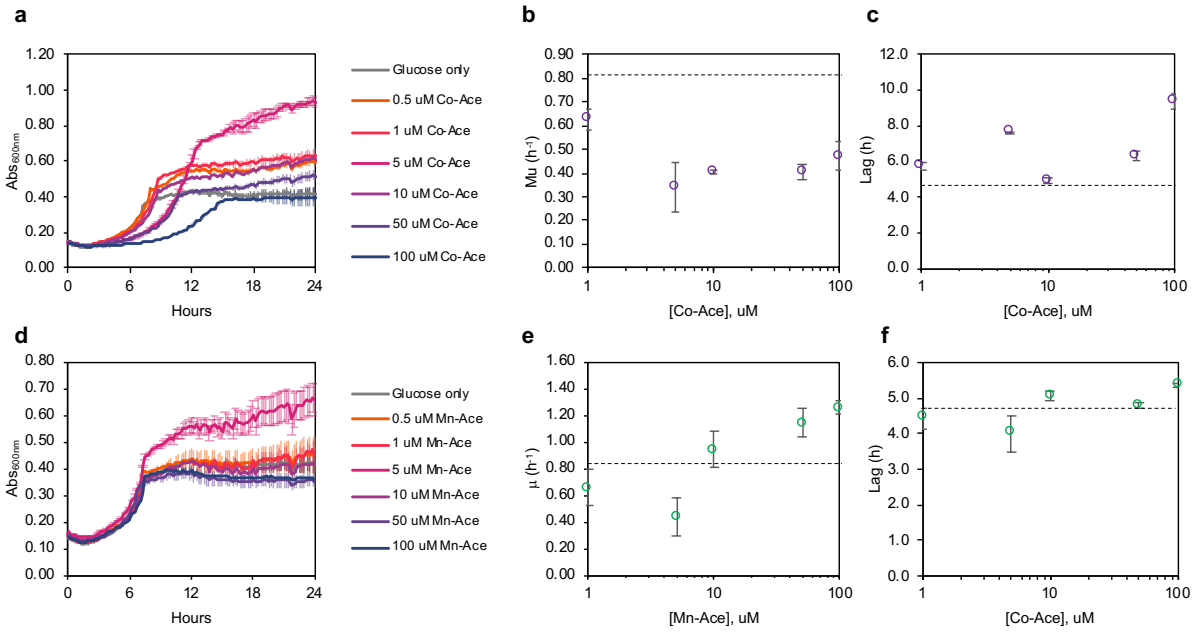

Figure S36. Effect of cobalt and manganese on the growth of AW162 in 10 mM glucose. (**a**) Growth curves for AW162 cultivated in 10 mM of glucose only, or 10 mM glucose plus 0.5, 1, 5, 10, 50, or 100 mM of cobalt acetate (Co-Ace). (**b**) Growth rate and (**c**) lag phase for each concentration of Co-Ace supplementation as calculated by a Gompertz fit (*53*) of the data in (**a**) (**d**) Growth curves for AW162 cultivated in 10 mM of glucose only, or 10 mM glucose plus 0.5, 1, 5, 10, 50, or 100 mM of manganese acetate (Mn-Ace) supplementation. (**e**) Growth rate and (**f**) lag phase for each concentration of Mn-Ace supplementation as calculated by a Gompertz fit (*53*) of the data in (**c**) . Dashed lines indicate the growth rate or lag observed without any supplemented metals. Plots depict average ± standard deviation, n=3. Cultivations were performed in a BioscreenC. Note that (**b-c**) and (**e-f**) plot [Co-Ace] and [Mn-Ace] on a $\log_{10}$ scale.

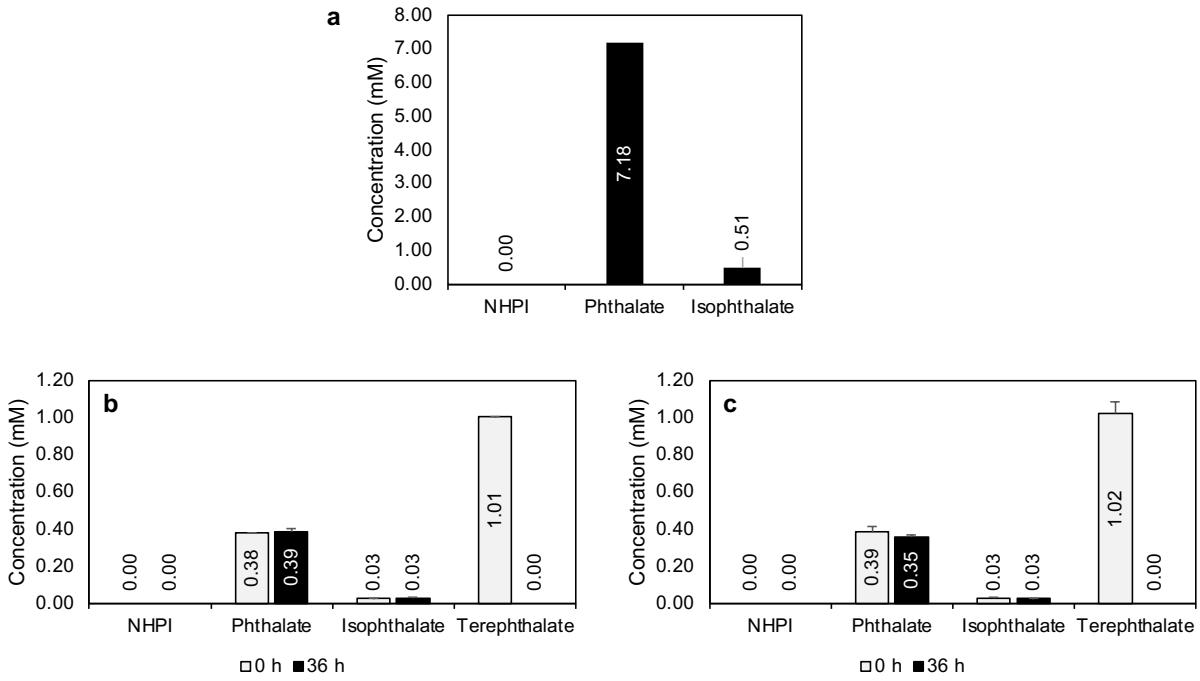

Figure S37. *N*-hydroxyphthalimide concentrations in microbial cultivations.
(**a**) Concentration of *N*-hydroxyphthalimide (NHPI), phthalate, and isophthalate in effluent prepared from mixed HDPE, PS, and PET commercial resin. NHPI, phthalate, isophthalate, and terephthalate concentrations in initial (t_0) and final (t_f) time-points from (**c**) AW162 and (**d**) AW307 cultivations in effluent from mixed PET, PS, and HDPE commercial resin. Plot depicts average ± standard deviation, n=3.

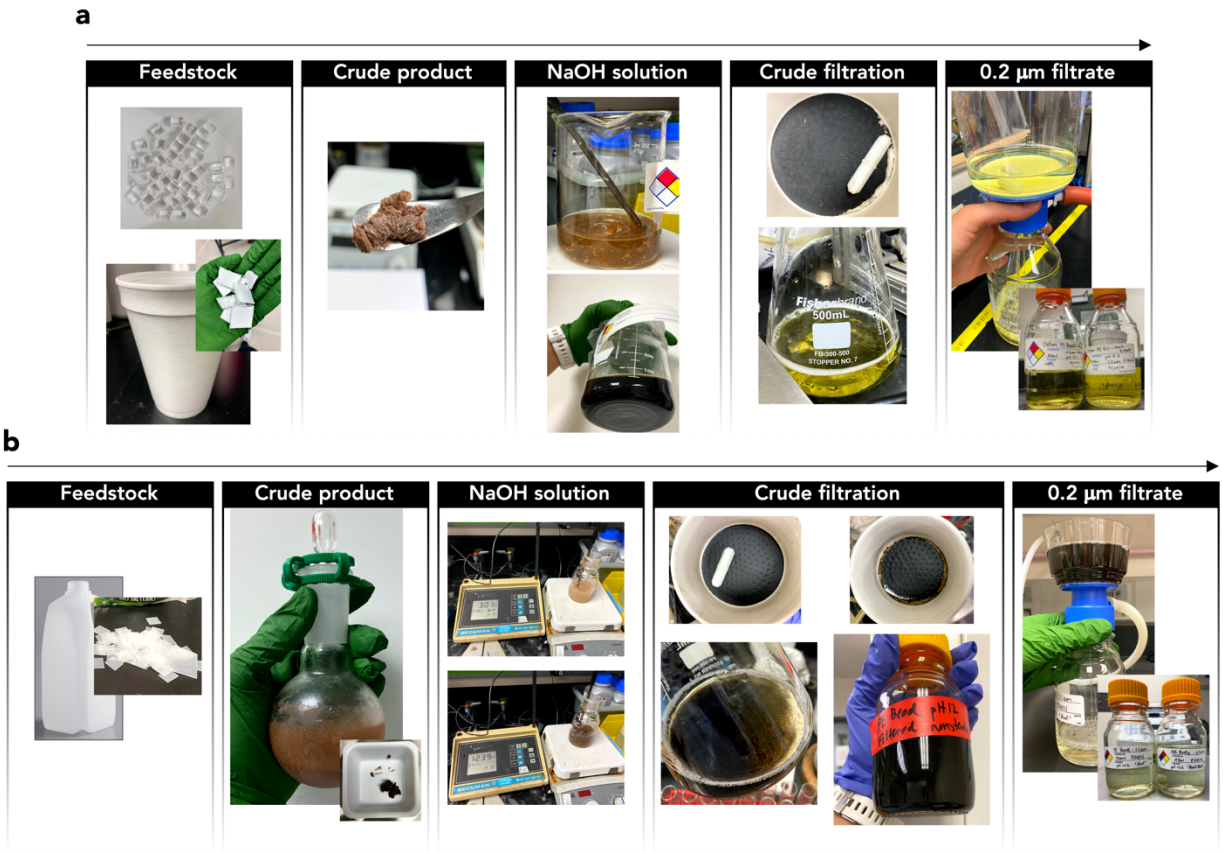

Figure S38. Workflow for preparation of effluent from single-component and mixed plastics.

(**a**) Photos of preparation of PS feedstocks for bioconversion. PS beads or post-consumer EPS cups were catalytically deconstructed, and the crude product was added to water. NaOH was added to solution to pH-adjust (top, upon addition of water to crude product; bottom, after pH adjusting to pH >8). The crude filtrate (top, filter cake; bottom, filtrate), and the sterilized filtrate. (**b**) Photos of HDPE feedstock (top, HDPE beads; bottom, post-consumer HDPE bottle), the crude deconstructed product, the NaOH adjusted solution (top, upon addition to water, pH 3.01; bottom, upon pH adjustment to 12.39), the crude filtration (top, crude filter cake; bottom, the crude filtrate), and the filtration for sterilization. The final solution is referred to as the effluent. The 0.2 mM filtrate (yellow solutions on far left-hand side of (a) and (b)) were mixed with solutions of M9 minimal medium components (1 M calcium chloride, 100 mM iron sulfate, 1 M magnesium sulfate, 10X M9 Salts containing disodium phosphide, monopotassium phosphate, sodium chloride, ammonium chloride, and water). This results in a dilution of the concentration of plastic-derived substrates present in the microbial cultivations as compared to the effluent solution. Measured concentrations in the effluent solutions are provided in **Tables S9-11** and measured concentrations at t_0 in each shake flask are provided in **Supplementary Excel 1**."

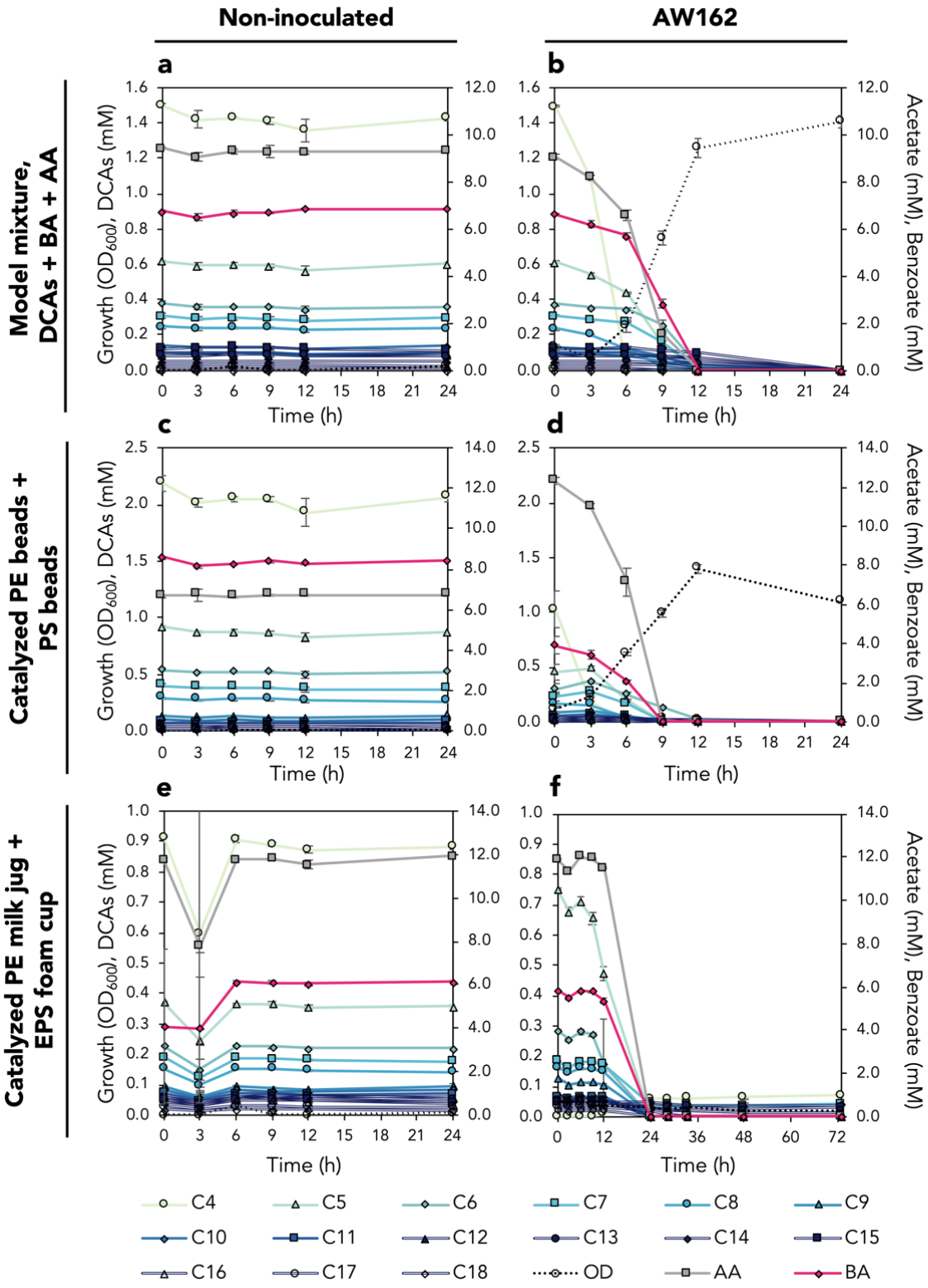

Figure S39. Microbial growth and dicarboxylate utilization from effluent from mixed PS and HDPE (commercial polymer resin or post-consumer products) by engineered *P. putida*. (**a**) Non-inoculated and (**b**) AW162 cultivations in commercial benzoate, acetate, and dicarboxylates with 4, 5, 6, 7, 8, 9, 10, 11, 12, 13, 14, 15, 16, 17, or 18 carbons (C_4-C_{18},

respectively). (**c**) Non-inoculated and (**d**) AW162 cultivations in effluent from mixed HDPE beads and PS beads. (**e**) Non-inoculated and (**f**) AW162 cultivations in effluent from mixed post-consumer HDPE bottle and EPS cups. n=3; average ± standard deviation. Cultivations were performed in shake flasks. Strain genotypes are provided in **Table S6**. BA, benzoate; AA, acetate; C_4, succinic acid; C_5, glutaric acid; C_6, adipic acid; C_7, pimelic acid; C_8, suberic acid; C_9, azelaic acid; C_{10}, sebacic acid; C_{11}, undecanedioic acid; C_{12}, dodecanedioic acid; C_{13}, tridecanedioic acid; C_{14}, tetradecanedioic acid; C_{15}, pentadecanedioic acid; C_{16}, hexadecanedioic acid; C_{17}, heptadecanedioic acid; C_{18}, octadecanedioic acid; OD, optical density measured at 600 nm. Note that y-axis scales are different across the panels.

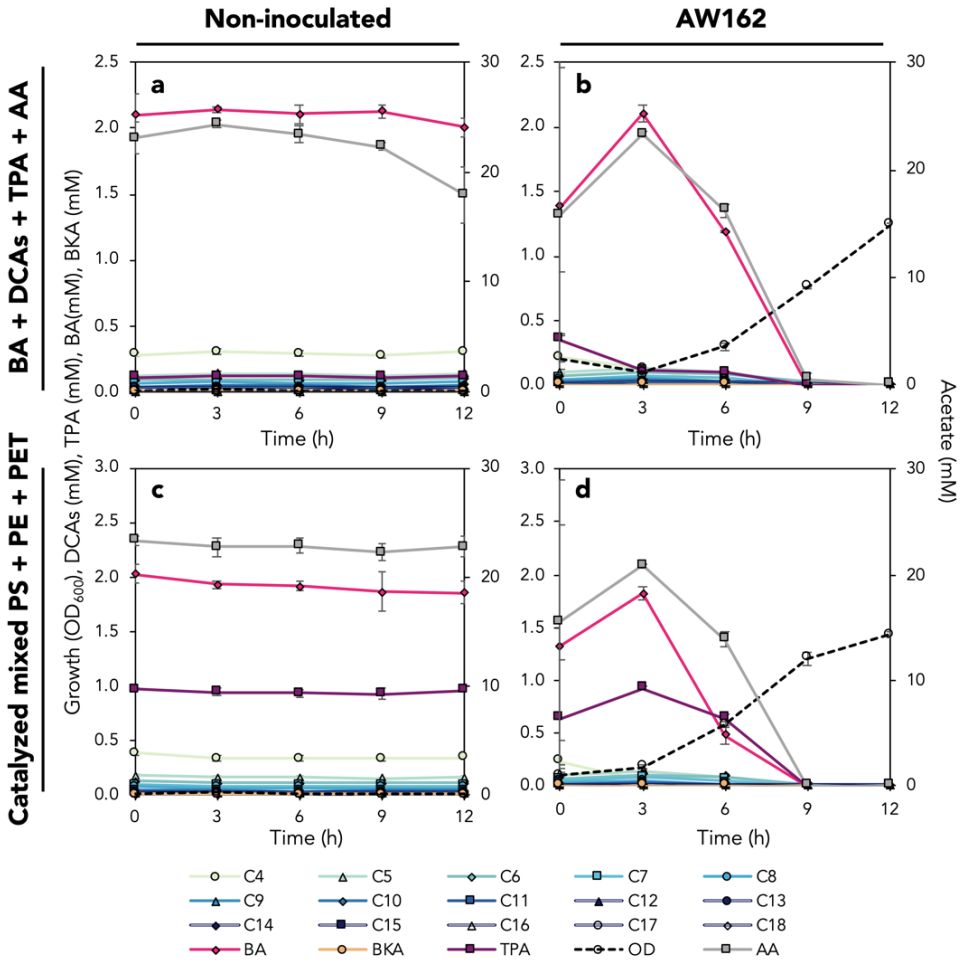

Figure S40. Microbial growth in effluent from mixed PS, HDPE, and PET commercial polymer resin.
(**a**) Non-inoculated and (**b**) AW162 cultivations in commercial benzoate, dicarboxylates with 4, 5, 6, 7, 8, 9, 10, 11, 12, 13, 14, 15, 16, 17, or 18 carbons (C_4-C_{18}, respectively), terephthalate, and acetate. (**c**) Non-inoculated and (**d**) AW162 cultivations in effluent from mixed HDPE beads, PS beads, and PET powder. n=3; average ± standard deviation. Cultivations were performed in shake flasks. Strain genotypes are provided in **Table S6**. BA, benzoate; TPA, terephthalate; AA, acetate; C_4, succinic acid; C_5, glutaric acid; C_6, adipic acid; C_7, pimelic acid; C_8, suberic acid; C_9, azelaic acid; C_{10}, sebacic acid; C_{11}, undecanedioic acid; C_{12}, dodecanedioic acid; C_{13}, tridecanedioic acid; C_{14}, tetradecanedioic acid; C_{15}, pentadecanedioic acid; C_{16}, hexadecanedioic acid; C_{17}, heptadecanedioic acid; C_{18}, octadecanedioic acid; OD, optical density measured at 600 nm.

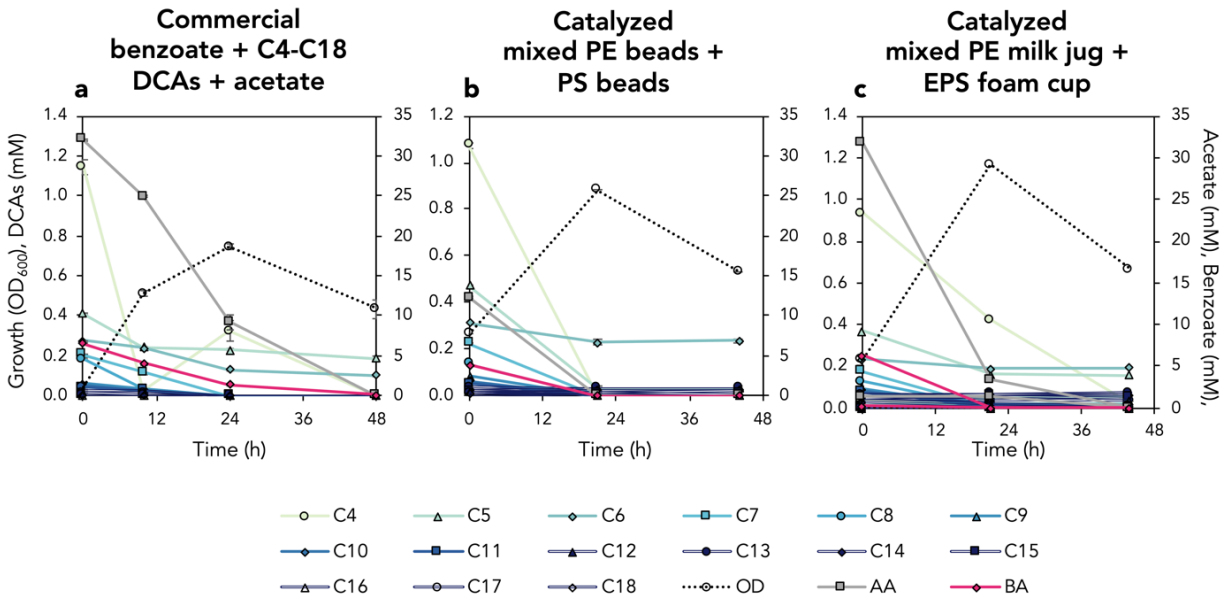

Figure S41. Growth and substrate utilization during conversion of effluent from mixed PS and HDPE (beads or post-consumer products) to polyhydroxyalkanoates by engineered *P. putida*.

AW162 cultivations in nitrogen-deplete M9 minimal medium supplemented with (**a**) commercial benzoate, dicarboxylates from C_4-C_{18}, and acetate, (**b**) effluent from mixed PS beads and HDPE beads, or (**c**) effluent from mixed post-consumer HDPE bottle and EPS cup. (**b**) and (**c**) cultivations did not grow from 0-48 h following inoculation at OD_{600}~0.05; at 48 h they were split into fresh flasks and inoculated to OD 0.2. Growth and metabolite concentrations from 49 h to 93 h are shown here. Cultivation (**a**) was harvested for polyhydroxyalkanoate analysis at 48 h. Cultivations (**b**) and (**c**) were harvested for polyhydroxyalkanoate analysis at 93 h. n=3; average ± standard deviation. Cultivations were performed in shake flasks. Strain genotypes are provided in **Table S6**. BA, benzoate; AA, acetate; C_4, succinic acid; C_5, glutaric acid; C_6, adipic acid; C_7, pimelic acid; C_8, suberic acid; C_9, azelaic acid; C_{10}, sebacic acid; C_{11}, undecanedioic acid; C_{12}, dodecanedioic acid; C_{13}, tridecanedioic acid; C_{14}, tetradecanedioic acid; C_{15}, pentadecanedioic acid; C_{16}, hexadecanedioic acid; C_{17}, heptadecanedioic acid; C_{18}, octadecanedioic acid; OD, optical density measured at 600 nm.

a

	Total PHA per sample (mg)		PHA/DCW (mg/mg)	
	Avg.	Stdev.	Avg.	Stdev.
AW162, Model mixture of BA + DCAs + AA	2.41	0.58	0.118	0.029
AW162, Effluent from mixed PS beads + HDPE beads	0.133	0.019	0.008	0.002
AW162, Effluent from mixed EPS cup + HDPE bottle	0.128	0.023	0.008	0.002

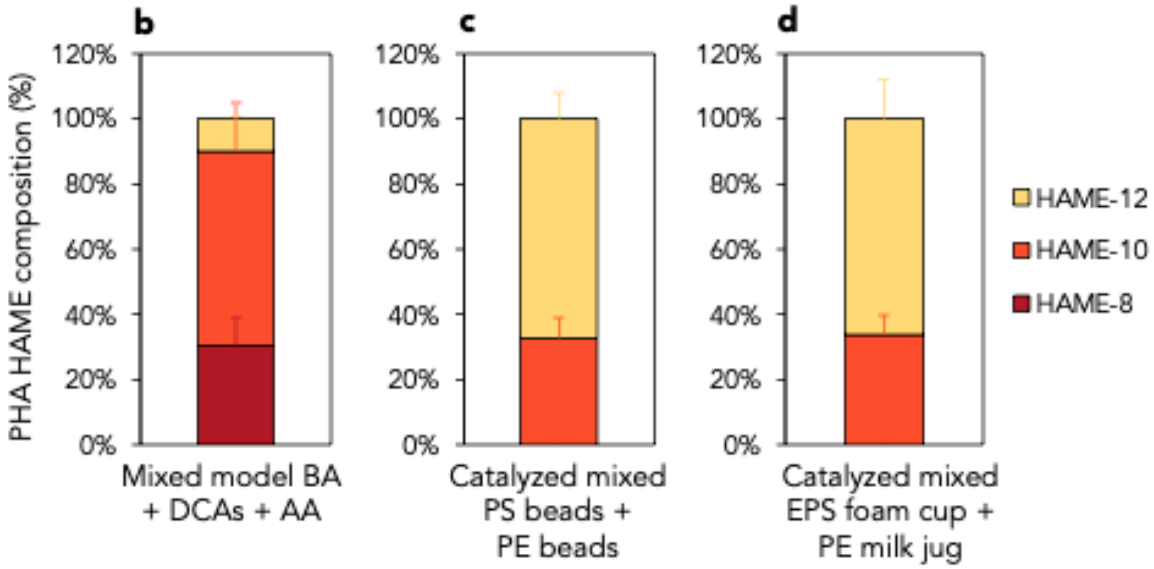

Figure S42. Polyhydroxyalkanoate production from intermediates in effluent from mixed PS and HDPE by engineered *P. putida*.
(**a**) Total polyhydroxyalkanoate (PHA) production per sample and polyhydroxyalkanoate yield per dry cell weight (DCW). See **Figure S41** for growth and metabolite utilization corresponding to the three cultivations: (**b**) AW162 in nitrogen limited M9 minimal medium supplemented with mixed benzoate, dicarboxylates, and acetate (harvested at 48 h), (**c**) AW162 in nitrogen limited M9 minimal medium supplemented with effluent from mixed PS beads and HDPE beads (harvested at 93 h), or (**d**) AW162 in nitrogen limited M9 minimal medium supplemented with effluent from mixed post-consumer EPS cup and HDPE bottle (harvested at 93 h). n=3; average ± standard deviation. Cultivations were performed in shake flasks. Strain genotypes are provided in **Table S6**.

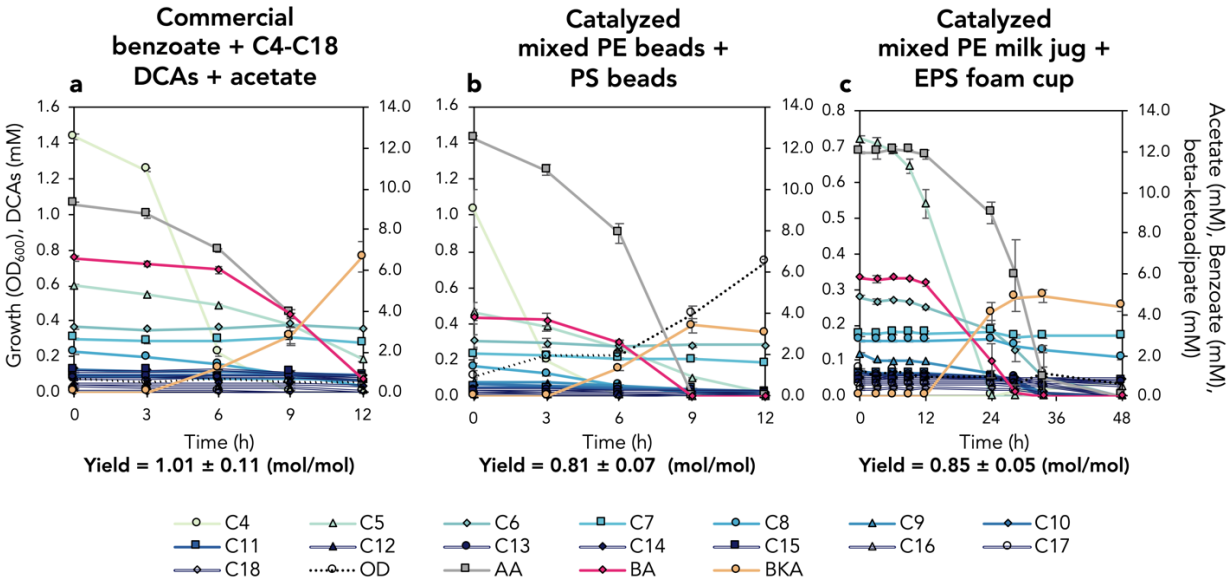

Figure S43. Conversion of intermediates in effluent from mixed PS and HDPE (commercial polymer resin or post-consumer products) to β-ketoadipate by engineered *P. putida*.
Growth and benzoate conversion to β-ketoadipate in AW307 cultivations in M9 minimal medium supplemented with (**a**) commercial benzoate, mixed dicarboxylates, and acetate, (**b**) effluent from mixed HDPE beads and PS beads, or (**c**) effluent from mixed post-consumer HDPE bottle and EPS cups. Molar yield (%) at 12 h is listed below the chart. n=3; average ± standard deviation. Cultivations were performed in shake flasks. Strain genotypes are provided in **Table S6**. BA, benzoate; AA, acetate; C_4, succinic acid; C_5, glutaric acid; C_6, adipic acid; C_7, pimelic acid; C_8, suberic acid; C_9, azelaic acid; C_{10}, sebacic acid; C_{11}, undecanedioic acid; C_{12}, dodecanedioic acid; C_{13}, tridecanedioic acid; C_{14}, tetradecanedioic acid; C_{15}, pentadecanedioic acid; C_{16}, hexadecanedioic acid; C_{17}, heptadecanedioic acid; C_{18}, octadecanedioic acid; BKA, β-ketoadipate; OD, optical density measured at 600 nm. Note that axis scales are different across the panels.

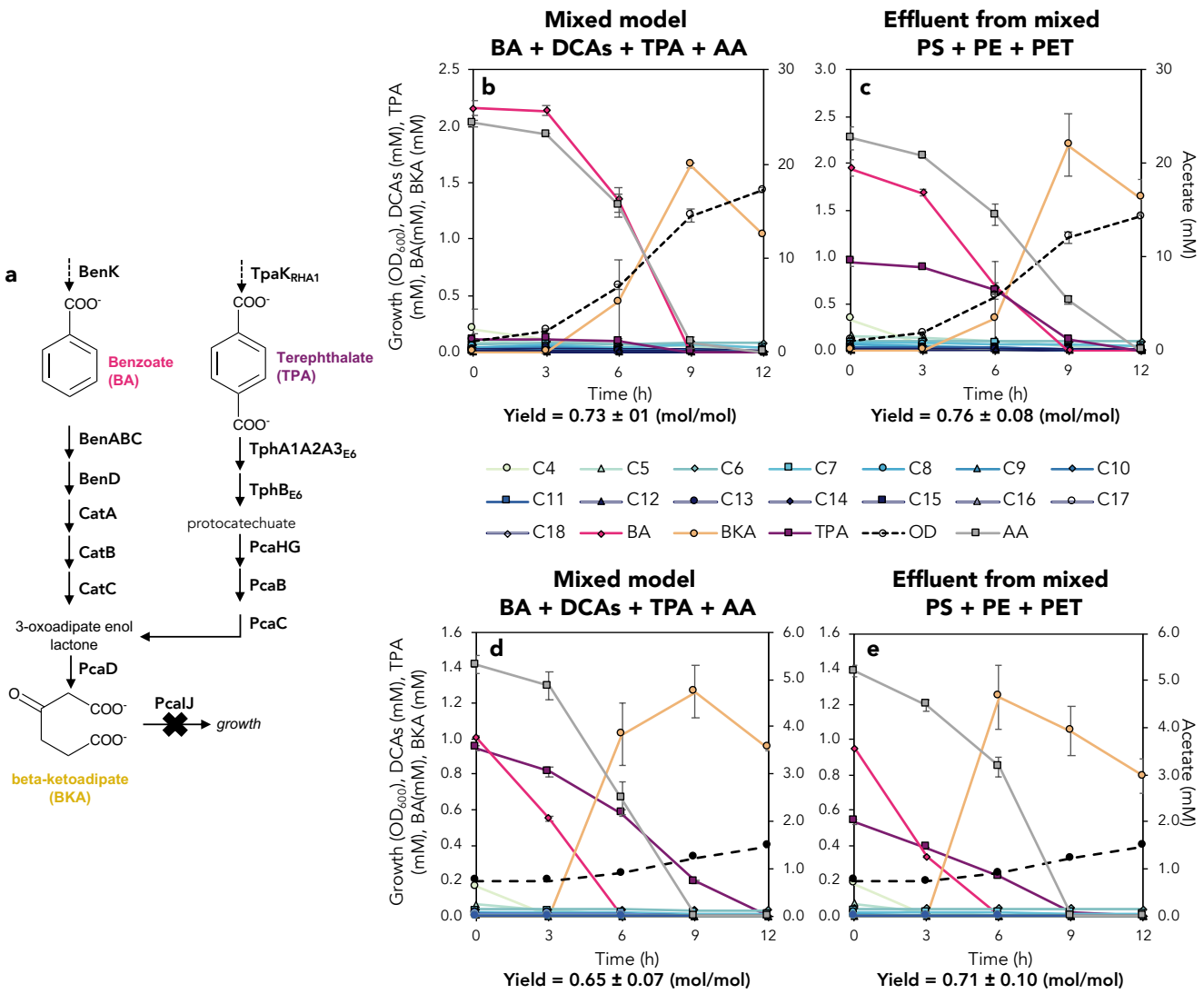

Figure S44. Conversion of benzoate and terephthalate in effluent from mixed PS, HDPE, and PET commercial polymer resin to β-ketoadipate by engineered *P. putida*.

(**a**) Metabolic pathway for conversion of benzoate and terephthalate to β-ketoadipate. Dashed lines indicate cellular import; subscript indicates organism of origin for heterologous genes (E6=*Comamonas* sp. E6, RHA1=*Rhodococcus jostii* RHA1). Growth and benzoate conversion to β-ketoadipate in AW307 cultivations in M9 minimal medium supplemented with (**b**) commercial benzoate, mixed dicarboxylates, terephthalate, and acetate, or (**c**) effluent from mixed HDPE beads, PS beads, and PET powder. Molar yield at 9 h is listed below the chart. (**d-e**) Reactions were performed in a second prepared effluent from mixed HDPE beads, PS beads, and PET powder using optimized deconstruction parameters; notably the effluent was dried more and thus contained less acetate. AW307 was cultivated as before in (**d**) commercial benzoate, mixed dicarboxylates, terephthalate, and acetate, or (**c**) effluent from mixed HDPE beads, PS beads, and PET powder. Molar yield at 9 h is listed below the chart. Cultivations were performed in shake flasks; n=3; average ± standard deviation. Strain genotypes are provided in **Table S6**. BA, benzoate; terephthalate, terephthalate; AA, acetate; C_4, succinic acid; C_5, glutaric acid; C_6, adipic acid; C_7, pimelic acid; C_8, suberic acid; C_9, azelaic acid; C_{10}, sebacic acid; C_{11}, undecanedioic acid; C_{12}, dodecanedioic acid; C_{13}, tridecanedioic acid; C_{14}, tetradecanedioic acid; C_{15}, pentadecanedioic acid; C_{16}, hexadecanedioic acid; C_{17}, heptadecanedioic acid; C_{18}, octadecanedioic acid; BKA, β-ketoadipate; OD, optical density measured at 600 nm.

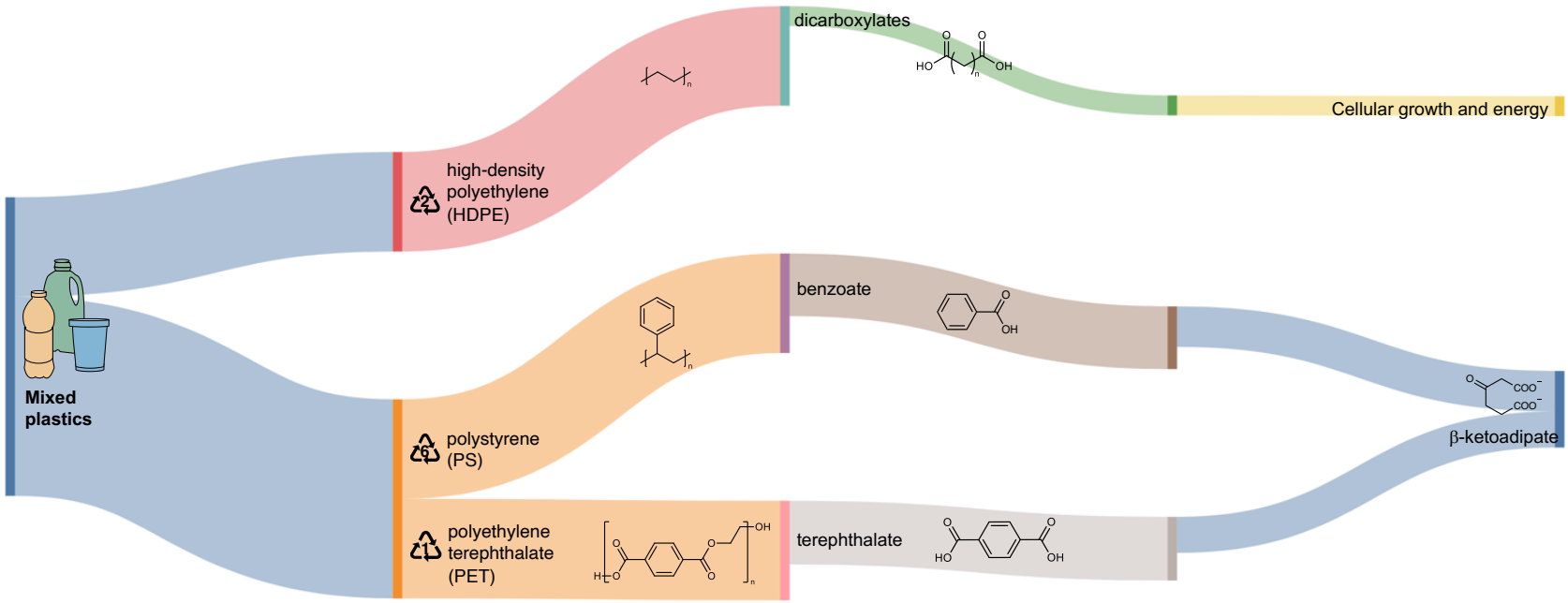

Figure S45. Sankey diagram illustrating the flow of carbon (carbon yield) from each process and the corresponding fate for mixed PS, HDPE, and PET.

HDPE is an aliphatic polymer and both PS and PET are aromatic-containing polymers. In the oxidation step: dicarboxylates were produced at 20 mol% carbon from HDPE, benzoate was produced at 62.9 mol% carbon from PS, and terephthalate was produced at 63.6 mol% carbon. Dicarboxylates were utilized for cellular growth and energy. Benzoate and terephthalate were both converted to beta-ketoadipate at a molar yield of 75.5%; given that one carbon was lost from benzoate and two were lost from terephthalate, this results in an overall carbon yield of 61% from the aromatic constituents.

Supplementary Tables

Table S1. Molecular weight and dispersity of PS during deconstruction.

GPC determination of molecular weight and dispersity during oxidation of PS. Refer to **Figure S4** for reaction conditions.

Sample	M_n (kDa)	M_w (kDa)	$Đ$ (M_w/M_n)
Unreacted PS	100.0	255.0	2.5
0.5 hr	107.0	606.0	5.7
1.5 hr	14.3	25.5	1.8
2.5 hr	6.4	8.2	1.3
3.5 hr	5.8	7.8	1.4
4.5 hr	8.0	11.9	1.5
5.5 hr	6.9	11.0	1.6

Table S2. Multiple reaction monitoring transitions for dicarboxylic acids.

Optimized quantifying and qualifying multiple reaction monitoring (MRM) transitions and coupled fragmentor voltages (V) and collision energies (CE) for UHPLC-MS/MS quantitative analysis for all dicarboxylic acids s and deuterated dicarboxylic acids internal standards.

Carbon Length	Analyte	*m/z* Precursor Ion	Fragmentor (V)	MRM quantifying transition	CE (V)	MRM qualifying transition	CE (V)
3	malonic acid	103	50	103 → 59.1	8	103 → 103	0
4	succinic acid	117	55	117 → 73.1	12	117 → 99	8
5	glutaric acid	131.1	60	131.1 → 87.1	12	117 → 113	8
6	adipic acid	145.1	70	145.1 → 83.1	12	145.1 → 127	8
7	pimelic acid	159	70	159 → 97.1	12	159 → 141.1	8
8	suberic acid	173.1	75	173.1 → 111	12	173.1 → 83	20
9	azelaic acid	187.1	85	187.1 → 125	16	187.1 → 97	16
10	sebacic acid	201.1	85	201.1 → 139	16	201.1 → 183	12
11	undecanedioic acid	215.1	105	215.1 → 197	16	215.1 → 153	20
12	dodecanedioic acid	229.1	105	229.1 → 211.1	16	229.1 → 167.1	20
13	tridecanedioic acid	243.2	110	243.2 → 225.1	16	243.2 → 181.1	20
14	tetradecanedioic acid	257.2	100	257.2 → 239.1	16	257.2 → 195.1	20
15	1,15-pentadecanedioic acid	271.2	105	271.2 → 253	20	271.2 → 209	24
16	hexadecanedioic acid	285.2	120	285.2 → 223.1	24	285.2 → 267.1	20
17	heptadecanedioic Acid	299.2	115	299.2 → 237	24	299.2 → 281	20
18	octadecanedioic Acid	313.2	140	313.2 → 251.1	24	313.2 → 295.1	20
19	nonadecanedioic acid	327.2	130	327.2 → 265.1	24	327.2 → 309.1	20
20	eicosanedioic acid	341.3	135	341.3 → 279.1	28	341.3 → 323.1	24
21	heneicosanedioic acid	355.3	140	355.3 → 293.1	28	355.3 → 337.1	24
22	docosanedioic acid	369.3	100	369.3 → 307.2	32	369.3 → 351.2	20
4	succinic-2,2,3,3-d4 acid	121	55	121 → 77.1	12	121 → 119.5	8
5	pentanedioic-2,2,4,4-d4 acid	135.1	55	135.1 → 91.1	12	135.1 → 72.1	16

6	hexanedioic-2,2,5,5-d4 acid	149.1	60	149.1 → 105.1	12	149.1 → 86.1	12
12	1,12-dodecanedioic-2,2,11,11-d4 acid	233.2	90	233.2 → 214.1	16	233.2 → 170.2	20

Table S3. *m/z* for dicarboxylic acids and lactone acids.

High resolution LC-MS accurate *m/z* values corresponding to Series 1 (dicarboxylic acids) and Series 2 (lactone acids).

Measured *m/z* $[M-H]^-$	Theoretical *m/z* $[M-H]^-$	Mass error (ppm)	Chemical Formula of the compound
Series 1			
103.0025	103.0031	-5.83	$C_3H_4O_4$
117.0182	117.0188	-4.99	$C_4H_6O_4$
131.0340	131.0344	-3.31	$C_5H_8O_4$
145.0496	145.0501	-3.38	$C_6H_{10}O_4$
159.0654	159.0657	-2.14	$C_7H_{12}O_4$
173.0811	173.0814	-1.68	$C_8H_{14}O_4$
187.0968	187.097	-1.29	$C_9H_{16}O_4$
201.1125	201.1127	-0.95	$C_{10}H_{18}O_4$
215.1283	215.1283	-0.20	$C_{11}H_{20}O_4$
229.1435	229.144	-2.15	$C_{12}H_{22}O_4$
243.1593	243.1596	-1.41	$C_{13}H_{24}O_4$
257.1750	257.1753	-1.14	$C_{14}H_{26}O_4$
271.1905	271.1909	-1.64	$C_{15}H_{28}O_4$
285.2061	285.2066	-1.73	$C_{16}H_{30}O_4$
299.2221	299.2222	-0.48	$C_{17}H_{32}O_4$
313.2375	313.2379	-1.26	$C_{18}H_{34}O_4$
327.2533	327.2535	-0.75	$C_{19}H_{36}O_4$
353.2687	353.2692	-1.37	$C_{21}H_{38}O_4$
367.2840	367.2848	-2.27	$C_{22}H_{40}O_4$
381.2998	381.30048	-1.80	$C_{23}H_{42}O_4$
395.3153	395.3161	-2.11	$C_{24}H_{44}O_4$
411.3460	411.3474	-3.40	$C_{25}H_{46}O_4$
425.3619	425.3631	-2.82	$C_{26}H_{48}O_4$
439.3766	439.3787	-4.78	$C_{27}H_{50}O_4$
453.3951	453.3944	1.54	$C_{28}H_{52}O_4$
Series 2			
129.0193	129.0188	3.88	$C_5H_6O_4$
143.0350	143.0344	4.19	$C_6H_8O_4$
157.0502	157.0501	0.64	$C_7H_{10}O_4$
171.0655	171.0657	-0.91	$C_8H_{12}O_4$
185.0812	185.0814	-1.11	$C_9H_{14}O_4$
199.0967	199.097	-1.29	$C_{10}H_{16}O_4$
213.1120	213.1127	-3.31	$C_{11}H_{18}O_4$
227.1277	227.1283	-2.45	$C_{12}H_{20}O_4$
241.1433	241.144	-2.93	$C_{13}H_{22}O_4$

255.1591	255.1596	-1.79	$C_{14}H_{24}O_4$
269.1745	269.1753	-3.00	$C_{15}H_{26}O_4$
283.1908	283.1909	-0.20	$C_{16}H_{28}O_4$
297.2065	297.2066	-0.36	$C_{17}H_{30}O_4$
311.2220	311.2222	-0.51	$C_{18}H_{32}O_4$
325.2372	325.2379	-2.10	$C_{19}H_{34}O_4$
339.2527	339.2535	-2.34	$C_{20}H_{36}O_4$
353.2687	353.2692	-1.4	$C_{21}H_{38}O_4$
367.2842	367.2848	-1.73	$C_{22}H_{40}O_4$
381.3000	381.3005	-1.27	$C_{23}H_{42}O_4$
395.3153	395.3161	-2.11	$C_{24}H_{44}O_4$
409.3334	409.3318	3.91	$C_{25}H_{46}O_4$
423.3463	423.3474	-2.60	$C_{26}H_{48}O_4$
437.3645	437.3631	3.20	$C_{27}H_{50}O_4$
451.3790	451.3787	0.66	$C_{28}H_{52}O_4$

Table S4. Multiple reaction monitoring transitions for lactone acids.
Optimized quantifying and qualifying multiple reaction monitoring (MRM) transitions including coupled fragmentor voltages (V) and collision energies (CE) for UHPLC-MS/MS quantitative analysis for lactone acid analytes and internal standard.

Analyte	*m/z* Precursor Ion	Fragmentor (V)	MRM quantifying transition	CE (V)	MRM qualifying transition	CE (V)
(*R+S*)-5-oxo-2-tetrahydrofurancarboxylic acid (C_5-Lac)	129	95	129 → 85	8	129 → 57.1	16
(5-oxo-tetrahydrofuran-2-yl)acetic acid (C_6-Lac)	143	55	143 → 99	4	143 → 55.1	8
3-(5-oxo-tetrahydrofuran-2-yl)propionic acid (C_7-Lac)	157.1	95	157.1 → 113	4	157.1 → 59	20
4-hydroxybenzoic-2,3,5,6-d4 acid (ISTD)	141.05	60	141.05 → 97	16	141.05 → 69.1	36

Table S5. Plasmids utilized in this study.

Plasmid	Utility	Construction details
pK18mobsacB	Suicide vector for kanamycin/sucrose selection and counterselection-mediated gene replacements in *P. putida* KT2440; Confers kanamycin resistance	ATCC® 87097™, as described in Schäfer *et al.* (1994) (*54*).
pK18sB	A derivative of the plasmid pK18mobsacB that exclude the mobilization factor and other extraneous DNA	Genbank: MH166772, as described in Jayakody *et al.* (2018) (*55*).
pAW020	To integrate the P_{tac}:*dcaAIJ*$_{ADP1}^{CO}$ (codon optimized with synthetic RBSs) operon into the *paaX* chromosomal locus of *P. putida* KT2440 and derived strains with simultaneous *paaX* deletion	Genes from *A. baylyi* ADP1 (*dcaA, dcaI,* and *dcaJ*) were codon optimized using the *Pseudomonas putida* codon tables within the IDT Optimizer tool (https://www.idtdna.com/CodonOpt). Synthetic ribosome binding sites were designed for each gene using the RBS Calculator V2.0 (https://salislab.net/software/design_rbs_calculator) and a TIR target of ~10,000 au. The synthetic operon was driven by P_{tac}, terminated by TonB, and flanked by 1 kB homology arms for deletion of *paaX*. The entire expression cassette (see P_{tac}:*dcaAIJ*$^{CO\text{-}KT}$ in **Table S11** for the DNA sequence) was inserted between the HindIII and EcoRI sites in pK18sB and ordered for synthesis by Twist. Sanger sequencing (GENEWIZ, Inc.) with oAW189, oAW190, oAW191, oAW192, and oAW193 verified the sequence.
pAW021	To integrate the P_{549}:*dcaKP*$_{ADP1}^{CO}$ (codon optimized with synthetic RBSs) operon into the *fpvA* chromosomal locus of RC026	Genes from *A. baylyi* ADP1 (*dcaK* and *dcaP*) were codon optimized using the *Pseudomonas putida* codon tables within the IDT Optimizer tool (https://www.idtdna.com/CodonOpt). Synthetic ribosome binding sites were designed for each gene using the RBS Calculator V2.0 (https://salislab.net/software/design_rbs_calculator) and a TIR target of ~10,000 au. The synthetic operon was driven by P_{549}, terminated by TonB, and flanked by a 1 kB homology arms *tpaK* (already inserted into the *fpvA* chromosomal locus in RC026) and a 1 kB homology arm for the *fpvA* site. The entire expression cassette (see P_{549}:*dcaKP*$^{CO\text{-}KT}$ in **Table S11** for the DNA sequence) was inserted between the HindIII and EcoRI sites in pK18sB and ordered for synthesis by Twist. Sanger sequencing (GENEWIZ, Inc.) with oAW199, oAW200, oAW201, oAW202, oAW203, oAW204 and oAW205 verified the sequence.
pAW040	To delete the *psrA* gene from the genome of *P. putida* KT2440 and derived strains	A 937 bp upstream homology region (HR) was amplified from gDNA with oAW291 and oAW292, a 971 bp downstream HR was amplified from gDNA with oAW293 and oAW294, and the pK18mobsacB backbone was prepared by digesting pAW004 with EcoRI-HF and BamHI-F followed by purification of the 5391 bp band. Three fragments were assembled with NEB HiFi Assembly and transformed into E. coli DH5A F'Iq, a correct colony was identified by cPCR with oAW295 and oAW296 (Tm=57 with MyTaq, 1.4 kB) and sequence verified with oAW295, oAW297, oAW298, and oAW299.
pAW042	To constitutively express the *PP_0370* gene in *P. putida* KT2440 and derived strains	A 1000 bp upstream homology region (HR) was amplified from gDNA with oFB130 and oFB131, and a 1067 bp downstream HR was amplified from gDNA with oFB132 and oFB133. The primers for amplifying these homology regions had overhangs containing a Salis-designed RBS and P14-d promoter. The pK18sB backbone was prepared by digesting pAW028 with EcoRI-HF and HindIII-HF followed by purification of the 2987 bp band. Three fragments were assembled with NEB HiFi Assembly and transformed into E. coli DH5A F'Iq. One correct colony was identified by cPCR with oFB157 and oFB158 (Tm=58 with MyTaq, 2403 bp, Book #7420-106) and sequence verified with oFB157, oFB146, oFB147, oFB148 and oFB149.

pIP126	To integrate the P_{tac}:*dcaAKIJP*$_{ADP1}$ (not codon optimized) operon into the *paaX* chromosomal locus of *P. putida* KT2440 and derived strains with simultaneous *paaX* deletion	Upstream and downstream homology arms for *paaX* were amplified from *P. putida* KT2440 gDNA with primer pairs oIP515/oIP516 and oIP521/oIP522, respectively. *rrnB* T1 terminator and P_{tac} sequences were amplified from gBlock IP_tph_tpi-Opt_ADP1-1 (see IP_tph_tpi-Opt_ADP1-1 in **Table S11** for the DNA sequence) with oIP517/oIP518. *dcaAKIJP* was amplified from *Acenitobacter baylyi* ADP1 gDNA with oIP519/oIP520. PCR products were assembled into pK18sB (linearized with SacI and XbaI) with NEBuilder HiFi DNA assembly kit. See P_{tac}:*dcaAKIJP*^{ADP1} in **Table S11** for the DNA sequence of the integration. Sanger sequencing (GENEWIZ, Inc.) with oIP523–oIP531 and universal primers M13F and M13R verified the sequence.
pCJ059	To delete *pcaIJ* from the genome of *P. putida* KT2440 and derived strains	As described in Johnson et al. (2019) (*24*).
pFB003	To integrate the P_{tac}:*dcaAKIJP*$_{ADP1}$ (codon optimized with synthetic RBSs) operon into the *paaX* chromosomal locus of *P. putida* KT2440 and derived strains with simultaneous *paaX* deletion	Genes from *A. baylyi* ADP1 (*dcaA, dcaK, dcaI, dcaJ,* and *dcaP*) were codon optimized using the *Pseudomonas putida* codon tables within the IDT Optimizer tool (https://www.idtdna.com/CodonOpt). Synthetic ribosome binding sites were designed for each gene using the RBS Calculator V2.0 (https://salislab.net/software/design_rbs_calculator) and a TIR target of ~10,000 au. The synthetic operon was driven by P_{tac}, terminated by TonB, and flanked by 1 kB homology arms for deletion of *paaX*. The entire expression cassette (see P_{tac}:*dcaAKIJP*$^{CO\text{-}KT}$ in **Table S11** for the DNA sequence) was designed between the HindIII and EcoRI sites in pK18SB. The 1st part of the expression cassette, P_{tac}:dcaA, was in the backbone of the sequence-verified pAW020 plasmid. The 2nd part of the expression cassette, *dcaKIJP*$^{CO\text{-}KT}$, was ordered for synthesis by Twist in pK18sB. The Twist insert was then assembled with the pAW020 backbone, constructing a complete expression cassette. Sanger sequencing (GENEWIZ, Inc.) with oFB092, oFB093, oFB094, oFB095, oFB096, oFB097, oFB098, and oFB099 verified the sequence.

Table S6. Bacterial strains utilized in this study.

Strain Name	Genotype	Desc. and construction details
Wild-type *P. putida*	*Pseudomonas putida* KT2440 (*P. putida* KT2440)	ATCC® 47054
TDM461	*P. putida* Δ*hsdMR*::P_{tac}:*tphA2*$_{II}$*A3*$_{II}$*B*$_{II}$*A1*$_{II\text{-}E6}$ *fpvA*:P_{tac}:*tpaK*$_{RHA1}$	As described in Werner et al. (2021) (*25*).
RC025	*P. putida* KT2440 Δ*hsdMR*::P_{tac}:*tphA2*$_{II}$*A3*$_{II}$*B*$_{II}$*A1*$_{II\text{-}E6}$ *fpvA*:P_{tac}:*tpaK*$_{RHA1}$ Δ*glcR*	As described in Werner et al. (2021) (*25*).
RC026	*P. putida* KT2440 Δ*hsdMR*::P_{tac}:*tphA2*$_{II}$*A3*$_{II}$*B*$_{II}$*A1*$_{II\text{-}E6}$ *fpvA*:P_{tac}:*tpaK*$_{RHA1}$ Δ*glcR* P_{tac}:*glcDEFG:PP_3749*	As described in Werner et al. (2021) (*25*).
AW061	*P. putida* KT2440 Δ*hsdMR*::P_{tac}:*tphA2*$_{II}$*A3*$_{II}$*B*$_{II}$*A1*$_{II\text{-}E6}$ *fpvA*:P_{tac}:*tpaK*$_{RHA1}$ Δ*glcR* P_{tac}:*glcDEFG:PP_3749* Δ*paaX*::P_{tac}:*dcaAKIJP*$_{ADP1}$	pIP126 was transformed into RC026 and confirmed by cPCR with oIP532 and oIP533 (1.9 kB, Tm=53.8°C).
AW072	*P. putida* KT2440 Δ*hsdMR*::P_{tac}:*tphA2*$_{II}$*A3*$_{II}$*B*$_{II}$*A1*$_{II\text{-}E6}$ *fpvA*:P_{tac}:*tpaK*$_{RHA1}$ Δ*glcR* P_{tac}:*glcDEFG:PP_3749* Δ*paaX*::P_{tac}:*dcaAIJ*$_{ADP1}$	pAW020 was transformed into RC026 and confirmed by cPCR with oAW213/oAW214 (3.5 kB, Tm=68°C) and oAW213/oAW215 (5.1 kB, Tm=68°C).
AW074	*P. putida* KT2440 Δ*hsdMR*::P_{tac}:*tphA2*$_{II}$*A3*$_{II}$*B*$_{II}$*A1*$_{II\text{-}E6}$ *fpvA*:P_{tac}:*tpaK*$_{RHA1}$:P_{549}:*dcaKP*$_{ADP1}$ Δ*glcR* P_{tac}:*glcDEFG:PP_3749* Δ*paaX*::P_{tac}:*dcaAIJ*$_{ADP1}$	pAW021 was transformed into AW072 and confirmed by cPCR with oCJ822 and oCJ312 (Tm=63°C, 3.9 kB).
AW128	*P. putida* KT2440 Δ*hsdMR*::P_{tac}:*tphA2*$_{II}$*A3*$_{II}$*B*$_{II}$*A1*$_{II\text{-}E6}$ *fpvA*:P_{tac}:*tpaK*$_{RHA1}$ Δ*glcR* P_{tac}:*glcDEFG:PP_3749* Δ*paaX*::P_{tac}:*dcaAKIJP*$_{ADP1}^{CO}$	pFB003 was transformed into RC026 and confirmed to be correct via cPCR with oIP532 and oIP522.
AW160	*P. putida* KT2440 Δ*hsdMR*::P_{tac}:*tphA2*$_{II}$*A3*$_{II}$*B*$_{II}$*A1*$_{II\text{-}E6}$ *fpvA*:P_{tac}:*tpaK*$_{RHA1}$:P_{549}:*dcaKP*$_{ADP1}$ Δ*glcR* P_{tac}:*glcDEFG:PP_3749* Δ*paaX*::P_{tac}:*dcaAIJ*$_{ADP1}$ Δ*psrA*	pAW040 was transformed into AW074. Correct integration was confirmed by cPCR (oAW306/oAW307, Tm=68 MyTaq, 2.5 kB).
AW162	*P. putida* KT2440 Δ*hsdMR*::P_{tac}:*tphA2*$_{II}$*A3*$_{II}$*B*$_{II}$*A1*$_{II\text{-}E6}$ *fpvA*:P_{tac}:*tpaK*$_{RHA1}$ Δ*glcR* P_{tac}:*glcDEFG:PP_3749* Δ*paaX*::P_{tac}:*dcaAKIJP*$_{ADP1}^{CO}$ Δ*psrA*	pAW040 was transformed into AW128. Correct integration was confirmed by cPCR (oAW306/oAW307, Tm=68 MyTaq, 2.5 kB).
AW170	*P. putida* KT2440 Δ*hsdMR*::P_{tac}:*tphA2*$_{II}$*A3*$_{II}$*B*$_{II}$*A1*$_{II\text{-}E6}$ *fpvA*:P_{tac}:*tpaK*$_{RHA1}$ Δ*glcR* P_{tac}:*glcDEFG:PP_3749* Δ*paaX*::P_{tac}:*dcaAKIJP*$_{ADP1}^{CO}$ Δ*psrA* Δ*gnuR*	pAW041 was transformed into AW162. Correct integration was confirmed by cPCR (oFB152/oFB153, Tm=66, 2244 bp).
AW177	*P. putida* KT2440 Δ*hsdMR*::P_{tac}:*tphA2*$_{II}$*A3*$_{II}$*B*$_{II}$*A1*$_{II\text{-}E6}$ *fpvA*:P_{tac}:*tpaK*$_{RHA1}$ Δ*glcR* P_{tac}:*glcDEFG:PP_3749* Δ*paaX*::P_{tac}:*dcaAKIJP*$_{ADP1}^{CO}$ Δ*psrA* P_{14d}:*PP_0370*	pAW042 was transformed into AW162. Correct integration was confirmed by cPCR with oFB163/oFB164 (Tm=60 with MyTaq, 1251 bp). Inserted P-14d promoter and synthetic RBS were sequence verified with oFB137 and oFB147.
AW179	*P. putida* KT2440 Δ*hsdMR*::P_{tac}:*tphA2*$_{II}$*A3*$_{II}$*B*$_{II}$*A1*$_{II\text{-}E6}$ *fpvA*:P_{tac}:*tpaK*$_{RHA1}$ Δ*glcR* P_{tac}:*glcDEFG:PP_3749* Δ*paaX*::P_{tac}:*dcaAKIJP*$_{ADP1}^{CO}$ Δ*psrA* Δ*gnuR* P_{14d}:*PP_0370*	pAW042 was transformed into AW170. Correct integration was confirmed by cPCR with oFB163/oFB164 (Tm=60 with MyTaq, 1251 bp). Inserted P-14d promoter and synthetic RBS were sequence verified with oFB137 and oFB147.
AW307	*P. putida* KT2440 Δ*hsdMR*::P_{tac}:*tphA2*$_{II}$*A3*$_{II}$*B*$_{II}$*A1*$_{II\text{-}E6}$ *fpvA*:P_{tac}:*tpaK*$_{RHA1}$ Δ*glcR* P_{tac}:*glcDEFG:PP_3749* Δ*paaX*::P_{tac}:*dcaAKIJP*$_{ADP1}^{CO}$ Δ*psrA* Δ*pcaIJ*	pCJ059 was transformed into AW162. Correct integration was confirmed with cPCR (oCJ366/oCJ367, MyTaq Tm=54, 2 kB).

Table S7. Oligonucleotides utilized in this study.

Primer	Sequence (5′→3′)
oAW189	gagcgagcaggagctggc
oAW190	CCTGAAAACCACCGCGGTGAAAG
oAW191	CTATCGGGATGTGCGCCTCTTCC
oAW192	CGCTGATAAGGCTGATCGCTGGG
oAW193	CGTTTCAGGTGGCCCTCAATGGTG
oAW199	ctgagatacctacagcgtgagctatgag
oAW200	gtcgatcatgacgagcctggactacg
oAW201	GGATAGCATCACCACGAGCCAACC
oAW202	GGGTACTACGGGGTGTCGAACTGG
oAW203	GGTGACCTGGACCGACAACGTG
oAW204	CCTCAACGCCGCGGGTG
oAW205	caactggcatcggtcaccggg
oAW213	ctcgtcgttcccggcagcctgcagc
oAW214	CCGCCACGCATGATGTCAAACGAATCCCCGTGATGC
oAW215	ggccctgatgaacgtttacgtcgagaagaatactgagcaggg
oAW291	cgcaattaatgtgagttagGAATTCCCGGTTCCCTGGCTTTCAGG
oAW292	TAGCCGAACCGGTCTTTGTGGACTACTCCGACTACTCCGTCAGAC
oAW293	TGACGGAGTAGTCGGAGTAGTCCACAAAGACCGGTTCGGCTACCG
oAW294	agctagGGATCCCGGCCATCGACAGGTCATCACTGAAAATCACCC
oAW295	gaagagcgcccaatacgcaaac
oAW297	CCTTGGCTTCCAGGCCAGGGATG
oAW298	CATGACTGTCAGCCTGCAAGGCTCC
oAW299	GATGCCGGCGCATGTCATCTAC
oAW306	GCTTGGCGGTGGGGCGATCAGGGTC
oAW307	GGCCAAAGGGGGATAGAGCGTAGGAGCGG
oCJ312	CACGCCTGCTTCATTGAAC
oCJ822	TCGGCAGAAAGTCATTCG
oCJ366	CGATTGCGCCATGAACAG
oCJ367	AGGCTGCCGAGTATCATG
oIP515	atgacatgattacGAATTCGAGCTCgcctgcacatcgatatatcg
oIP516	cgcggataaagcaccgac
oIP517	tatagtcggtgctttatccgcgcacagttcgcccccagacatcaaataaaacgAAAG
oIP518	catcgcgaatcatTAAACCTCCTgtgtgaaattgttatccgctc
oIP519	ataacaatttcacacAGGAGGTTTAatgattcgcgatgaagg
oIP520	agcctccgaccggaggcttttgactttaaaacttgtacattgacacg
oIP521	agcctccggtcggaggcttttgactggggagtgctcgcctc
oIP522	TGCATGCCTGCAGGTCGACTCTAGAggcttacaagccgcctc
oIP532	ctgccggtaatcactgtgg

oIP533	cctggtgtattggcttctacc
oFB092	CTCTTCCGGCTGTATGAAGG
oFB093	CTACGAAGCATCGGACCAC
oFB094	GGCTTCCTGTACGGGATTC
oFB095	GCTCGTATCCTAAATCCATTAGCTC
oFB096	CGCTAAATATCTGCCTAAGGACAAG
oFB097	CCAACTCCGTTAACAGAACTATTACC
oFB098	CCTATAAGAATTGGACCTTTGGGC
oFB099	GGAGCGCATCGATCTTTAAGTATG
oFB130	AGGAAACAGCTATGACATGATTACGAATTCGTGGCGGTGGCCCTC
oFB131	TAAAAATTAtcaacttattatacagtcgcgaatgtcggatgtcaagtagaGACAACCTCTCGCTAGTCGGGTC
oFB132	cgcgactgtataataagttgaTAATTTTTATTAAGGTAGGGAAAAATATACTGatgGCTGACTATAAAGCGCCGCTG
oFB133	GACGTTGTAAAACGACGGCCAGTGCCAAGCTTTCGATCAGCGCCTTCATGGTCAAC
oFB137	CATTCAGTACGAAGCGCATGTC
oFB146	GTGGCGGTGGCCCTCCAG
oFB147	CGTGAAGTGATCGCCAATTACGTGATGC
oFB148	CCGTGCTGGAAGAAGCCGGC
oFB149	CCGAAGTTCCTGGTCAATGAAGACGGC
oFB152	GTACGCCGCCAAAACCGTCCTGGAACGATTTCATGAC
oFB153	CACAATCTGCCCGATCACATCCGACTGCCTGTTTACCG
oFB157	GAAACGCCTGGTATCTTTATAGTCCTGTCGG
oFB158	CAATCATGCGAAACGATCCTCATCCTGTTTG
oFB163	GCTGACGGTGTACATCGCCTACTTTCTG
oFB164	caacttattatacagtcgcgaatgtcggatgtcaagtagaGAC
oIP523	tcgtcaaagctggcttcg
oIP524	aatggcattggttcaagtgg
oIP525	caaattcatggtggggcagg
oIP526	gccattgtaccagtcgtcc
oIP527	ctgatacacatgatcagtcttcac
oIP528	cagataaggcagatcgctgg
oIP529	tgagctgaaagatggacagg
oIP530	ggacatttggtcagacatgg
oIP531	gtcaaaagcctccggtcg
M13F	GTAAAACGACGGCCAG
M13R	CAGGAAACAGCTATGAC

Table S8. Synthesized DNA utilized in this study.

Name	Sequence (5'→3')	Desc.
IP_tph_tpi-Opt_ADP1-1	As described in Pardo *et al. (56)*.	
P_{tac}:*dcaAIJ*$^{CO\text{-}KT}$	gcctgcacatcgatatatcgcggcatctcgggttcctctggctgcacgcacggcacatcgcttggccggcat tttttggaattgtttgcagggacgtaatgcgggatcacgaccaggtgtggtcagtatatgctctatgcgata caacaatgcaaggcgcaaaatgttttcgcgtatctctttttttactttctatgatcacagctccagtgcaat gcttgctgaagaatcgtttaacctttgcattttctagtacttacagcgggtttttgccttgcagcattaatt caacacaagtgatacacgattgacgaccaaacagcatctgatacaagatcgactgacattccaaatcatttc gagagtgttgccatgccttgctatcgactggacggcctgacgcctgtggttcacccgacagcctacgtgcac cccagcgcagtcctgatcggtgacgtcatcgtcggcccccgctgctacattggcccgctggcatcgctcagg ggcgatttcggccgcatcgtgctggaggagggcgccaacttgcaggacacctgcgtgatgcatggtttcccg gggggcgacaccgtagtggaacgtaacgggcatgtcggccacgggcgccgtgctgcacggctgtcgcgtcggc gaagattcattgatcggcatgaacgccgtggtgatggatggcgcccatgtagcacctcgctgcatcgtcgcg gccaccgccttcgtcaaagctggcttcgaatgtgcggcgcagagcctggtgatggggtcgccagcccaggtc aaacgcccactgagcgagcaggagctggcctggaaacagcgcgggacggcggagtaccagcacctggcgcag cgctgcatgaacagcatggtcgaatgcccaccgctggccgaggcagagccggggcgcccgcgcatggaagac accggggtcaggcccaagggccaggcaagcgcatgagcctggcagcgacacgcaatggccaggcggcccgcc gcacaggtatagtcggtgctttatccgcgcacagttcgccccccagacatCAAATAAAACGAAAGGCTCAGTC GAAAGACTGGGCCTTTCGTTTTATCTGTTGTTTGTCGGTGAACGCTCTCattaattaatccagaggcatgag ctgttgacaattaatcatcggctcgtataatgtgtggAattgtgagcggataacaatttcacactagttcta ccccctttactttaaggttatattATGATTCGCGATGAAGGCATGCTCCAACAACTGTTGTCCACGATCCGCG ATTTTGTCAAGAATGAGTTGATTCCACGGGAGCATGAAGTCGCTGAGAAAGACTGTATTCCTGAAGACATCA TTCAGCAAATGCGCGAGCTGGGGCTCTTCGGTTTGACCATCCCTGAGGAGTATGGCGGGCTCGGGATTACGA TGGAGGAAGAAGTCAACGTGGCGTTCGAATTGGGGCAGACGTCGCCAGCATTTCGGTCGTTGATCGGTACCA ACAACGGTATCGGTTCGTCGGGGCTGATCATTGATGGTACCGAAGAACAGAAGCAGAAATATCTGCCGCGTT ATGCATCGGGTGAGATCATCGGTTCGTTTTGTTTGACGGAACCTGAAGCCGGTTCGGACGCGGCAAGCCTGA AAACCACCGCGGTGAAAGATGGGGACTTCTACATTCTGAATGGGACGAAACGCTTCATTACGAACGCTCCCC ACGCGGCTACCTTTACGGTGATGGCACGCACGAATCCTGCCATCAAAGGCGCAGGCGGGATCAGCGCATTCC TCGTCGAAGCCAACACCCCGGGCATCACCCTCGGGAAAATCGACCAAAAAATGGGCCAAAAGGGGAGCCATA CGTGCGATGTGATCTTCGAAAACTGTCGTGTGCCGGCCTCCGCTCTGATCGGTGGTGTCGAGGGCGTGGGGT TCAAAACGGCCATGAAAGTGCTCGATAAAGGCCGGCTCCATATCGGTGCCTATAGCGTGGGGGTCGCGGAAC GCATGCTCAATGACGCGTTGCATTACGCTGTCGAACGCAAACAATTCGGTCAACCAATCGCAAACTTCCAGT TGATCCAAGCGATGCTGGCTGATAGCAAAGCCGAAATTTACGCGGCGAAGTGTATGGTCCTCGACGCGGCAC GCCGCCGTGACGAGGGCCAGAACATTTCGACCGAGGCATCCTGCGCCAAGATGTTCGCGACGGAGATGTGCG GTCGTGTCGCTGACCGTTGCGTCCAAATCCACGGCGGGGCAGGCTACATTTCCGAATACAGCATTGAACGTT TCTATCGGGATGTGCGCCTCTTCCGGCTGTATGAAGGCACCACGCAGGTGCAGCAAATTATTATCGCGAAGA ACATGATTAAAGAGGTCACCTCGTAAgaaatccagcacaaacgagcgcaatcgtttaaggaagtaaaTATGA TCAATAAGATCATCAACGACATTGAACCCATTCTCAAATCGATTCCCGATGGGTCCACGATCATGACCTCCG GTTTTGGTACGACGGGCCAACCAGAAGCTCTCCTCGAGGCCCTGATTGATTTTGCGCCAAAGGAACTCACCA TCATTAATAACAATGCGTCGAGCGGCCCGAATGGTCTGACCCAGCTGTTTACCGCCGGGTTGGTCAAAAAAT TGATTTGCTCGTATCCTAAATCCATTAGCTCGACGGTGTTCCCAGACCTGTATCGTGCCGGTAAAATTGAGT TGGAGCTCGTCCCACAAGGGAATCTCGCCTGTCGCATCCAGGCAGCGGGTGCTGGGCTCGGGGCGGTCTTCA CGCCTACGGGCTACGGGACCAAAATTGCTGAAGGTAAGGAAACCCGGATCATTAACGGCAAAAATTACGTCC TCGAGTATCCACTCGAAGCAGACTACGCGTTTATTTACGCTGATAAGGCTGATCGCTGGGGCAACTTGACCT ATCGGAAGGCTGCCCGGAATTTCGGGCCTATCATGGCCAAAGCTGCTAAGACGACCATTGCCCAGGTCAATC	Upstream and downstream homology regions for *paaX* shown in grey dotted underline. rrnB T1 terminator shown in dark red. Tac promoter shown in green squiggle underline. ORFs for *dcaA, dcaI,* and *dcaJ* codon optimized for *Pseudomonas putida* shown in UPPER CASE BLUE UNDERLINE, in that order. Synthetic ribosome binding sites for each gene shown in lower case blue double underline. TonB terminator show in red.

	AGACCGTGGAATTGGGTGATCTCGATCCCGAATGCATCATTACCCCAGGTATTTTTGTGCAACATGTCGTGC GCCTGGGCGATATTAAATAAtgacttataacctacctagaaggaacattggATGACGATCCAGAAACGCAGC CGCGAAGACATCGCCATCATGATCGCAAAAGATATTCCGGATGGTAGCTATGTCAACTTGGGCATCGGCCTG CCGACCCACGTCGCTAAATATCTGCCTAAGGACAAGGAAATTTTTTTGCATTCCGAAAATGGGGTCCTGGCG TTTGGCCCGCCACCAGCTGAAGGCGAGGAAGATCAAGATTTGGTGAATGCTGGTAAAGAATTGGTCACCCTG CTGTCCGGTGGTTGTTTTATGCATCACGGGGATTCGTTTGACATCATGCGTGGCGGTCATTTGGATATCTGC GTCATTGGGGCGTTTCAGGTGGCCCTCAATGGTGATCTGGCAAATTGGCATACCGGTAAGGATGATGATGTC CCGGCAGTGGGTGGGGCAATGGACTTGGCGGTCGGGGCTAAACGTATTTTTGTCTATATGGAACATACCACG AAAAAAGGCGAGCCCAAGATTGTCAAGCATCTGACCTACCCAATCACCGGCGAGCAGTGTGTCGATCGGATT TATACGGACTTGTGTACGATCGAATTGAAGGATGGGCAGGCGTATGTGATCGAAATGGTCGATGGCCTCGAC TTTGACACGTTGCAGGCCCTGACGGAGTGCCCCCTCATTGACCATTGTACGTACTCCTCCCTCATCCAACTC CGTTAAagtcaaaagcctccggtcggaggcttttgactggggagtgctcgcctcacagcgccgcggccaaca ttcacggcgtcgagcagggtgccttcaggggcccttggcctcacattcaccgccaccttgttcgagcgccat gagtgcaggcatatcaagaatttctaccaacctgccatgcaggtcgacgatacccagcgcgcgcagacgggc gacggatcggcacacggtttccaggcgtaaacccaggtacgaagccatgtcttcacgagacatccgcaacat gaagccatgggcagagtaaccgcggctgacgaagcgcctggagagccccaccaggaagctggccagccgctg ttctgcagtcaggttgcacagcatcagcacacgcccgtgctcacgcacgatctcccggctcatcaggcgatt caggctttgctgcaggtccggaaactcacgcgccagggtttgcaagcggcgatagggaacagggcagacttc gctgtcttccagggcaatggcgtcacagacatggtgctctgtggcgatggcatcgaggccgattacatcgcc cggcatccagaagttgatcaccacgccttgcccctcggcggtgttcaggctggtcttgaaactgccgcagcg taaggcatagagcatggtcagcggatcgttggcattgaacagcgcggcgcccttgcgaatgcgcatgcgtgg gcctatcaacgcgcccaggcagctgttttcgtcaactggcaggccagtggggaggcacaggccgcttacccg gcaatccatgcagtggttcaccagcggtttcaggtgaatagggtttgccttggacaaagggttgggggagtc gagcagggtgaccttcagctggccaggcattttcaggcctccttcgcattacggaggccccttttgggccccc gtgccattacgcgcaccgagcccgacggtaaccccggtatggggcgaccaatcagcaagcatgtcccgcgag tgggggggcattgaggcggcttgtaagcc	
P_{549}:*dcaKP*$^{CO\text{-}KT}$	ctattgcggcttctccctcggattcgtcgcggcagggctggtctccggttggctgatcccgatcctcggctg gcggtcggtactcgtcgtcggcgcagtagcaccgctgctcctgctcccggcgttgctgcgctacctgccgga ctcactcacctcaatgatcaaccgaggcgcggagcccaacagaatccaggcgatcttccgcaaaatggatcc cgccctcgccgtcggccccgacatcacctacgaggccgagaagcggaccgacggacaacgcactgcactgag gagcctgttcacccgtgaccgggtcttgggaaccctgctgctgtggctggtcttcgtcatcaacctcggcga gttttacgcgctgcagagctggctaccgtcgatcatgacgagcctggactacgacatgggtacggtggtcac cgccaccaccctcacgactgtcggcggcatcgccgctgcatttgtcaccgggccctgtatggaccgactcgg cgcgtacgtcaccctcggaaccgtttatgtcgtcggattcgcattcgttgcgctgaccggtgtcgcctttac ggcgccgttgtgggtcctattgacggccaatttttttgcgggggtctgcatcagcggtggacagaagagcct catcgcgctgtccgcggtgttctatccgacaccgatgcggtccaccggggttggatgggcgttgggtgttgg ccgcctcggcggcatcgtcgggccgatcgcggtcggagcggcactcggcatgggctggtccgccagtgcagt cttctacgcaatgtcagtcccatgctcgtcgccggagctgcggtcttcctcctcggccgctgggtccgaag cgacaatcaccccgatcgcaagtcggcagaaagtcattcgctcgcccgcaagtagtgtggatcggcaacacc ggccgggtgatctcaaggcctgcgatactagtagtcaaaagcctccgaccggaggcttttgactGAATTCga gctgattacaattaatcatcggctcgtttaatgtgtggaattgtgagcggataacaatttcacacgaatcac acacacagggtcaaggacaaaagctATGCATATTCTCTCGGAAGACATTGACATGACGACGGATAGCATCAC CACGAGCCAACCTAACCAGGCTATTCAGACCCCAAAAAAAATCTGGATTACGGCCTTCATCTTTGCGTTTCT GGCGCTGCTCTGTGATGGGGCAGATTTGGGCTTCTTGGCGTTGTCCCTGACGTCCTTGAAGAGCGAGTTCCA CCTGACCGGGCTCCAAGCGGGGACCTTGGGGTCGCTGACCCTCTTCGGTTCCGCTATCGGTGGGTTGTTCGG TGGCTGGGCCTGTGATCGTTTTGGCCGGGTCCGTATTATTGTCTTTTTCATCGCCTATTCGAGCATTCTCAC	Upstream homology region for *tpaK* (already integrated into the *fpvA* site in host strain) shown in grey dotted underline. TonB terminators shown in lower case red. P_{549} promoter shown in light green squiggle underline. ORFs for *dcaK* and *dcaP* codon optimized for *Pseudomonas putida* shown in UPPER CASE BLUE UNDERLINE, in that order. Synthetic ribosome binding sites for each gene shown in lower case blue double underline. Downstream homology region for *fpvA* shown in grey dashed underline

GTGTGCTTTGGGTTTCACGCACTCCTTTGAGCAATTTGCGATTGTGCGCGTCTTCGGTTCGATGGGCCTCGG
CGCTCTCTATATTGCATGTAACGTCTTGATGAGCGAAATGGTCCCTACGAAGCATCGGACCACGGTGCTGGC
GACGCTCATGACGGGCTACACCCTGGGCAGCTTGTTGGCCACGCTGCTGGCCGGCCACATCATTCCGGAGCA
CGGTTGGCGCTATTTGTACTGGCTCGCAATCGTCCCTGTCGTCTTGAGCTTTTTTATGCATTACATGGTCCC
TGAACCAGAGTCCTGGAAAAAATCCCGTCAAATCCGTGCCCAACAAGCTACGGGTGGGATGAAGGAGGTGAA
GCGTGAGAATCCTTACCGTGAAATTTTTAAGGAGAAAAAACACGGCATTATGTTTTTGCTGTGGGTGGTCTC
CACCGGCGCTTTGCAGTTCGGGTACTACGGGGTGTCGAACTGGTTGCCGGCATACTTGGAATCGGAGCTCGG
GATTAAGTTTAAGGAAATGGCCATGTATATGGTCGGTACCTTCATCATTATGATTTTCGCTAAGATTATCGC
TGGTATGATCGCAGATAAATTGGGGCGCCGCGCTGTGTTCGCATTTGGGACGATTGGGACGGCCCTCTTTAT
CCCGGTCATCGTCTATCTCAATACGCCTGCTAATATCCTCTGGATGATGCTGTTTTTCGGCTTCCTGTACGG
GATTCCCTACGCGATTAATGCTACGTATATGACGGAATCGTTTCCGACCTCGATTCGCGGTAGCGCGGTGGG
CGGTGCGTATAACGTCGGTAAAGTCTTGTCGATTTTCTCCCCGCTGACCATCGGCTATTTGTCCCAGTCCGG
TTCCATTGGGTTGGGCCTCCTCGTGATGGCTGCTGCGTACTTTATTTGCGGCGTGATCCCGCTCCTGTTTAT
CAAAGATCGTCTGTATAATCCACAGAAGGCCGACTAAcagaactattaccaagagttaagaaagaaactaAT
GAAGAAATTGATCCTGGCCGTCGCATGTGCTACGGCGTCCGGGACGCTGCTCGCTAATAGCACCGAGAACAA
ATCCACGGAGCAGCGTATTAACGCACTGGAGGCCGAATTGCAACGCCTCAAAGCAGAGTTGGAGTTGCAGAA
GACCAATCAACAGAATATGCTCGCTGAGTCGAAGGTCAAGACCCAGAATGCAAATGAGATCCAAACGAAAGA
GAAAGTCATCGCACCCTCCTGGGTGACCTGGACCGACAACGTGAAAATTTACGGCATTGCTCGCTTGGATGC
TGCGGTGGATTTCAAGTCCTCGCCTGACTCGGGCGGGCGGACCACGTCGTCCCTGTACCGCGCCCCTTTTGA
ATCCTCGACGCGTTCCAATCATGCGCGCTCGGACGCCTCCATTAACGCGTCGCGCCTCGGTGTCTATTTTAA
TTCGCCCGACAAGAAGATTACGGGCAATATCGAGGCTGATTTTTTTGATTCGTCCACGATGGGCACGGGTGA
CGGCAAATTTCGGATCCGCCATGCCTTTTTCACCTATAAGAATTGGACCTTTGGGCAGACGTGGAGCTTGAT
GTCGAACATGGAGACGCGTACGGAATCCGTGGATTATACCCAATTCCTCGGTACCAGCTATACGCGCTTGCC
TCAAATTCGTTACGACTGGAAAATTGACCAAAACCATGACTTGAAGGTGGCGGTGGAGTACACGGGTAGCCG
GGTCTCCGCCCTGCCTTCCCTCACCTCCCGCTATAGCTATAAGAATGGGCCGCTGTTGCTGTTGGCGCAAGG
CTTCATCAATGAAAAGTCCGTCGACGTGACGACGGACAATGTCAAGAAACTGAGCTGGGGGGCAGGGGGCGG
GGTGAAGTACCAAATCACCCCACAGCACTCCATTCAAGCCAACTACCAACACATTGTGGGCGATCAGAAGTT
CATGCCTTACACCACCCAATCGGGTCTCGCAAACGCTTCGAGCCTCAACGCCGCGGGTGATTTCTCGTTGAA
TCGGGAGAAAACCGATCTGGTGATGAACACCCTCGACGTGGCCAATATCGGCTACACGTATAAATTCAACGA
GTATTGGCGCACGAATTGGAGCGCATCGATCTTTAAGTATGACGATAATTCGGCGTATGCAGAGATTAATCC
TGACGCTAATGAACGGCTCATTGACTATGCTGCAAATCTGTTCTACTCCCCTACCGCTCAAATGGATTTTGG
GGTCGAATATCATCAAGGGGAACGGAAAGTGTTCGACGGTCGTAAAGCAGACGTGAGCCGGATTAATTTTGT
GAGCATGTATAAGTTTTAAACTAGTagtcaaaagcctccgaccggaggcttttttactcatggatgcctgaaa
ggctcccttacagatgctgctgcagtgcctcgaccaccatcgccaggccttcatcggcctcctcgatgatcg
aacccatacgcatgaagtcatgggtcactcccgggatcaccgcaagctgcaccgccaccccggcttgctcca
agtgccgtgcataagcgacaccctggtcatgcagcgggtcgcactcggcaatcagcatcagtgcaggtgcac
tgttgctggcgacgctgcccagcaacggtgaaaaacgcggatcgtgacggtctgccggcaccgtggcgtatt
gctggtagaaccactccagggtctgcgcttcaagcaggtaaccgctgccatagcgctgcaccgaaggccgcc
ggcaactggcatcggtcaccgggtagatcattacctgcaggcgcggtgccggcagctcgcgctgcgcagcca
actggttggccagaatggtagccaggctaccaccgacactgtcgcccaccaccgccagtcgctgcgcatcga
tgcccagcgcctcggcctgctcgaccaaccagcgccaggcatccagggcatcgtcactggctgtcgggaaac
gccactgcggcgccagccggtagcccacggcaatcaccggcaccccggcatcctgcgccaggttccagcaca
gcgtgtcatgcgaatcgaggctgcccaccacgtagccgccgccatgcaggtacagcagcgccgcgccggcca
gtgcagggtcggcctgcggcgggcggtacaagcgcaccggcaaggtatggccatcgcgggtggtcaacgaaa
ggtcgctgatgcagtccggctcgtcggccttgcccgcaatcagcgccgaggactcttcgaactggcggcgcg

	cctcgtccgccgccagggcatgcatgggcagcaccttgccggcgctgcgtccggcctccaccagttgcaggt aggccgccaggtcagggttcagggacatcgttcgattctccagaggggc	
P_{tac}:*dcaAKIJP*$^{CO\text{-}KT}$	gcctgcacatcgatatatcgcggcatctcgggttcctctggctgcacgcacggcacatcgcttggccggcat ttttttggaattgtttgcagggacgtaatgcgggatcacgaccaggtgtggtcagtatatgctctatgcgata caacaatgcaaggcgcaaaatgttttcgcgtatctctttttttactttctatgatcacagctccagtgcaat gcttgctgaagaatcgtttaacctttgcattttctagtacttacagcgggtttttgccttgcagcattaatt caacacaagtgatacacgattgacgaccaaacagcatctgatacaagatcgactgacattccaaatcatttc gagagtgttgccatgccttgctatcgactggacggcctgacgcctgtggttcacccgacagcctacgtgcac cccagcgcagtcctgatcggtgacgtcatcgtcggccccgctgctacattggcccgctggcatcgctcagg ggcgatttcggccgcatcgtgctggaggagggcgccaacttgcaggacacctgcgtgatgcatggtttcccg gggggcgacaccgtagtggaacgtaacgggcatgtcggccacggcgccgtgctgcacggctgtcgcgtcggc gaagattcattgatcggcatgaacgccgtggtgatggatggcgcccatgtagcacctcgctgcatcgtcgcg gccaccgccttcgtcaaagctggcttcgaatgtgcggcgcagagcctggtgatggggtcgccagcccaggtc aaacgcccactgagcgagcaggagctggcctggaaacagcgcgggacggcggagtaccagcacctggcgcag cgctgcatgaacagcatggtcgaatgcccaccgctggccgaggcagagccggggcgcccgcgcatggaagac accggggtcaggcccaagggccaggcaagcgcatgagcctggcagcgacacgcaatggccaggcggcccgcc gcacaggtatagtcggtgctttatccgcgcacagttcgcccccagacatcaaataaaacgAAAGGCTCAGTC GAAAGACTGGGCCTTTCGttttatctgttgtttgtcggtgaacgctctcattaattaatccagaggcatgag ctgttgacaattaatcatcggctcgtataatgtgtggAattgtgagcggataacaatttcacactagttcta ccccttactttaaggttatattATGATTCGCGATGAAGGCATGCTCCAACAACTGTTGTCCACGATCCGCG ATTTTGTCAAGAATGAGTTGATTCCACGGGAGCATGAAGTCGCTGAGAAAGACTGTATTCCTGAAGACATCA TTCAGCAAATGCGCGAGCTGGGGCTCTTCGGTTTGACCATCCCTGAGGAGTATGGCGGGCTCGGGATTACGA TGGAGGAAGAAGTCAACGTGGCGTTCGAATTGGGGCAGACGTCGCCAGCATTTCGGTCGTTGATCGGTACCA ACAACGGTATCGGTTCGTCGGGGCTGATCATTGATGGTACCGAAGAACAGAAGCAGAAATATCTGCCGCGTT ATGCATCGGGTGAGATCATCGGTTCGTTTTGTTTGACGGAACCTGAAGCCGGTTCGGACGCGGCAAGCCTGA AAACCACCGCGGTGAAAGATGGGGACTTCTACATTCTGAATGGGACGAAACGCTTCATTACGAACGCTCCCC ACGCGGCTACCTTTACGGTGATGGCACGCACGAATCCTGCCATCAAAGGCGCAGGCGGGATCAGCGCATTCC TCGTCGAAGCCAACACCCCGGGCATCACCCTCGGGAAAATCGACCAAAAAATGGGCCAAAAGGGGAGCCATA CGTGCGATGTGATCTTCGAAAACTGTCGTGTGCCGGCCTCCGCTCTGATCGGTGGTGTCGAGGGCGTGGGGT TCAAAACGGCCATGAAAGTGCTCGATAAAGGCCGGCTCCATATCGGTGCCTATAGCGTGGGGGTCGCGGAAC GCATGCTCAATGACGCGTTGCATTACGCTGTCGAACGCAAACAATTCGGTCAACCAATCGCAAACTTCCAGT TGATCCAAGCGATGCTGGCTGATAGCAAAGCCGAAATTTACGCGGCGAAGTGTATGGTCCTCGACGCGGCAC GCCGCCGTGACGAGGGCCAGAACATTTCGACCGAGGCATCCTGCGCCAAGATGTTCGCGACGGAGATGTGCG GTCGTGTCGCTGACCGTTGCGTCCAAATCCACGGCGGGGCAGGCTACATTTCCGAATACAGCATTGAACGTT TCTATCGGGATGTGCGCCTCTTCCGGCTGTATGAAGGCACCACGCAGGTGCAGCAAATTATTATCGCGAAGA ACATGATTAAAGAGGTCACCTCGTAAgaatcacacacacagggtcaaggacaaaagctATGCATATTCTCTC GGAAGACATTGACATGACGACGGATAGCATCACCACGAGCCAACCTAACCAGGCTATTCAGACCCCAAAAAA AATCTGGATTACGGCCTTCATCTTTGCGTTTCTGGCGCTGCTCTGTGATGGGGCAGATTTGGGCTTCTTGGC GTTGTCCCTGACGTCCTTGAAGAGCGAGTTCCACCTGACCGGGCTCCAAGCGGGGACCTTGGGGTCGCTGAC CCTCTTCGGTTCCGCTATCGGTGGGTTGTTCGGTGGCTGGGCCTGTGATCGTTTTGGCCGGGTCCGTATTAT TGTCTTTTTCATCGCCTATTCGAGCATTCTCACGTGTGCTTTGGGTTTCACGCACTCCTTTGAGCAATTTGC GATTGTGCGCGTCTTCGGTTCGATGGGCCTCGGCGCTCTCTATATTGCATGTAACGTCTTGATGAGCGAAAT GGTCCCTACGAAGCATCGGACCACGGTGCTGGCGACGCTCATGACGGGCTACACCCTGGGCAGCTTGTTGGC CACGCTGCTGGCCGGCCACATCATTCCGGAGCACGGTTGGCGCTATTTGTACTGGCTCGCAATCGTCCCTGT CGTCTTGAGCTTTTTTATGCATTACATGGTCCCTGAACCAGAGTCCTGGAAAAAATCCCGTCAAATCCGTGC CCAACAAGCTACGGGTGGGATGAAGGAGGTGAAGCGTGAGAATCCTTACCGTGAAATTTTTAAGGAGAAAAA	Upstream and downstream homology regions for *paaX* shown in grey dotted underline. rrnB T1 terminator shown in dark red. Tac promoter shown in green squiggle underline. ORFs for *dcaA, dcaK, dcaI, dcaJ* and *dcaP* codon optimized for *Pseudomonas putida* shown in UPPER CASE BLUE UNDERLINE, in that order. Synthetic ribosome binding sites for each gene shown in lower case blue double underline. TonB terminator show in red.

ACACGGCATTATGTTTTTGCTGTGGGTGGTCTCCACCGGCGCTTTGCAGTTCGGGTACTACGGGGTGTCGAA
CTGGTTGCCGGCATACTTGGAATCGGAGCTCGGGATTAAGTTTAAGGAAATGGCCATGTATATGGTCGGTAC
CTTCATCATTATGATTTTCGCTAAGATTATCGCTGGTATGATCGCAGATAAATTGGGGCGCCGCGCTGTGTT
CGCATTTGGGACGATTGGGACGGCCCTCTTTATCCCGGTCATCGTCTATCTCAATACGCCTGCTAATATCCT
CTGGATGATGCTGTTTTTCGGCTTCCTGTACGGGATTCCCTACGCGATTAATGCTACGTATATGACGGAATC
GTTTCCGACCTCGATTCGCGGTAGCGCGGTGGGCGGTGCGTATAACGTCGGTAAAGTCTTGTCGATTTTCTC
CCCGCTGACCATCGGCTATTTGTCCCAGTCCGGTTCCATTGGGTTGGGCCTCCTCGTGATGGCTGCTGCGTA
CTTTATTTGCGGCGTGATCCCGCTCCTGTTTATCAAAGATCGTCTGTATAATCCACAGAAGGCCGACTAAga
aatccagcacaaacgagcgcaatcgtttaaggaagtaaatATGATCAATAAGATCATCAACGACATTGAACC
CATTCTCAAATCGATTCCCGATGGGTCCACGATCATGACCTCCGGTTTTGGTACGACGGGCCAACCAGAAGC
TCTCCTCGAGGCCCTGATTGATTTTGCGCCAAAGGAACTCACCATCATTAATAACAATGCGTCGAGCGGCCC
GAATGGTCTGACCCAGCTGTTTACCGCCGGGTTGGTCAAAAAATTGATTTGCTCGTATCCTAAATCCATTAG
CTCGACGGTGTTCCCAGACCTGTATCGTGCCGGTAAAATTGAGTTGGAGCTCGTCCCACAAGGGAATCTCGC
CTGTCGCATCCAGGCAGCGGGTGCTGGGCTCGGGGCGGTCTTCACGCCTACGGGCTACGGGACCAAAATTGC
TGAAGGTAAGGAAACCCGGATCATTAACGGCAAAAATTACGTCCTCGAGTATCCACTCGAAGCAGACTACGC
GTTTATTTACGCTGATAAGGCTGATCGCTGGGGCAACTTGACCTATCGGAAGGCTGCCCGGAATTTCGGGCC
TATCATGGCCAAAGCTGCTAAGACGACCATTGCCCAGGTCAATCAGACCGTGGAATTGGGTGATCTCGATCC
CGAATGCATCATTACCCCAGGTATTTTTGTGCAACATGTCGTGCGCCTGGGCGATATTAAATAAtgacttat
aacctacctagaaggaacattggATGACGATCCAGAAACGCAGCCGCGAAGACATCGCCATCATGATCGCAA
AAGATATTCCGGATGGTAGCTATGTCAACTTGGGCATCGGCCTGCCGACCCACGTCGCTAAATATCTGCCTA
AGGACAAGGAAATTTTTTTGCATTCCGAAAATGGGGTCCTGGCGTTTGGCCCGCCACCAGCTGAAGGCGAGG
AAGATCAAGATTTGGTGAATGCTGGTAAAGAATTGGTCACCCTGCTGTCCGGTGGTTGTTTTATGCATCACG
GGGATTCGTTTGACATCATGCGTGGCGGTCATTTGGATATCTGCGTCATTGGGGCGTTTCAGGTGGCCCTCA
ATGGTGATCTGGCAAATTGGCATACCGGTAAGGATGATGATGTCCCGGCAGTGGGTGGGGCAATGGACTTGG
CGGTCGGGGCTAAACGTATTTTTGTCTATATGGAACATACCACGAAAAAAGGCGAGCCCAAGATTGTCAAGC
ATCTGACCTACCCAATCACCGGCGAGCAGTGTGTCGATCGGATTTATACGGACTTGTGTACGATCGAATTGA
AGGATGGGCAGGCGTATGTGATCGAAATGGTCGATGGCCTCGACTTTGACACGTTGCAGGCCCTGACGGAGT
GCCCCCTCATTGACCATTGTACGTACTCCTCCCTCATCCAACTCCGTTAAcagaactattaccaagagttaa
gaaagaaactaATGAAGAAATTGATCCTGGCCGTCGCATGTGCTACGGCGTCCGGGACGCTGCTCGCTAATA
GCACCGAGAACAAATCCACGGAGCAGCGTATTAACGCACTGGAGGCCGAATTGCAACGCCTCAAAGCAGAGT
TGGAGTTGCAGAAGACCAATCAACAGAATATGCTCGCTGAGTCGAAGGTCAAGACCCAGAATGCAAATGAGA
TCCAAACGAAAGAGAAAGTCATCGCACCCTCCTGGGTGACCTGGACCGACAACGTGAAAATTTACGGCATTG
CTCGCTTGGATGCTGCGGTGGATTTCAAGTCCTCGCCTGACTCGGGCGGGCGGACCACGTCGTCCCTGTACC
GCGCCCCTTTTGAATCCTCGACGCGTTCCAATCATGCGCGCTCGGACGCCTCCATTAACGCGTCGCGCCTCG
GTGTCTATTTTAATTCGCCCGACAAGAAGATTACGGGCAATATCGAGGCTGATTTTTTTGATTCGTCCACGA
TGGGCACGGGTGACGGCAAATTTCGGATCCGCCATGCCTTTTTCACCTATAAGAATTGGACCTTTGGGCAGA
CGTGGAGCTTGATGTCGAACATGGAGACGCGTACGGAATCCGTGGATTATACCCAATTCCTCGGTACCAGCT
ATACGCGCTTGCCTCAAATTCGTTACGACTGGAAAATTGACCAAAACCATGACTTGAAGGTGGCGGTGGAGT
ACACGGGTAGCCGGGTCTCCGCCCTGCCTTCCCTCACCTCCCGCTATAGCTATAAGAATGGGCCGCTGTTGC
TGTTGGCGCAAGGCTTCATCAATGAAAAGTCCGTCGACGTGACGACGGACAATGTCAAGAAACTGAGCTGGG
GGGCAGGGGGCGGGGTGAAGTACCAAATCACCCCACAGCACTCCATTCAAGCCAACTACCAACACATTGTGG
GCGATCAGAAGTTCATGCCTTACACCACCCAATCGGGTCTCGCAAACGCTTCGAGCCTCAACGCCGCGGGTG
ATTTCTCGTTGAATCGGGAGAAAACCGATCTGGTGATGAACACCCTCGACGTGGCCAATATCGGCTACACGT
ATAAATTCAACGAGTATTGGCGCACGAATTGGAGCGCATCGATCTTTAAGTATGACGATAATTCGGCGTATG
CAGAGATTAATCCTGACGCTAATGAACGGCTCATTGACTATGCTGCAAATCTGTTCTACTCCCCTACCGCTC
AAATGGATTTTGGGGTCGAATATCATCAAGGGGAACGGAAAGTGTTCGACGGTCGTAAAGCAGACGTGAGCC

GGATTAATTTTGTGAGCATGTATAAGTTTTAAagtcaaaagcctccggtcggaggcttttgactggggagtg
ctcgcctcacagcgccgcggccaacattcacggcgtcgagcagggtgccttcaggggcccttggcctcacat
tcaccgccaccttgttcgagcgccatgagtgcaggcatatcaagaatttctaccaacctgccatgcaggtcg
acgatacccagcgcgcgcagacgggcgacggatcggcacacggtttccaggcgtaaacccaggtacgaagcc
atgtcttcacgagacatccgcaacatgaagccatgggcagagtaaccgcggctgacgaagcgcctggagagc
cccaccaggaagctggccagccgctgttctgcagtcaggttgcacagcatcagcacacgcccgtgctcacgc
acgatctcccggctcatcaggcgattcaggctttgctgcaggtccggaaactcacgcgccagggtttgcaag
cggcgatagggaacagggcagacttcgctgtcttccagggcaatggcgtcacagacatggtgctctgtggcg
atggcatcgaggccgattacatcgcccggcatccagaagttgatcaccacgccttgcccctcggcggtgttc
aggctggtcttgaaactgccgcagcgtaaggcatagagcatggtcagcggatcgttggcattgaacagcgcg
gcgcccttgcgaatgcgcatgcgtgggcctatcaacgcgcccaggcagctgttttcgtcaactggcaggcca
gtggggaggcacaggccgcttacccggcaatccatgcagtggttcaccagcggtttcaggtgaatagggttt
gccttggacaaagggttgggggagtcgagcagggtgaccttcagctggccaggcattttcaggcctccttcg
cattacggaggcccctttgggccccgtgccattacgcgcaccgagcccgacggtaaccccggtatggggcg
accaatcagcaagcatgtcccgcgagtgggggcattgaggcggcttgtaagcc

Table S9. Composition of effluent from PS feedstocks prepared for bioconversion. Concentration of key carbon sources in effluent from PS prepared for bioconversion.

Analyte	Effluent from PS beads (g/L)	Effluent from post-consumer EPS cup (g/L)
benzoic acid	3.13	3.43
benzaldehyde	0.02	0.02
acetic acid	1.00	1.63

Table S10. Composition of effluent from mixed PS plus HDPE feedstocks prepared for bioconversion.

Concentration of key carbon sources effluent from mixed HDPE+PS prepared for bioconversion. Two separate batches are indicated by "- #1" and "- #2".

Analyte	Effluent from mixed HDPE beads + PS beads - #1 (g/L)	Effluent from mixed post-consumer HDPE bottle + EPS cup - #1 (g/L)	Effluent from mixed HDPE beads + PS beads - #2 (g/L)	Effluent from mixed post-consumer HDPE bottle + EPS cup - #2 (g/L)
acetic acid	0.862	2.351	7.794	16.706
benzoic acid	2.287	2.573	5.004	6.107
malonic acid (C_3)	0.000	0.000	0.000	0.000
succinic acid (C_4)	0.529	0.361	1.156	0.716
glutaric acid (C_5)	0.279	0.180	0.596	0.328
adipic acid (C_6)	0.192	0.127	0.461	0.239
pimelic acid (C_7)	0.146	0.102	0.356	0.196
suberic acid (C_8)	0.122	0.096	0.361	0.211
azelaic acid (C_9)	0.056	0.064	0.140	0.119
sebacic acid (C_{10})	0.044	0.059	0.120	0.115
undecanedioic acid (C_{11})	0.035	0.054	0.096	0.108
dodecanedioic acid (C_{12})	0.026	0.047	0.081	0.101
tridecanedioic acid (C_{13})	0.020	0.046	0.069	0.100
tetradecanedioic acid (C_{14})	0.015	0.041	0.054	0.090
pentadecanedioic acid (C_{15})	0.012	0.039	0.042	0.080
hexadecanedioic acid (C_{16})	0.009	0.034	0.032	0.069
heptadecanedioic acid (C_{17})	0.007	0.031	0.025	0.064
octadecanedioic acid (C_{18})	0.006	0.027	0.019	0.051
nonadecanedioic acid (C_{19})	0.000	0.023	0.013	0.030
eicosanedioic acid (C_{20})	0.000	0.017	0.000	0.000
heneicosanedioic acid (C_{21})	0.000	0.009	0.000	0.000
docosanedioic acid (C_{22})	0.000	0.000	0.000	0.000

Table S11. Composition of effluent from mixed PS plus HDPE plus PET feedstocks prepared for bioconversion.

Concentration of key carbon sources in effluent from mixed HDPE+PS+PET prepared for bioconversion.

Analyte	Effluent from mixed HDPE beads + PS beads + PET powder (g/L) (#1, low TPA yield)	Effluent from mixed HDPE beads + PS beads + PET powder (g/L) (#2, high TPA yield)
acetic acid	20.995	2.516
benzoic acid	3.690	1.100
terephthalic acid	2.324	0.891
succinic acid (C_4)	0.574	0.195
glutaric acid (C_5)	0.285	0.097
adipic acid (C_6)	0.218	0.061
pimelic acid (C_7)	0.178	0.052
suberic acid (C_8)	0.177	0.040
azelaic acid (C_9)	0.093	0.032
sebacic acid (C_{10})	0.085	0.017
undecanedioic acid (C_{11})	0.078	0.014
dodecanedioic acid (C_{12})	0.069	0.011
tridecanedioic acid (C_{13})	0.064	0.009
tetradecanedioic acid (C_{14})	0.054	0.007
pentadecanedioic acid (C_{15})	0.046	0.006
hexadecanedioic acid (C_{16})	0.037	0.004
heptadecanedioic acid (C_{17})	0.032	0.003
octadecanedioic acid (C_{18})	0.023	0.003
nonadecanedioic acid (C_{19})	0.012	0.002
eicosanedioic acid (C_{20})	0.000	0.001

Table S12. Manganese and cobalt concentrations in the water-based solutions prepared for bioconversion.

Expected errors: for < 1 ppb, ~25% error; for 1-5 ppb, ~10% error; 5-150 ppb, < 5% error; >150 ppb, 5-10% error.

Filtrate from:	Mn (ppb)	Mn (µM)	Co (ppb)	Co (µM)
Effluent from PS beads	1.29	0.024	4.50	0.076
Effluent from EPS cup	1.20	0.022	77.8	1.32
Effluent from PS bead + HDPE bead	0.18	0.003	211	3.58
Effluent from post-consumer EPS cup + HDPE bottle	0.20	0.004	268	4.56
Effluent from PS + HDPE + PET powder	0.22	0.004	272	4.62

Table S13. Numerical data for β-ketoadipate yields in AW307 cultivations.
Dicarboxylates, benzoate, and terephthalate are derived from deconstructed polymers; acetate is present as residual solvent partially removed by rotary evaporation. The aliphatic constituents acetate and dicarboxylates are substrates for cellular growth. The aromatic constituents benzoate and terephthalate are substrates for conversion to beta-ketoadipic acid. The yield of β-ketoadipate (BKA) from aromatic substrates ((βKA/(BA+TPA)) is reported in column A (mol%, as reported throughout the manuscript). Mol β-ketoadipate per mol of all polymer-derived carbon substrates ((βKA/(BA+TPA+DCAs)) is reported in Column B.

M9 Minimal Media Plus	Bio. Rep.	Substrates (t0), mM				Product, mM		A			B		
								Yield: mol BKA per mol of aromatic constituent (βKA/(BA+TPA))			Yield: mol BKA per mol of total carbon from polymers (βKA/(BA+TPA+DCAs))		
		Acetate (AA)	Dicarboxylates (DCAs)	Benzoate (BA)	Terephthalate (TPA)	Beta-ketoadipate (βKA)	$Time_f$ (h)	Yield	Avg. (%)	Stdev. (%)	Yield	Avg. (%)	Stdev. (%)
Benzoate, dicarboxylates, terephthalate, acetate	Rep 1	24.58	0.84	2.22	0.11	1.67	9	0.718	72.9	1.2	0.528	53.7	0.7
	Rep 2	24.51	0.82	2.09	0.11	1.63	9	0.741			0.540		
	Rep 3	23.86	0.78	2.17	0.11	1.66	9	0.727			0.542		
Effluent from mixed HDPE beads, PS beads, and PET powder	Rep 1	22.13	0.85	1.85	0.90	1.81	9	0.657	75.5	8.5	0.503	57.5	6.3
	Rep 2	24.45	0.98	2.02	0.97	2.41	9	0.807			0.607		
	Rep 3	24.25	0.89	1.98	0.96	2.36	9	0.802			0.615		
Benzoate, dicarboxylates, acetate	Rep 1	9.20	3.59	6.62	n/a	7.43	12	1.123	101.1	11.3	0.728	65.1	7.5
	Rep 2	9.31	3.66	6.47	n/a	6.56	12	1.014			0.648		
	Rep 3	9.26	3.64	6.63	n/a	5.94	12	0.896			0.578		
Effluent from mixed HDPE beads and PS beads	Rep 1	12.46	2.81	3.41	n/a	3.05	12	0.894	81.0	7.2	0.490	48.5	1.2
	Rep 2	12.39	2.49	4.04	n/a	3.08	12	0.763			0.472		
	Rep 3	12.55	2.30	4.06	n/a	3.14	12	0.773			0.494		
Effluent from mixed post-consumer HDPE bottle and EPS cup	Rep 1	11.96	1.90	5.80	n/a	5.24	35.5	0.903	84.8	4.7	0.680	64.1	3.4
	Rep 2	11.97	1.88	5.78	n/a	4.72	35.5	0.816			0.616		
	Rep 3	11.98	1.84	5.84	n/a	4.82	35.5	0.825			0.627		
Effluent from mixed HDPE beads, PS beads, and PET powder	Rep 1	5.109	0.336	0.952	0.553	0.959	9	0.637	70.6	10.1	0.521	57.7	8.2
	Rep 2	5.169	0.334	0.948	0.527	1.212	9	0.822			0.670		
	Rep 3	5.324	0.325	0.944	0.532	0.972	9	0.659			0.540		

Table S14. Calculation of total molar β-ketoadipate yields from aromatic constituents of polymers.

		Yield, molar basis				Yield, carbon basis				
		A	B	C	D	E	F	G	H	I
Substrate	**Aromatic oxygenate**	**Molar yield from oxidation (mol%)**	**Total aromatic yield (mol%)**	**β-ketoadipate molar yield, mol/mol (%)**	**Estimated total molar β-ketoadipate yield (B*C)**	**Carbon yield from oxidation (carbon mol%)**	**Total carbon yield from oxidation (carbon mol%)**	**# carbons in product/# carbons in substrate)**	**Carbons captured in β-ketoadipate per substrate (C*G)**	**Estimated total carbon β-ketoadipate yield**
PS bead + HDPE bead	Benzoic acid	78.8%	78.8%	81.0%	**63.8%**	68.8%	68.8%	0.86	69.4%	**69.4%**
EPS cup + HDPE bottle	benzoic acid	81.2%	81.2%	84.8%	**68.9%**	65.0%	65.0%	0.86	72.7%	**72.7%**
PS bead + HDPE bead + PET powder, #2	terephthalic acid	63.6%	63.2%	70.6%	**53.4%**	63.6%	63.2%	0.75	53.0%	**56.7%**
	benzoic acid	62.9%				62.9%		0.86	60.5%	

References

1. S. B. Borrelle *et al.*, Predicted growth in plastic waste exceeds efforts to mitigate plastic pollution. *Science* **369**, 1515-1518 (2020).
2. A. Milbrandt, K. Coney, A. Badgett, G. T. Beckham, Quantification and evaluation of plastic waste in the United States. *Resour. Conserv. Recycl.* **183**, 106363 (2022).
3. K. Ragaert, L. Delva, K. Van Geem, Mechanical and chemical recycling of solid plastic waste. *Waste Manage.* **69**, 24-58 (2017).
4. A. Rahimi, J. M. García, Chemical recycling of waste plastics for new materials production. *Nat. Rev. Chem.* **1**, 1-11 (2017).
5. G. W. Coates, Y. D. Getzler, Chemical recycling to monomer for an ideal, circular polymer economy. *Nat. Rev. Mater.*, 1-16 (2020).
6. I. Vollmer *et al.*, Beyond mechanical recycling: Giving new life to plastic waste. *Angew. Chemie* **59**, 15402-15423 (2020).
7. L. D. Ellis *et al.*, Chemical and biological catalysis for plastics recycling and upcycling. *Nat. Catal.* **4**, 539-556 (2021).
8. S. C. Kosloski-Oh, Z. A. Wood, Y. Manjarrez, J. P. de los Rios, M. E. Fieser, Catalytic methods for chemical recycling or upcycling of commercial polymers. *Mater. Horiz.* **8**, 1084-1129 (2021).
9. A. J. Martín, C. Mondelli, S. D. Jaydev, J. Pérez-Ramírez, Catalytic processing of plastic waste on the rise. *Chem*, (2021).
10. C. Jehanno *et al.*, Critical advances and future opportunities in upcycling commodity polymers. *Nature* **603**, 803-814 (2022).
11. S. R. Nicholson *et al.*, The critical role of process analysis in chemical recycling and upcycling of waste plastics. *Ann. Rev. Chem. Biomolec. Eng.* **13**, (2021).
12. R. Wei *et al.*, Possibilities and limitations of biotechnological plastic degradation and recycling. *Nat. Catal.* **3**, 867-871 (2020).
13. R. A. F. Tomás, J. C. M. Bordado, J. F. P. Gomes, *p*-Xylene oxidation to terephthalic acid: A literature review oriented toward process optimization and development. *Chem. Rev.* **113**, 7421-7469 (2013).
14. W. Partenheimer, Valuable oxygenates by aerobic oxidation of polymers using metal/bromide homogeneous catalysts. *Catal. Today* **81**, 117-135 (2003).
15. A. Pifer, A. Sen, Chemical recycling of plastics to useful organic compounds by oxidative degradation. *Angew. Chemie* **37**, 3306-3308 (1998).
16. E. Bäckström, K. Odelius, M. Hakkarainen, Trash to treasure: Microwave-assisted conversion of polyethylene to functional chemicals. *Ind. Eng. Chem. Res* **56**, 14814-14821 (2017).
17. M. W. Guzik *et al.*, Robust process for high yield conversion of non-degradable polyethylene to a biodegradable plastic using a chemo-biotechnological approach. *Waste Manage.* **135**, 60-69 (2021).
18. Y. Ishii, S. Sakaguchi, Recent progress in aerobic oxidation of hydrocarbons by N-hydroxyimides. *Catal. Today* **117**, 105-113 (2006).
19. F. Gugumus, Re-examination of the thermal oxidation reactions of polymers 2. Thermal oxidation of polyethylene. *Polym. Degrad. Stab.* **76**, 329-340 (2002).
20. J. G. Linger *et al.*, Lignin valorization through integrated biological funneling and chemical catalysis. *Proc. Natl. Acad. Sci.* **111**, 12013-12018 (2014).

21. I. Poblete-Castro, J. Becker, K. Dohnt, V. M. Dos Santos, C. Wittmann, Industrial biotechnology of *Pseudomonas putida* and related species. *Appl. Microbiol. Biotechnol.* **93**, 2279-2290 (2012).
22. P. I. Nikel, V. de Lorenzo, *Pseudomonas putida* as a functional chassis for industrial biocatalysis: From native biochemistry to trans-metabolism. *Metab. Eng.* **50**, 142-155 (2018).
23. M. P. Mezzina, M. T. Manoli, M. A. Prieto, P. I. Nikel, Engineering native and synthetic pathways in *Pseudomonas putida* for the production of tailored polyhydroxyalkanoates. *Biotechnol. J.* **16**, e2000165 (2021).
24. C. W. Johnson *et al.*, Innovative chemicals and materials from bacterial aromatic catabolic pathways. *Joule* **3**, 1523-1537 (2019).
25. A. Z. Werner *et al.*, Tandem chemical deconstruction and biological upcycling of poly(ethylene terephthalate) to β-ketoadipic acid by *Pseudomonas putida* KT2440. *Metab. Eng.* **67**, 250-261 (2021).
26. Y. S. Ackermann *et al.*, Engineering adipic acid metabolism in *Pseudomonas putida*. *Metab. Eng.* **67**, 29-40 (2021).
27. D. Parke, M. A. Garcia, L. N. Ornston, Cloning and genetic characterization of *dca* genes required for beta-oxidation of straight-chain dicarboxylic acids in *Acinetobacter* sp. strain ADP1. *Appl. Environ. Microbiol.* **67**, 4817-4827 (2001).
28. G. Thompson Mitchell *et al.*, Fatty acid and alcohol metabolism in *Pseudomonas putida*: Functional analysis using random barcode transposon sequencing. *Appl. Environ. Microbiol.* **86**, e01665-01620 (2020).
29. C. Fernández, E. Díaz, J. L. García, Insights on the regulation of the phenylacetate degradation pathway from *Escherichia coli*. *Environ. Microbiol. Rep.* **6**, 239-250 (2014).
30. N. A. Rorrer *et al.*, Production of β-ketoadipic acid from glucose in *Pseudomonas putida* KT2440 for use in performance-advantaged nylons. *Cell Rep. Phy. Sci.*, (2022).
31. S. Y. Lee *et al.*, A comprehensive metabolic map for production of bio-based chemicals. *Nat. Catal.* **2**, 18-33 (2019).
32. C. Shi *et al.*, Design principles for intrinsically circular polymers with tunable properties. *Chem* **7**, 2896-2912 (2021).
33. Y. Kato, T. Wakabayshi, A convenient synthesis of γ-carboxymethylbutanolide. *Synth. Commun.* **7**, 125-130 (1977).
34. L. J. Missio, J. V. Comasseto, Enantioselective synthesis of (−)-γ-jasmolactone. *Tetrahedron Asymmetry* **11**, 4609-4615 (2000).
35. M. Sankar *et al.*, The benzaldehyde oxidation paradox explained by the interception of peroxy radical by benzyl alcohol. *Nature Comm.* **5**, 3332 (2014).
36. D. Salvachúa *et al.*, Metabolic engineering of *Pseudomonas putida* for increased polyhydroxyalkanoate production from lignin. *Microb. Biotechnol.* **13**, 290-298 (2020).
37. C. W. Johnson, G. T. Beckham, Aromatic catabolic pathway selection for optimal production of pyruvate and lactate from lignin. *Metab. Eng.* **28**, 240-247 (2015).
38. L. G. Migas, A. P. France, B. Bellina, P. E. Barran, ORIGAMI: A software suite for activated ion mobility mass spectrometry (aIM-MS) applied to multimeric protein assemblies. *bioRxiv*, 152686 (2017).
39. M. Liu *et al.*, Improved WATERGATE pulse sequences for solvent suppression in NMR spectroscopy. *J. Magn. Reson.* **132**, 125-129 (1998).

40. I. Agilent Technologies. (https://www.agilent.com/cs/library/technicaloverviews/public/5990-8496EN.pdf, 2015).
41. C. E. Frank, Hydrocarbon Autoxidation. *Chem Rev* **46**, 155-169 (1950).
42. J. F. Black, Metal-catalyzed autoxidation. The unrecognized consequences of metal-hydroperoxide complex formation. *JACS* **100**, 527-535 (1978).
43. F. Gugumus, Physico-chemical aspects of polyethylene processing in an open mixer. Part 29: Experimental kinetics and mechanisms of γ-lactone formation. *Polym. Degrad. Stab.* **92**, 143-157 (2007).
44. J. Tu, Z. Zhou, T. Li, Z.-J. Zhu, The emerging role of ion mobility-mass spectrometry in lipidomics to facilitate lipid separation and identification. *Trends Anal. Chem.* **116**, 332-339 (2019).
45. P. P. Hoet, R. Y. Stanier, The dissimilation of higher dicarboxylic acids by *Pseudomonas fluorescens*. *Eur. J. Biochem.* **13**, 65-70 (1970).
46. R. Y. Stanier, N. J. Palleroni, M. Doudoroff, The aerobic pseudomonads: a taxonomic study. *J. Gen. Microbiol.* **43**, 159-271 (1966).
47. L. N. Ornston, D. Parke, Properties of an inducible uptake system for beta-ketoadipate in *Pseudomonas putida*. *J. Bacteriol.* **125**, 475-488 (1976).
48. P. P. Hoet, R. Y. Stanier, Existence and functions of two enzymes with beta-ketoadipate: succinyl-CoA transferase activity in *Pseudomonas florescens*. *Eur J Biochem* **13**, 71-76 (1970).
49. M. Zhang *et al.*, Increased glutarate production by blocking the glutaryl-CoA dehydrogenation pathway and a catabolic pathway involving l-2-hydroxyglutarate. *Nat. Commun.* **9**, 2114 (2018).
50. A. Ferrández, J. L. García, E. Díaz, Transcriptional regulation of the divergent *paa* catabolic operons for phenylacetic acid degradation in *Escherichia coli*. *J. Biol. Chem.* **275**, 12214-12222 (2000).
51. P. Fonseca, F. de la Peña, M. A. Prieto, A role for the regulator PsrA in the polyhydroxyalkanoate metabolism of *Pseudomonas putida* KT2440. *Int. J. Biol. Macromol.* **71**, 14-20 (2014).
52. S. Zobel *et al.*, Tn7-Based Device for Calibrated Heterologous Gene Expression in *Pseudomonas putida*. *ACS Synth. Biol.* **4**, 1341-1351 (2015).
53. S. H. Saunders. (Zenodo, 2022).
54. A. Schäfer *et al.*, Small mobilizable multi-purpose cloning vectors derived from the *Escherichia coli* plasmids pK18 and pK19: selection of defined deletions in the chromosome of *Corynebacterium glutamicum*. *Gene* **145**, 69-73 (1994).
55. L. N. Jayakody *et al.*, Thermochemical wastewater valorization via enhanced microbial toxicity tolerance. *Energy Environ. Sci.* **11**, 1625-1638 (2018).
56. I. Pardo *et al.*, Gene amplification, laboratory evolution, and biosensor screening reveal MucK as a terephthalic acid transporter in *Acinetobacter baylyi* ADP1. *Metab. Eng.* **62**, 260-274 (2020).